NASA CR-179471
R86AEB361

National Aeronautics and
Space Administration

EFFECTS OF SURFACE CHEMISTRY ON HOT CORROSION LIFE

FINAL REPORT

By

R.E. Fryxell
General Electric Company
Aircraft Engine Business Group
Cincinnati, Ohio 45215

G.E. Leese
TRW, Inc.
Aircraft Components Group
Cleveland, Ohio 44117

June 1986

Prepared for
National Aeronautics and Space Administration

Lewis Research Center
Contract NAS3-23926

1. Report No.	2. Government Accession No.	3. Recipient's Catalog No.
NASA CR-179471		

4. Title and Subtitle	5. Report Date
Effects of Surface Chemistry on Hot Corrosion Life	June 1986
	6. Performing Organization Code 533-04-11

7. Author(s)	8. Performing Organization Report No.
R.E. Fryxell and G.E. Leese	R86AEB361
	10. Work Unit No.

9. Performing Organization Name and Address	11. Contract or Grant No.
General Electric Company Aircraft Engine Business Group Evendale, OH 45215-6301 TRW Inc. Cleveland, OH 44117	NAS3-23926
	13. Type of Report and Period Covered Final Contractor Report

12. Sponsoring Agency Name and Address	14. Sponsoring Agency Code
National Aeronautics and Space Administration Washington, DC 20546	

15. Supplementary Notes

Project Manager: Nathan S. Jacobson
NASA Lewis Research Center
Cleveland, OH

16. Abstract

Burner rig tests were conducted under the follcwing conditions: 900° C, hourly thermal cycling, 0.5 ppm sodium as NaCl in the gas stream, Mach 0.3 velocity. The alloys tested were Udimet 700 (U700) and René 80, uncoated and with RT21, Codep, or NiCoCrAlY coatings. The tests, up to 1000 hours, included specimens in the as-processed condition and after aging at 1100° C in oxidizing or inert environments for up to 600 hours. Coil-inductance changes were measured for periodic non-destructive inspection of specimens and found useful in following the course of corrosion.

Typical sulfidation observed in all cases was similar to that observed in service-run turbine components. Aging at 1100° C caused severe decrease in the hot corrosion life of RT21 and Codep coatings and a significant but lesser decrease in the life of NiCoCrAlY coatings. The extent of these decreases was much greater for all three coatings on U700 substrates than on René 80 substrates. Further studies of Codep-coated specimens, including aging at other temperatures, indicated (a) that life decrease is predominantly caused by changes in morphological features of the diffusion zone and (b) the threshold temperature for deleterious changes is less than 1050° C with U700 substrates and greater than 1100°/less than 1135° C with René 80 substrates.

A coating hot corrosion life-prediction model is proposed that recognizes the above findings. The model requires time/temperature information for a turbine component at takeoff conditions as well as environmental contaminant information. The penalties of aging, as defined, must be separately determined for materials systems other than Codep/U700 and Codep/René 80.

17. Key Words (Suggested by Author(s))	18. Distribution Statement
Hot Corrosion Gas Turbine Life Prediction Methodology	General Release

19. Security Classif. (of this report)	20. Security Classif. (of this page)	21. No. of Pages	22. Price*
Unclassified	Unclassified	103	

* For sale by the National Technical Information Service, Springfield, Virginia 22161

NASA-C-168 (Rev. 10-75)

N86-28087#

FOREWORD

This final report describes work performed for the NASA Lewis Research Center under Contract NAS3-23926 and represents collaborative efforts of the Engineering Materials Technology Laboratories (EMTL) of the General Electric Aircraft Engine Business Group and the Materials and Manufacturing Technology Center (MMTC) of TRW Inc. Aircraft Components Group. R.E. Fryxell of General Electric was the principal investigator; G.E. Leese and C.S. Kortovich of TRW and B.K. Gupta, formerly of TRW, presently with General Electric, participated under subcontract. N.S. Jacobson and, formerly, J.P. Merutka of the Lewis Research Center served as Project Manager for NASA.

TABLE OF CONTENTS

LIST OF ILLUSTRATIONS

LIST OF ILLUSTRATIONS (Continued)

LIST OF ILLUSTRATIONS (Continued)

LIST OF ILLUSTRATIONS (Concluded)

LIST OF TABLES

LIST OF TABLES (Concluded)

SUMMARY

This is the final report of a 3-year program. The objectives were to ascertain the surface-chemistry effects of oxide scale on the hot corrosion life of selected alloys, coated and uncoated, and to provide data for the development of a hot corrosion life-prediction model. Effects and efficacy of coating composition and heat treatment were also explored.

The coated alloys were evaluated by high-velocity hot corrosion rig testing in the as-processed condition and after various aging treatments designed to simulate the surface-chemistry effects of in-service conditions. Uncoated alloys were also tested in the heat-treated condition. The selected alloys were Udimet 700 (U700) and René 80; RT21, Codep, or NiCoCrAlY coatings were used. All specimens were periodically removed from test for inspection and nondestructive tracking of corrosion by measuring the change in 10-MHz coil inductance (technique developed at NASA Lewis).

Results for all three coatings showed that life at 900° C was shortened significantly by preaging at 1100° C for 100 hours or more; this was far more severe for U700 than for René 80 substrates. Aging in vacuum also degraded life, similar to aging in air, suggesting that interdiffusion effects are more important than surface-composition changes caused by oxidation.

Therefore the life-prediction model proposed is a combination of two unrelated parameters: average contaminant environment and coating/substrate interdiffusion phenomena occurring at takeoff temperatures. Proper definition and modeling of the effects of these parameters requires detailed information concerning engine operating conditions and flight route structure.

To obtain some further information in support of this model, additional burner rig tests were performed on Codep/U700 and Codep/René 80 specimens. These tests identified a temperature in the range 1100° - 1135° C at which relatively short exposures of Codep/René 80 degrade hot corrosion life. For Codep/U700, this threshold temperature is somewhat below 1050° C. One test performed at half the standard salt-ingestion level confirmed the expected decrease in hot corrosion rates.

In addition to the laboratory test program, a comprehensive evaluation of six service-run turbine components was performed to: (1) establish the extent and mechanism of hot corrosion degradation and (2) correlate observations to engine operating history, where possible. Typical sulfidation was identified in five of the six components. The extent of corrosion observed appeared to be inversely proportional to the average length of mission; however, with such a limited sampling it was not possible to determine whether this reflects fraction of time under takeoff conditions (higher temperatures), fraction of time near ground level (higher propensity for contamination), or some other related parameter. Nevertheless, these observations plus the results of the laboratory test program define a new perspective for future field-service evaluation and life-prediction modeling.

INTRODUCTION

This program was a 36-month, joint effort of the Engineering Materials Technology Laboratories of General Electric Company Aircraft Engine Business Group and the Materials and Manufacturing Technology Center of TRW, Inc. It comprised the following five tasks.

Task I involved evaluation of six turbine components, showing visual evidence of hot corrosion and having known operating history, to establish the degree of degradation and mechanisms in the corroded areas. Corrosion was correlated with operating conditions to the extent possible. Evaluation included chemical and X-ray diffraction analyses of surface scales/deposits as well as metallography, scanning electron microscopy, and electron microprobe examination. Both uncoated and coated hardware was included, and emphasis was placed on the cause and effect parameters associated with hot corrosion. The results of this study served as a point of reference for laboratory testing in the remainder of this program. All burner rig tests were performed by TRW Inc., Cleveland, Ohio.

Task II established a hot corrosion baseline for the selected alloys and coatings in the as-processed condition. This involved up to 1000 hours of exposure of duplicate specimens in a Mach 0.3 burner rig using Jet A fuel (0.045 - 0.065% sulfur); 0.5 ppm sodium by weight, as NaCl, was added to the combustion air. The test cycle was one hour at 900° C followed by six minutes of forced-air cooling to ambient temperature. Specimens were inspected at approximately 20-cycle intervals and removed from test when evidence of hot corrosion was noted in three successive inspections. Additional specimens were tested for time periods of 100, 300, and 500 hours if these time periods did not exceed 2/3 of the time the original specimen of the same material was exposed. Specimens tested in this task included U700 and René 80, uncoated and with the following coatings:

- Pack aluminide RT21 (Chromalloy) and Codep (General Electric)
- Low-pressure plasma sprayed NiCoCrAlY (Ni-23Co-18Cr-12Al-0.3Y), applied by General Electric

In Task III, triplicate specimens of the above coated alloys were aged at 1100° C under a variety of conditions, both oxidizing and inert environments, to induce coating/alloy interdiffusion with and without surface oxidation. These specimens were subsequently hot corrosion tested in Task IV, under the same conditions as in Task II, to determine the effects of aging on hot corrosion behavior. The aging treatments in Task III were as follows:

- Isothermal for 100 hours in a vacuum
- Isothermal air furnace oxidation for 100, 300, and 600 hours
- One-hour air furnace cycles for 100 hours
- Cyclic burner rig oxidation for 100, 300, and 600 hours

One specimen representing each of the above conditions was evaluated using the methods outlined in Task I.

In Task IV, the remaining duplicate specimens representing each condition were used, and an empirical hot corrosion life-prediction model was proposed. All data were consolidated, including the effects of aging on hot corrosion behavior.

Task V was a hot corrosion cyclic burner rig test designed to check the validity of the proposed life-prediction model. Duplicate specimens of the selected coated alloys were tested for up to a maximum of 1000 hours and evaluated as in Tasks II and IV. The Task V experiment was designed to test two aspects of the proposed life-prediction model:

- Environmental variable (a different salt flux)
- Surface chemistry and internal changes (modification of the aging conditions used in Task III)

TASK I - EVALUATION OF TURBINE COMPONENTS FROM FIELD SERVICE

This study involved comprehensive evaluation of six turbine components, blades and vanes, that showed evidence of hot corrosion in addition to normal oxidation degradation. These were selected from uncleaned engines for which operating history was reasonably well defined in order to provide a basis for estimating cause and effect parameters.

In the course of searching for suitable examples, it became very clear that, although uncleaned components were readily available, they generally had suffered some handling. This reduces, to a certain extent, the reliability of surface analysis for airborne contamination; results may either be high due to handling contamination or low due to loss of relatively nonadherent surface deposits. This uncertainty, however, in no way jeopardizes metallographic evaluation and correlation with operating history. Actually, evidence of corrosive contamination, such as sodium compounds on airfoil surfaces, is of second-order importance; ingestion of such contaminants by an airborne turbine is intermittent, and the amount found may only represent ingestion during the final landing before engine teardown.

It should be pointed out that hot corrosion is not frequently observed in the high-pressure turbines (HPT) of engine models available for this study. A large majority of engines run considerably longer before first removal, than the selected examples, without life-limiting environmental degradation. The five HPT examples selected were obtained only after examining blades from a large number of disassembled engines. On the other hand, hot corrosion is more frequently encountered in low-pressure turbines (LPT) since, at the lower temperatures involved, corrosive contaminants are more likely to accumulate in significant amounts and/or be present a greater percentage of the time. The sixth component selected was an LPT vane.

Table I identifies the six components, with associated provenance, and is a summary of available operating history. Four are the same component from engines of the same model to afford maximum cause-and-effect correlations, thus eliminating design and operational differences known to be significant. Evaluation of these components followed the sequence below:

1. Examine visually and photograph.

2. For the three components that have duplicate parts available, rinse concave and convex airfoil surfaces separately for the duplicates. Analyze water-soluble sodium, calcium, magnesium, cobalt, nickel, and sulfate.

3. Based on visual examination, select suitable locations for cutting which represent regions of maximum distress. Cut dry, prepare metallographic mounts, and polish under kerosene.

4. Examine mounts in the as-polished condition up to 500× for evidence of sulfidation.

Table I. Components Selected for Evaluation.

Carrier Base	Aircraft	Component	Total Hours	Number of Cycles	% Takeoffs at Coastal Airports
Southern Asia	A300B	1*	2,694	1560	67
Northern Africa	A300B	1	4,641	2169	77
Southern Africa	A300B	1	1,830	1471	50
Western Europe	DC10-30	1	2,625	610	46
South America	DC10-30	2*	15,155	2987	72
U.S. Military	F-4	3*	2,700		

Component 1: CF6-50 Stage 1 HPT Blade, Codep Coated René 80
Component 2: CF6-50 Stage 1 LPT Vane, Uncoated René 77
Component 3: J79 Stage 1 HPT Blade, Codep Coated René 80

* Duplicate parts were available for determining composition of water-soluble deposits.

5. Selectively analyze scale and underlying metal by scanning electron microscopy, energy-dispersive analysis of X-ray (SEM-EDAX) and by electron microprobe (EMP).

6. Etch mounts and examine for evidence of alloy depletion.

7. Measure maximum distress, including metal loss and alloy depletion, at various locations.

8. Define type of attack: oxidation, Type 1 hot corrosion, or Type 2 "intermediate temperature" hot corrosion. The two types of hot corrosion are typified as:

   - Type 1 - A zone of alloy depletion containing sulfide particles.
   - Type 2 - No alloy depletion in the affected area, and sulfides only at the scale/alloy interface. The scale is dense and layered.

9. Document typical regions of distress with photomicrographs.

10. Analyze, by X-ray diffraction, selected samples of scale from areas as close as possible to locations of maximum distress.

The four CF6-50 turbine blade evaluations are described in the following discussion individually and then as a group to correlate operating history to

the extent possible. Metallographic mounts were prepared of three transverse cuts of each airfoil. After preliminary examination, one mount from each blade was eliminated from detailed study because environmental degradation was clearly less. The intent of the study was to identify locations of maximum distress and to establish whether oxidation or hot corrosion was causing the distress. As is typical with HPT blades, the convex airfoil surfaces (CVX) exhibited minimal degradation; thus, the following discussion refers only to concave/pressure surfaces (CCV), in some cases including the leading edge (LE). Specific locations are designated by percent span (radial)/percent chord (distance from leading edge to trailing edge). Photographs of the concave surfaces of the four CF6-50 turbine blades are shown in Figure 1.

Southern Asia

At the 40%/70-90% location, the coating was breached, and some attack of the substrate was evident. Maximum distress was about 100 μm (0.004 inch). Type 1 subsurface sulfides were clearly visible (see Figure 2) within the remaining coating at the edge of the distressed region. EMP confirmed that these particles were sulfides (see Figure 3).

In the 60% radial section, similar Type 1 structures were observed with a maximum distress of about 50 μm (0.002 inch) at the LE; the diffusion zone of the coating was intact. EDAX examination confirmed the presence of subsurface sulfides, predominantly of Ti and Ni. The scale was rich in Al with lesser amounts of Cr, Ti, and some Ca. Calcium sulfate was identified by X-ray diffraction. The greatest distress, however, occurred at 60-80% chord (about 200 μm or 0.008 inch); thorough EDAX examination failed to reveal sulfides, and the scale was Cr rich with lesser amounts of Ti and Al. Thus, in this blade, although Type 1 hot corrosion was strongly evident, the most distressed region had both structural and compositional features of oxidation.

Northern Africa

At the 50%/60-90% location the coating was breached, and considerable loss of the substrate alloy had occurred to a total depth of about 230 μm (0.009 inch) including a depletion layer. Type 1 subsurface sulfides were clearly visible (Figure 4) together with strong EDAX confirmation of sulfur combined with Ti, Cr, and Ni. The scale was rich in Cr and Al with some Ti. Although Ca was not observed by EDAX, X-ray diffraction identified $CaSO_4$ from a scale specimen adjacent to the cut region. The depletion zone in the substrate had lower Cr, Al, and Ti levels than unaffected René 80. At the 80%/50-80% location, similar structures were observed, again to a maximum depth of about 230 μm (0.009 inch).

Southern Africa

Maximum distress, about 180 μm (0.007 inch), was observed on this blade at the 60%/90% location. The structural features indicate oxidation only

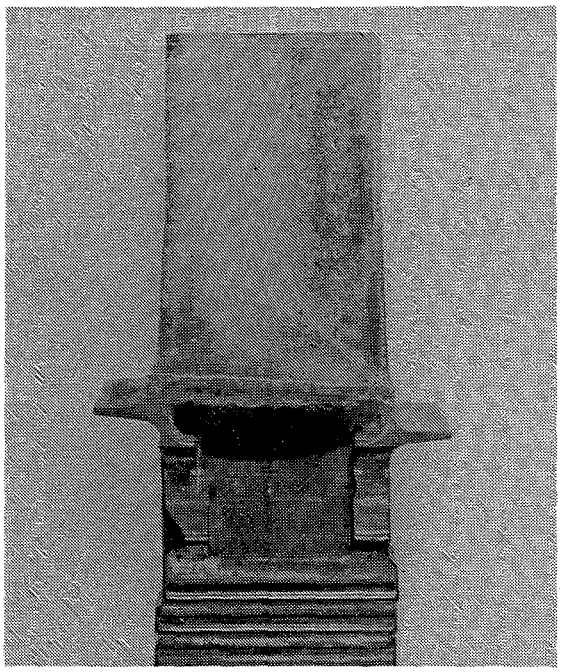

Southern Asia, A300B
2694 Hours, 1560 Cycles

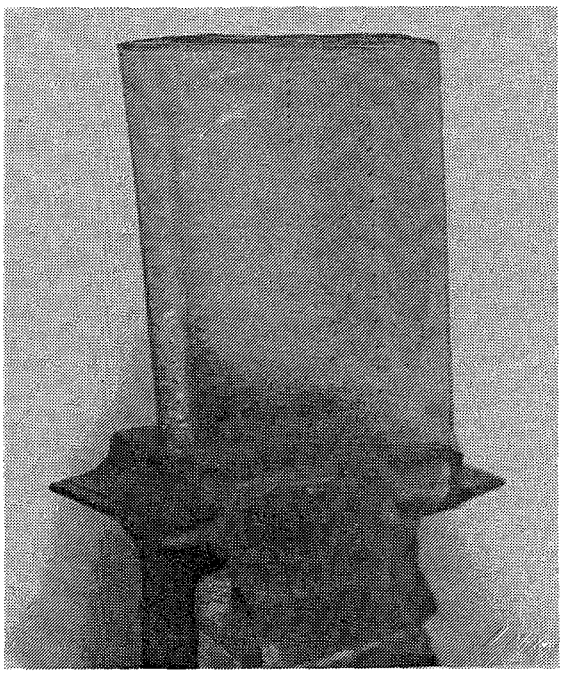

Northern Africa, A300B
4641 Hours, 2169 Cycles

Southern Africa, A300B
1830 Hours, 1471 Cycles

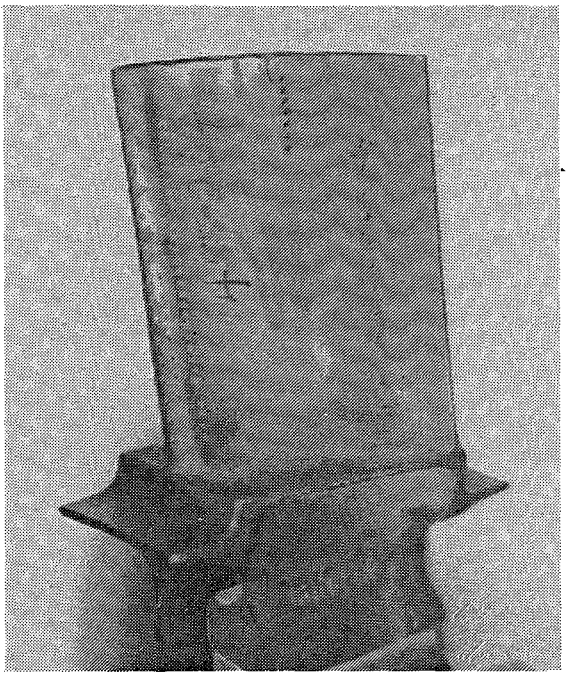

Western Europe, DC10-30
2625 Hours, 610 Cycles

Figure 1. CF6-50 HPT Stage 1 Blades.

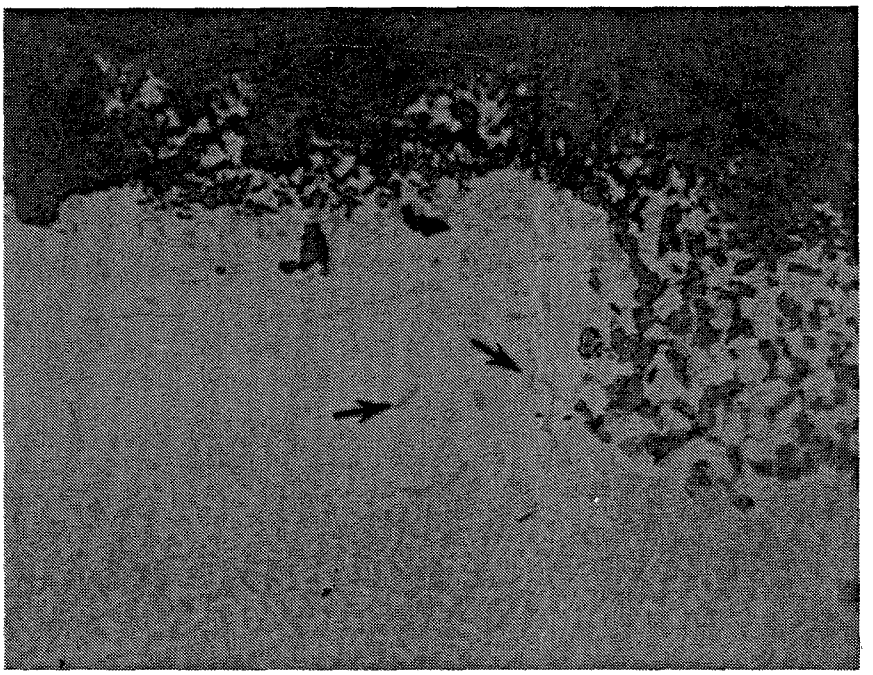

Arrows indicate presence of Type 1 sulfides.

Figure 2. Southern Asia CF6-50 HPT Stage 1 Blade, Concave Side, 40%/80% Location, As Polished (1000×).

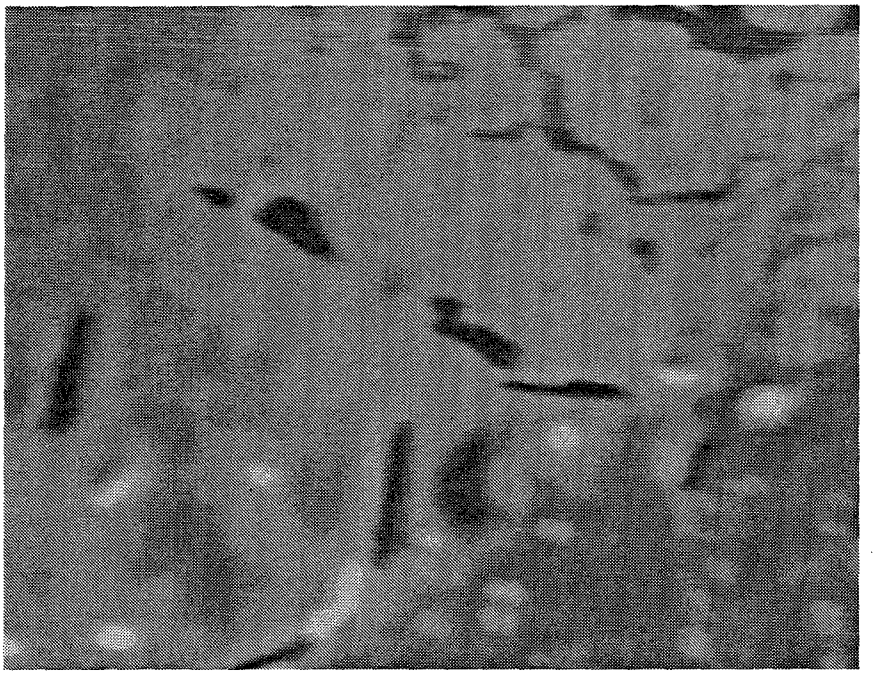

BSE

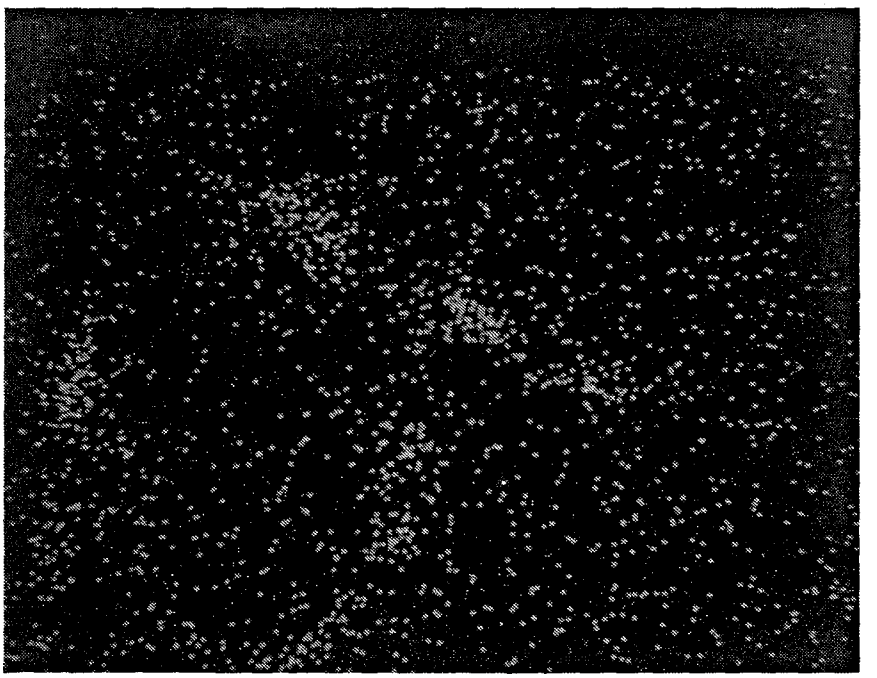

Sulfur

Figure 3. EMP Confirmation of Sulfides in the Subsurface Particles Indicated in Figure 2 (5000×).

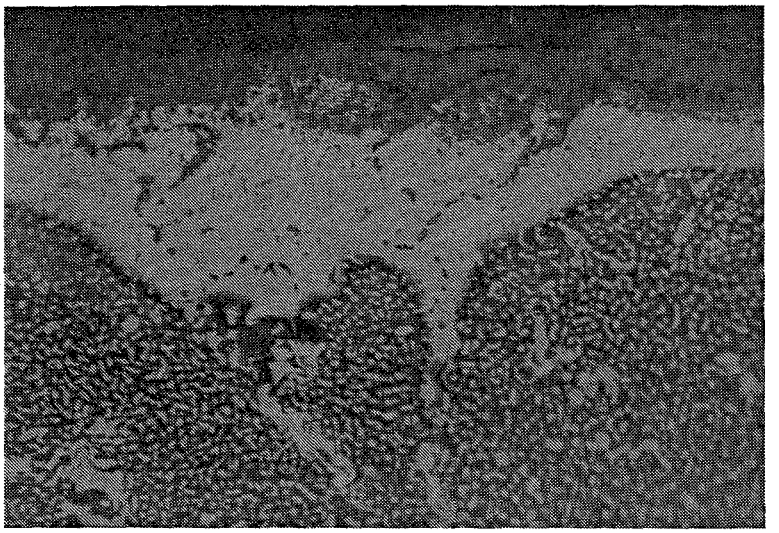

Etched 500×

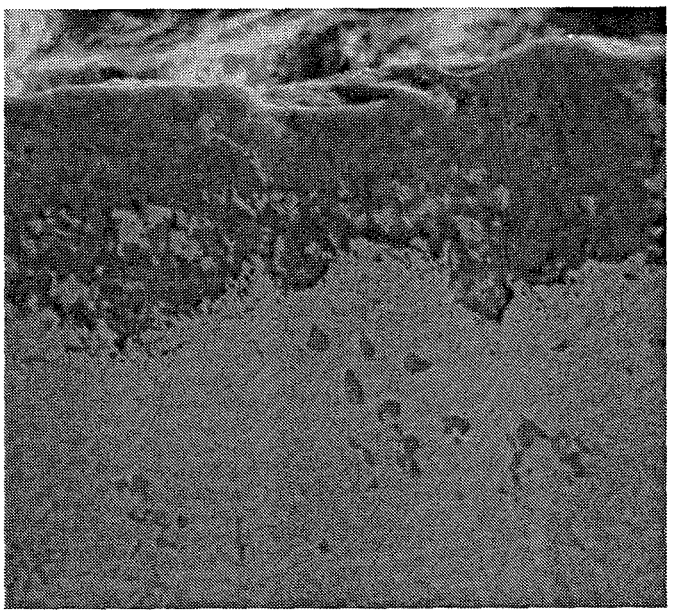

1450×

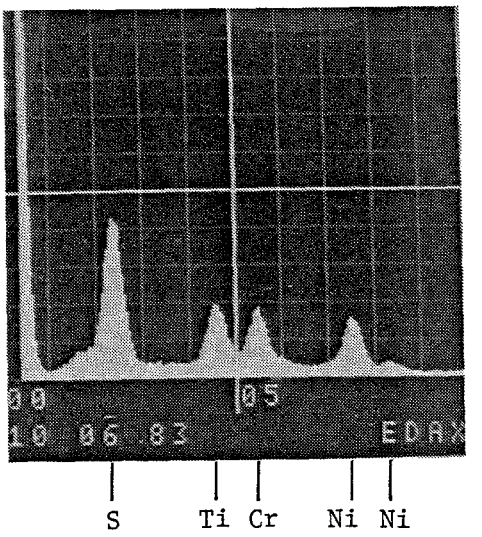

EDAX identifies gray subsurface particles as sulfides containing Ni, Cr, and Ti.

Figure 4. Northern Africa CF6-50 Engine HPT Stage 1 Blade, Concave Side, 50%/60-90% Location.

(Figure 5a). No sulfides were found by EDAX examination. The scale contained substantial amounts of Ca and some Fe (from the environment) as well as Al.

Type 1 sulfidation was confirmed by both EMP and EDAX in the 10% radial section at the leading edge (Figure 5b) and at 60-80% chord. Maximum distress was about 50 μm (0.002 inch) and 75 μm (0.003 inch) at these two locations, respectively. The outer scale was rich in Al with a lesser amount of Ti (LE), and the depletion zone in the exposed substrate at 60-80% chord again was lower in Cr, Al, and Ti than in the unaffected René 80.

Western Europe

This was the least distressed of the four CF6-50 turbine blades. There was faint visual evidence of Type 1 sulfidation within the coating (which was not breached) in the 10% section, at the leading edge, and at 60-80% chord; maximum penetration was about 45 μm (0.0018 inch). EDAX analysis of the scale showed strong Al and lesser amounts of Ti and Cr. Sulfur was not detected.

At the 20%/60-80% location the structure was quite similar (as shown in Figure 6). Maximum attack was about 50 μm (0.002 inch), and EMP analysis did provide evidence for sulfur, although weak, in the small particles within the residual coating barely visible in the photomicrograph. EDAX analysis of the scale showed considerable Ca as well as Al.

The above information is summarized in Table II. The listed temperatures refer to the blade surface at the location of maximum degradation; these must be regarded as approximate for two reasons: (1) observed distress occurs over some distance along the surface and (2) assigned temperatures are calculated and will, in general, change somewhat as the turbine ages.

The depletion zone that develops in an alloy such as René 80 is largely a loss of aluminum manifested in the disappearance of the γ' phase. This was confirmed by EDAX analysis of several etched metallographic mounts as well as the presence of subsurface sulfides. However, sulfides were found in the most distressed areas in only two of these blades; although sulfides were found in the other two, none was detectable in the most severely distressed regions.

This points up a primary difficulty in interpretation: contaminant ingestion occurs only when the aircraft is near ground level; during most of a mission, simple oxidation is probably to be expected. Table II exhibits one attempt to relate observed degradation to operating history. Using flight-pattern information and the criterion given in the first footnote, total times were estimated during which each engine might be considered vulnerable to contaminant ingestion: total hours near coastal airports and total hours in the life of an engine. One way of displaying this information is shown in Figure 7. The plot shows hot corrosion increasing with low-altitude operating time. The upwards curvature is reasonable; above about 60-80 μm degradation (nominal original coating thickness) the substrate alloy is exposed. However, with this limited sampling, it is not reasonable to make inferences concerning coastal versus total low-altitude exposure.

(a) 60%/90% Location, Concave Side; Ordinary Oxidation, No Evidence of Sulfides (Etched)

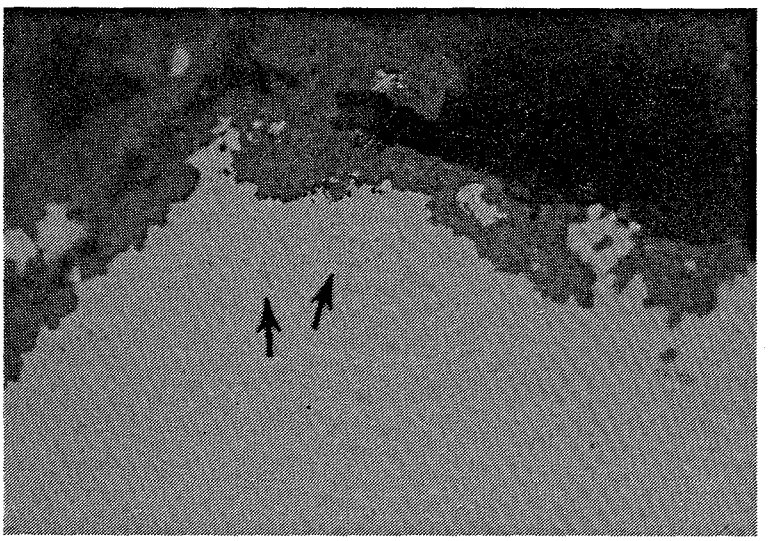

(b) 10% Leading-Edge Location; Considerable Subsurface Sulfides (Arrows) Within Residual Coating

Figure 5. Southern Africa CF6-50 Engine Stage 1 HPT Blade (500×).

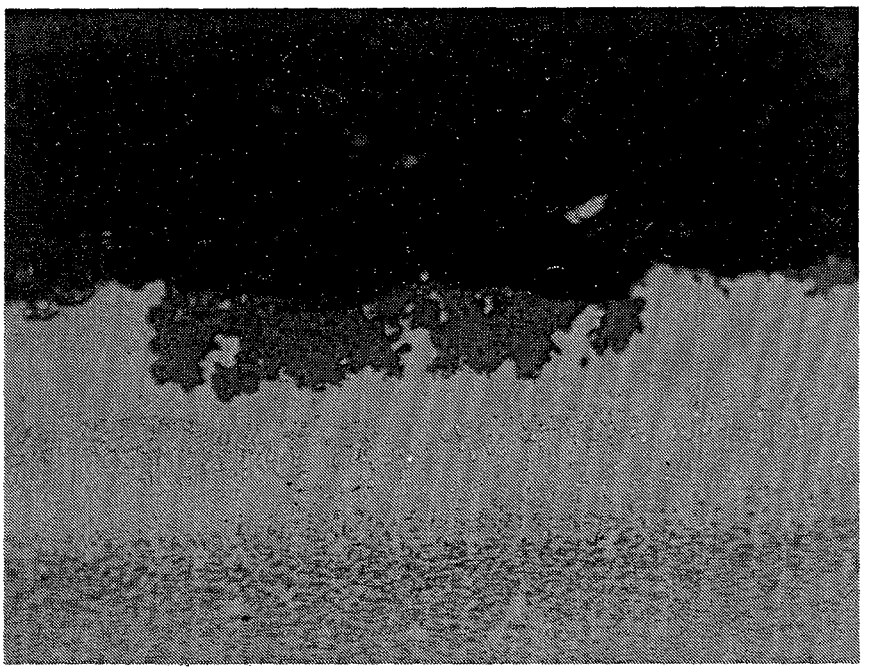

A few subsurface particles within the residual coating were confirmed as sulfides by EMP examination.

Figure 6. Western Europe CF6-50 HPT Stage 1 Blade, Concave Side, 20%/70% Location (Etched, 500×).

Table II. Summary of Metallographic Evaluations and Operating History for Four Stage 1 HPT Blades from CF6-50 Engines.

Carrier Base	Total Hours	Number of Cycles	Hours Per Cycle	Operating Hours Above 2000-ft Elevation *		Location, % Span/% Chord	Estimated Temp., ° C		Estimated Maximum** Depth of Attack, μm		Type 1 Sulfides
				Near Coastal Airport	Total		Max.	Avg.	Total	Per 1000 Hours	
Southern Africa	2694	1560	1.72	350	520	40/70-90	1090	820	100	37	Yes
						60/Leading Edge	980	740	50	20	Yes
						60/80	1090	820	200	75	No
Northern Africa	4641	2169	2.14	560	720	50/60-90	1090	820	230	50	Yes
						80/50-80	1090	820	230	50	Yes
Southern Africa	1830	1471	1.24	240	490	10/Leading Edge	910	680	50	27	Yes
						10/60-80	1020	760	75	40	Yes
						60/90	1090	820	180	100	No
Western Europe	2625	610	4.30	95	200	10/60-80	1020	760	45	17	No
						20/60-80	1020	760	50	20	Yes

* Estimated using 20 minutes as approximate total time per cycle; gate to takeoff, climb to 2000 ft.

** Including depletion zone.

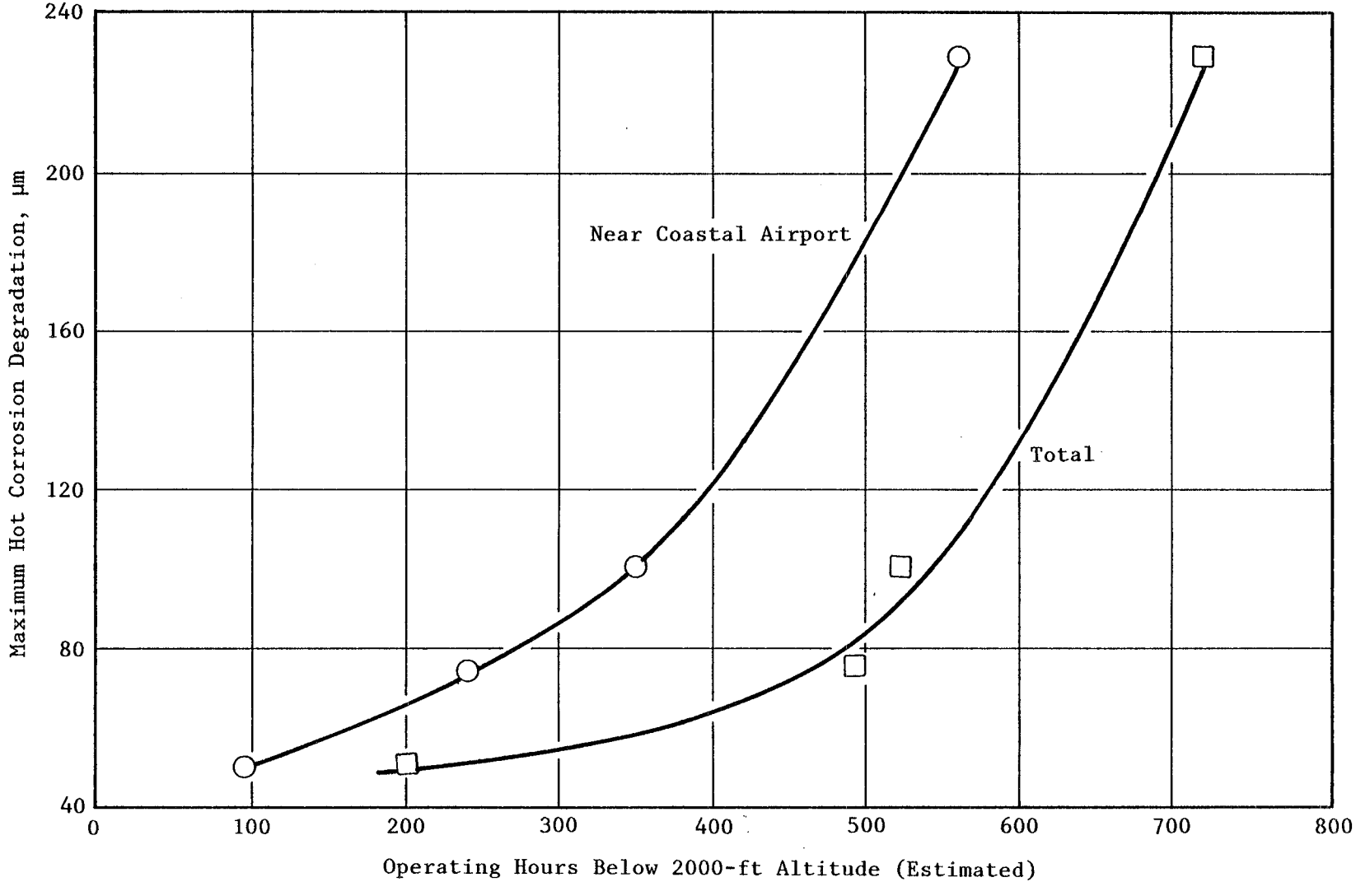

Figure 7. Hot Corrosion Degradation for Worst Case CF6-50 HPT Stage 1 Blades.

Alternatively, the trends shown in Figure 7 may reflect total times at takeoff/thrust reverse (higher) temperatures, a parameter clearly related to total hours at low altitude. This is shown in rate units in Figure 8. The highest rate corresponds to the shortest lengths of mission for which the percentage of time at higher temperatures (or lower altitude) is greater.

These are interesting and instructive exercises, but the four blades were selected as rather extreme examples, and the actual corrosive degradations (Table II and Figures 7 and 8) do not define curves which other examples should be expected to match. Further, since oxidation and hot corrosion rates are competitive in some cases (Table II), the cause-and-effect relationships with respect to environmental degradation have additional complexity. The trend shown in Figure 8 has, however, long been recognized in a qualitative sense; hopefully, continued quantitative evaluations coupled with compilations of operating histories will lead to a reliable choice among various possible correlations such as those depicted in Figures 7 and 8.

With respect to the ultimate blending of this type of information with the burner rig studies performed in this program and application to life-prediction methodology, it should be pointed out that previous burner rig corrosion tests at General Electric with very low salt-ingestion levels (at barely the threshold level for salt condensation) produced conventional Type 1 sulfidation but at rates indistinguishable from oxidation. This may relate to the results in Table II: oxidation and corrosion rates may vary relative to each other, depending on the circumstances. There are possible implications with respect to the design of somewhat more complex burner rig tests as well: temperature cycling, intermittent salt ingestion, etc.

Remaining to discuss are evaluations of two additional components and a variety of chemical and structural identifications of scales and deposits.

South America

This Stage 1 LPT vane was selected as an example of severe hot corrosion. LPT temperatures are considerably lower than in the HPT, and salt deposits are more likely to accumulate that may not evaporate during subsequent operation at high altitude. This is particularly true in relatively stagnant internal cavities. In the selected example, inside-out corrosion from such deposits was so severe it penetrated the airfoil in some locations. This evaluation, however, is confined to external surfaces that can be unambiguously related to operating parameters and to degradation of components elsewhere in the engine. Photographs of two adjacent vanes are shown in Figure 9.

Metallographic sections were prepared for the 80% span of both of these vanes (measured outwards from the inner flange). Type 1 sulfidation was prevalent and extensive at many locations on both concave and convex surfaces, unlike HPT blades where very little degradation occurs on the convex surface. Maximum attack was about 400 μm (0.016 inch), including depletion zone, at several locations on both sections examined. There was no evidence of Type 2 corrosion. Typical microstructures are shown in Figure 10, and EMP evidence

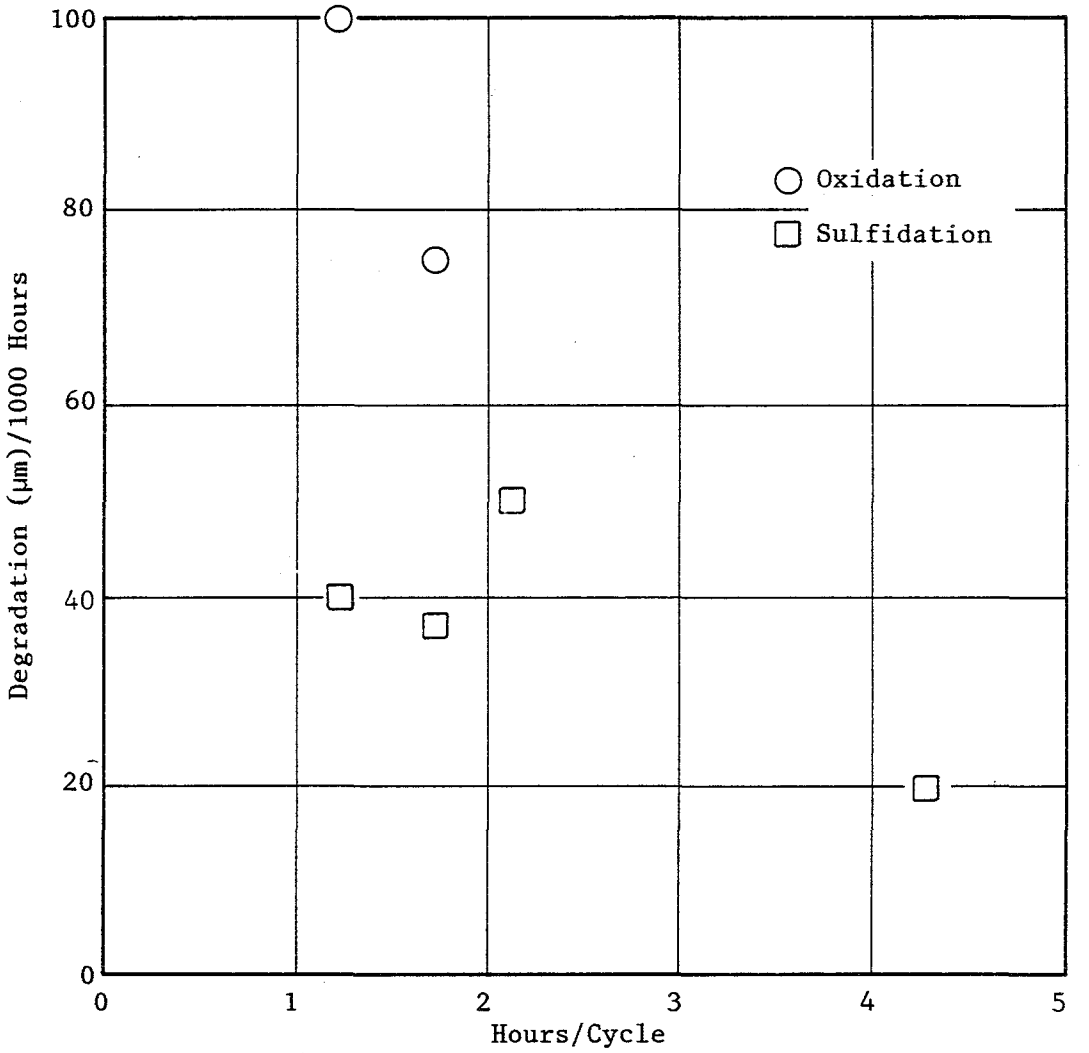

Figure 8. Maximum Degradation Rates for CF6-50 HPT Stage 1 Blades as a Function of Average Mission Duration.

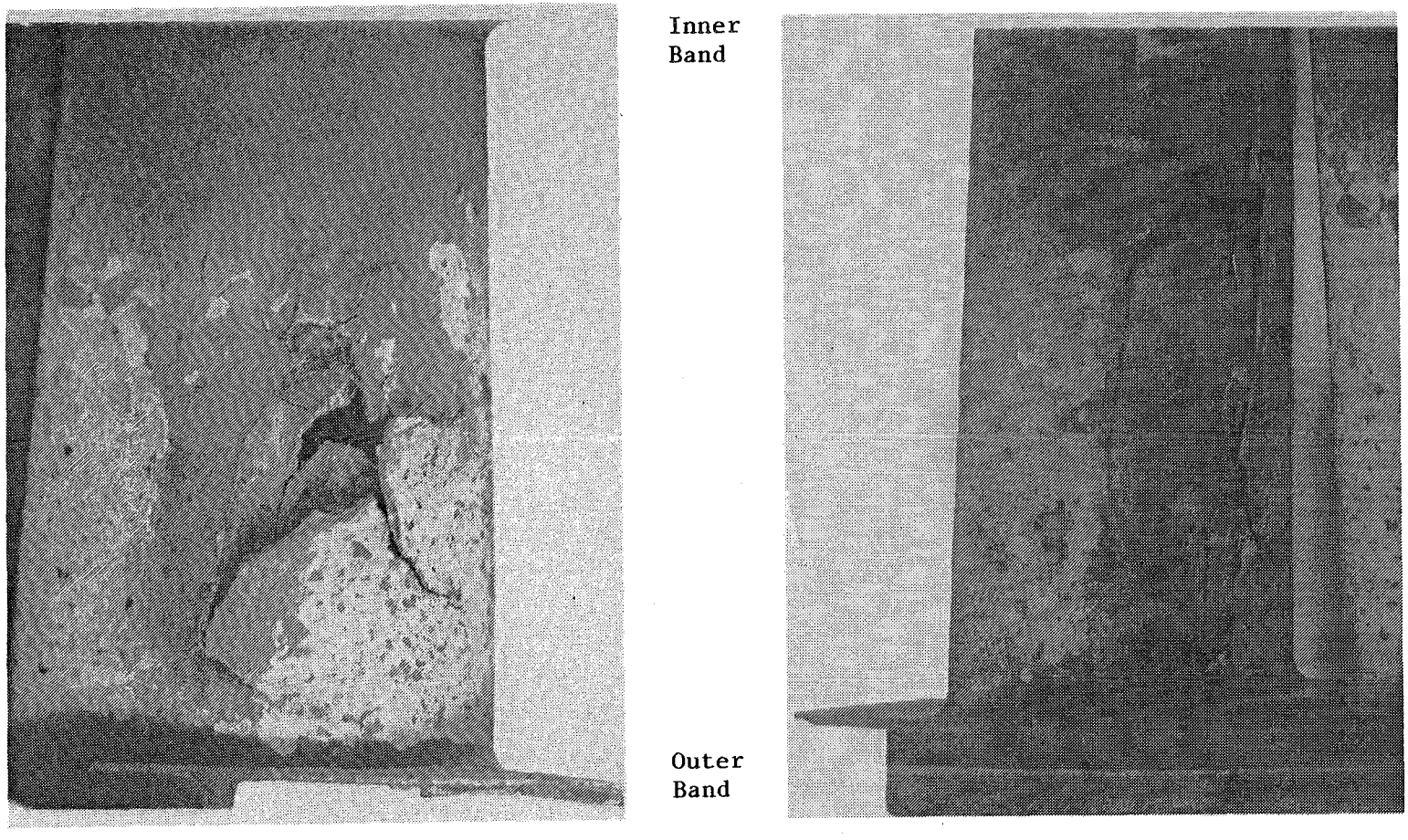

Figure 9. South American CF6-50 LPT Stage 1 Vanes After 15,155 Hours of Service.

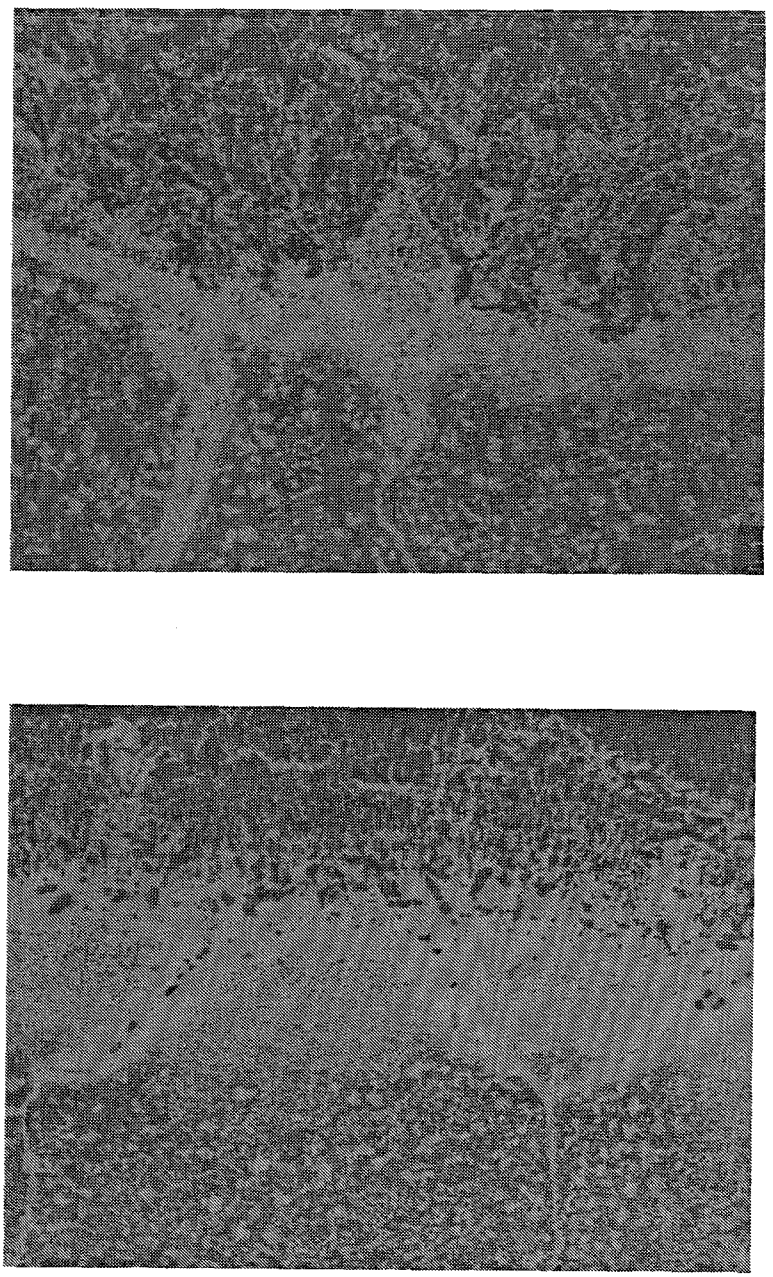

Figure 10. Type 1 Sulfidation on a South American CF6-50 LPT Stage 1 Vane (Etched, 500×).

for subsurface sulfides is illustrated in Figure 11. The scale is rich in Ni and Cr and low in Al, and the γ'-free region of the René 77 is typically depressed in Cr, Al, and Ti.

Pitch-line temperatures for this component are about 890° C at takeoff and 775° C at cruise. At the 80% span, temperatures are perhaps 25° - 50° C lower. It is interesting that the sulfidation rate of about 25 μm/1000 hours from this LPT vane (5.06 hours/cycle) falls in the same low range as that for the Western Europe long-mission HPT blade (Table II). Although conclusions cannot be drawn from a single example, this observation does include the counteracting effects of lower temperature (lower rate) and greater salt retention time (greater effective rate). Also, it should be pointed out that the LPT vane is not coated; therefore, it is more vulnerable to corrosion, at least for Type 1 attack.

U.S. Military

The J79 Stage 1 HPT blades were the least distressed components observed in this study. Detailed examination of 60% and 80% sections failed to reveal sulfides. The maximum distress was observed to be about 25 μm (0.001 inch) at the 80%/80% location; the maximum operating temperature there is estimated to be about 870° C. At this maximum-distress location, where the coating is less than half consumed, the scale is predominantly aluminum oxide and contains small amounts of Ca and Fe derived from the environment. A photograph of this blade and a typical microstructure are shown in Figure 12. (Sulfidation has been detected on other J79 HPT blades occasionally; the one depicted in Figure 12 is not an extreme example as was the case for the other five components in this survey).

Structural and Chemical Analyses

X-ray diffraction identification of $CaSO_4$ in scales has been cited in several instances. The patterns also invariably reveal NiO and a variety of spinel structures that cannot be explicitly identified. These compounds are considered inert and not involved in the hot corrosion process. It should be pointed out that in early stages of life, or relatively benign operating conditions, the scale which forms is nominally pure (and protective) aluminum oxide as described above for the J79 turbine blade. As the source of Al for reformation of this oxide is depleted, either with time or with more severe environmental parameters, the scale which forms becomes mixed with NiO and spinels. Such scales are far less protective; once they form, degradation proceeds at faster rates. The scales analyzed by X-ray diffraction in this study fall in the latter category.

Analyses of water-soluble constituents in deposits on the three duplicate parts identified in Table I are summarized in Table III. Results for inside surfaces are given for one of these. The deposits were removed ultrasonically in distilled water after all outer surfaces were scrubbed.

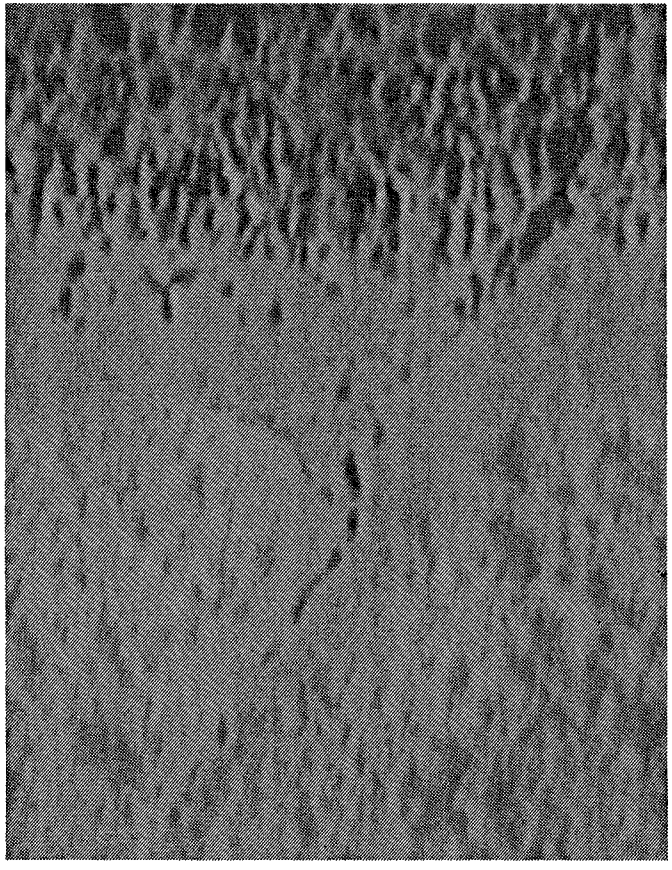

BSE

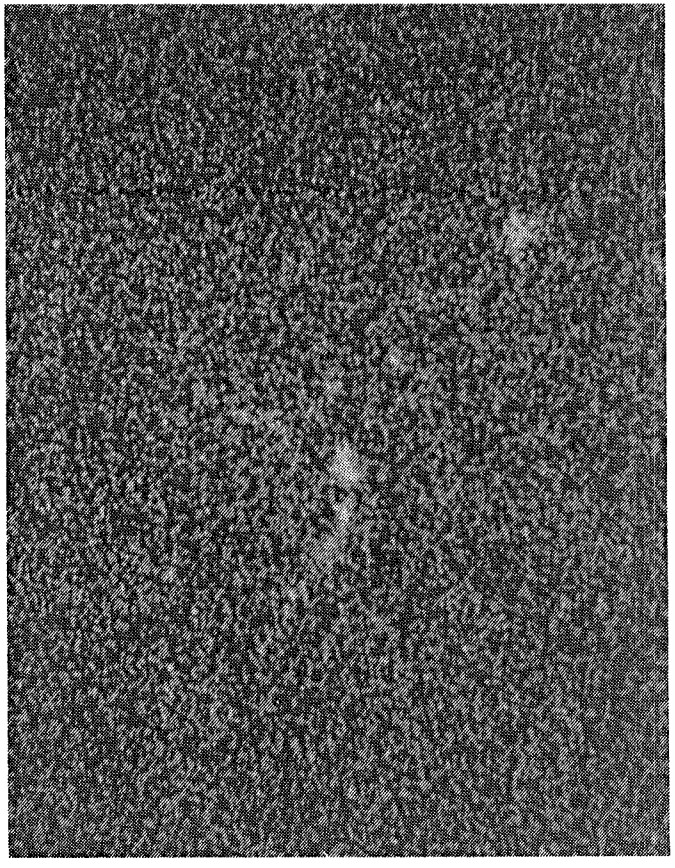

Sulfur

Figure 11. EMP Confirmation of Sulfides in the Subsurface Particles Shown in Figure 10 (2000×).

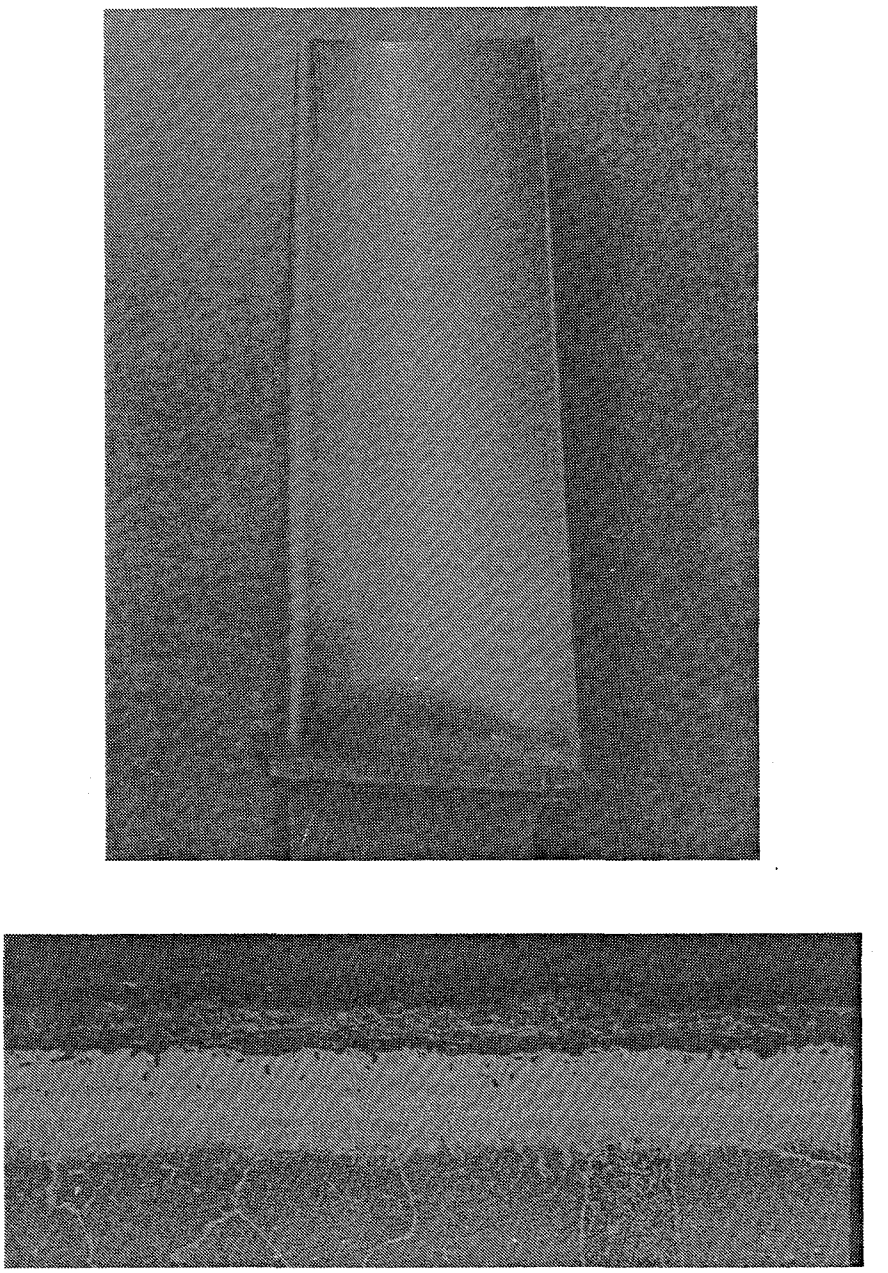

Etched, 200×

Figure 12. U.S. Military J79 HPT Stage 1 Blade Showing Degradation of the Codep Coating at the 80% Location on the Concave Side.

Table III. Analyses of Water-Soluble Deposits on Surfaces of Turbine Components from Field Service.

		Milligrams					
Component	Surface	Na	Ca	Mg	Co	Ni	SO_4
Southern Asia	Concave	0.24	0.32	0.09	0.01	0.01	2.39
Stage 1 HPT	Convex	0.21	0.14	0.09	0.01	0.01	1.93
Blade	Inside	0.25	5.84	0.12	0.01	0.01	40.6
South America	Concave (2)	0.49	0.22	0.18	0.01	0.04	2.65
Stage 1 LPT Vane	Convex (2)	0.48	0.28	0.19	0.04	0.07	3.21
U.S. Military	Concave	0.09	0.02	0.02	0.01	0.01	0.94
Stage 1 HPT	Convex	0.23	0.04	0.06	0.01	0.01	1.12
Blade							

Water-soluble Co and Ni (as sulfates) are formed in Type 2 hot corrosion at temperatures (≦750° C) appreciably lower than the range in which Type 1 hot corrosion occurs. Absence of these species in deposits on the two HPT blades is consistent with the operating temperatures and the Type 1 microstructures observed in metallographic evaluations. On the other hand, these species were found in significant amounts on the surface of the LPT vane which operates at lower temperatures. Apparently, the operating temperatures for this component are borderline; some chemical evidence of Type 2 hot corrosion is found, yet microstructural evidence indicates only Type 1. Details of the differences in these two mechanisms are amply discussed in References 1 and 2.

The other species listed in Table III are derived from the environment, specifically on the runway and at low elevations during takeoff and landing. The roughly equal amounts of these species on the concave and convex surfaces of the two HPT blades are unlike those found in marine engines (where the convex surface generally has far less) and supports the view that observed contamination is ingested during final landing. The larger amounts found internally are to be expected as contaminants accumulate during the use period of the engine. Calcium and magnesium compounds are known to be inert in hot corrosion; in fact, they act as inhibitors. The primary culprit is Na_2SO_4 according to ample evidence. On average, the metallic species listed in Table III account for about two-thirds of the measured sulfate, on a molar basis; possibly some other metals are present in the water-soluble deposits for which analyses were not made. Qualitative analyses detected no significant amounts of chloride. It should also be mentioned that Na was present in amounts too small to be detected by EDAX in metallographic sections, discussed earlier, which were prepared by nonaqueous procedures.

In summary, Type 1 hot corrosion was clearly identified in five of the six components evaluated in this study. Attempts have been made to correlate the extent of such degradation with operating histories. The observed microstructures will be used for comparison with those observed in the burner rig tests designed to induce Type 1 hot corrosion.

TASK II - BASELINE HOT CORROSION TESTS

Testing

All hot corrosion testing in this program was performed at TRW, Inc. in Cleveland, Ohio, using high-velocity (0.3 Mach) burner rigs operating at one atmosphere. In Task II, data on uncoated and coated alloys were obtained to be compared in Task IV with data obtained under the same test conditions, and on the same materials, but with specimens previously subjected to a variety of aging conditions (Task III). Materials for Task II burner rig hot corrosion testing included Udimet 700 and René 80 in the uncoated condition and with the following coatings:

- RT21 aluminide (Chromalloy American Corp.)
- Codep aluminide (General Electric Co.)
- Ni23Co18Cr12Al0.3Y applied by vacuum (low pressure) plasma spraying

The nominal major constituents of the substrate alloys in weight percent were:

- Udimet 700 14.5 Cr, 4.3 Al, 3.4 Ti, 15.0 Co, 4.2 Mo, balance Ni
- René 80 14.0 Cr, 3.0 Al, 5.0 Ti, 9.5 Co, 4.0 Mo, 4.0 W, balance Ni

Heat treatment sequences for these alloys were as follows:

U700	1.	1163° C (2125° F)/4 hours in vacuum/fast cool
	2.	1080° C (1975° F)/4 hours in vacuum/fast cool
	3.	927° C (1700° F)/24 hours in vacuum/fast cool
	4.	760° C (1400° F)/16 hours in vacuum/fast cool
René 80	1.	1093° C (2000° F)/2 hours in vacuum/helium quench
	2.	1052° C (1925° F)/4 hours in vacuum/furnace cool to 649° C (1200° F) in 20 minutes/air quench
	3.	843° C (1550° F)/4 hours in vacuum/air quench

Specimens (Figure 13) were cast slightly oversize and a serial number stamped on the bottom. The series were coded "X" for U700 or "L" for René 80. All specimens were given the first heat treatment and then centerless ground to a 32 AA finish. Top ends were also given a 32 AA finish, and corners were slightly chamferred to minimize the possibility of poor coating integrity.

At this point coatings were applied to a sufficient quantity of specimens for the entire program. For the two aluminides, the coating process fulfilled the function of the second step in the heat treatment; remaining heat treatments were performed, and the specimens were then ready for test. Diameters of each specimen were measured before and after coating.

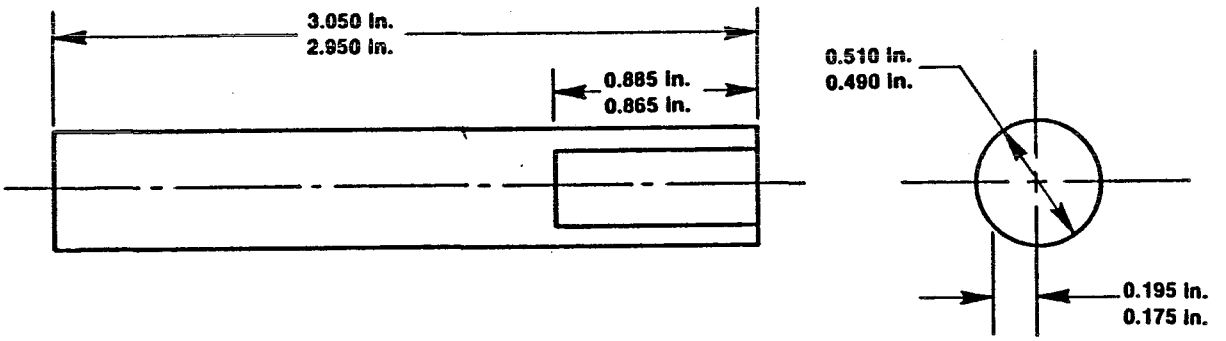

Figure 13. Hot Corrosion Test Specimen.

The plasma-sprayed coatings were applied to a thickness slightly greater than desired. Specimens were given the second heat treatment, which served also to provide a diffusion bond, and subsequent aging as well. The excess coating was then machined-off to give the desired nominal thickness of 0.10 mm (4.0 mils), surface finish 32 AA.

Photographs of typical specimens of all six coating/substrate systems are shown in Figure 14. Photomicrographs are shown in Figure 15; these structures are normal, and the two plasma-sprayed coatings exhibit excellent density. Thicknesses of these coatings, including diffusion zone, are:

Codep/René 80	50 μm
Codep/U700	84 μm
RT21/René 80	81 μm
RT21/U700	79 μm
NiCoCrAlY/René 80	98 μm
NiCoCrAlY/U700	98 μm

The four aluminide-coated systems were analyzed, by quantitative EMP, in a series of five locations in a line normal to the surface, three in the additive layer and one each in the diffusion zone and the substrate alloy. Results for the four systems were reasonably consistent in several respects.

1. Cr, Ti, and Mo are somewhat enriched in the diffusion zone relative to concentrations in the substrate. These elements are present in the additive layer, rather uniform across the thickness, averaging approximately 4%, 1%, and 1% respectively.

2. Cobalt is in the diffusion zone at about the same concentration as in the substrate and is roughly constant across the additive layer at about 2/3 the level in the substrate.

Concentrations of Ni and Al may be considered in terms of compound formation of NiAl. Noting that CoAl can also form and concentration of Co in the

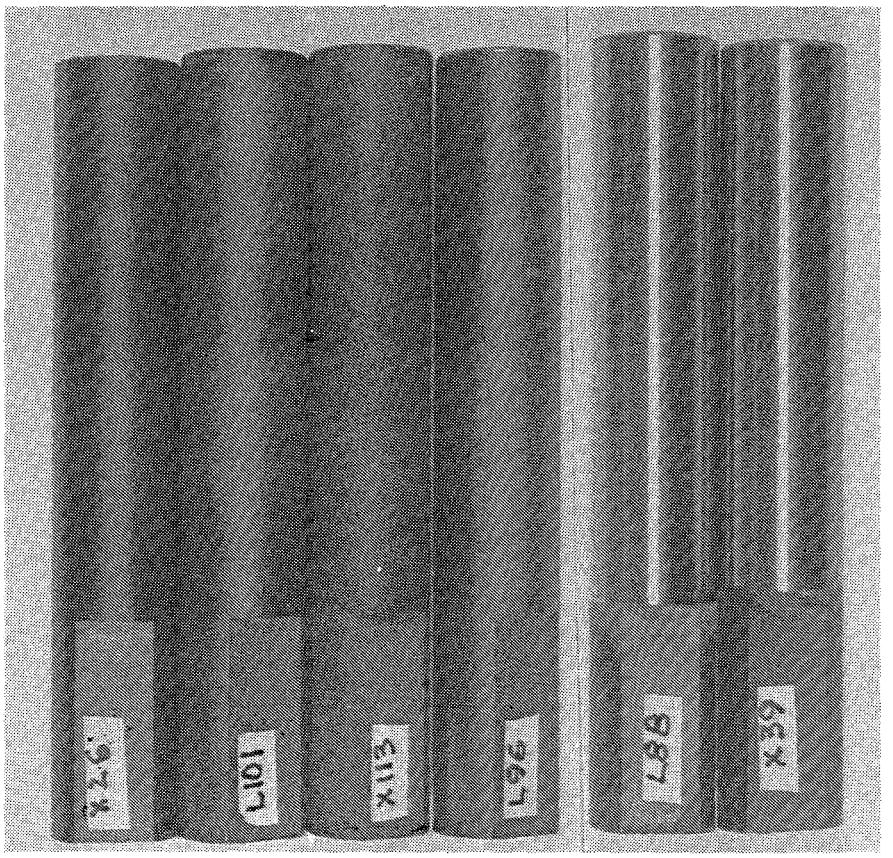

Coating:	Codep	RT21	RT21	Codep	NiCoCrAlY	
Substrate:	U700	René 80	U700	René 80	René 80	U700

Figure 14. As-Coated Burner Rig Specimens of Codep, RT21, and NiCoCrAlY on U700 and on René 80 (1.4×).

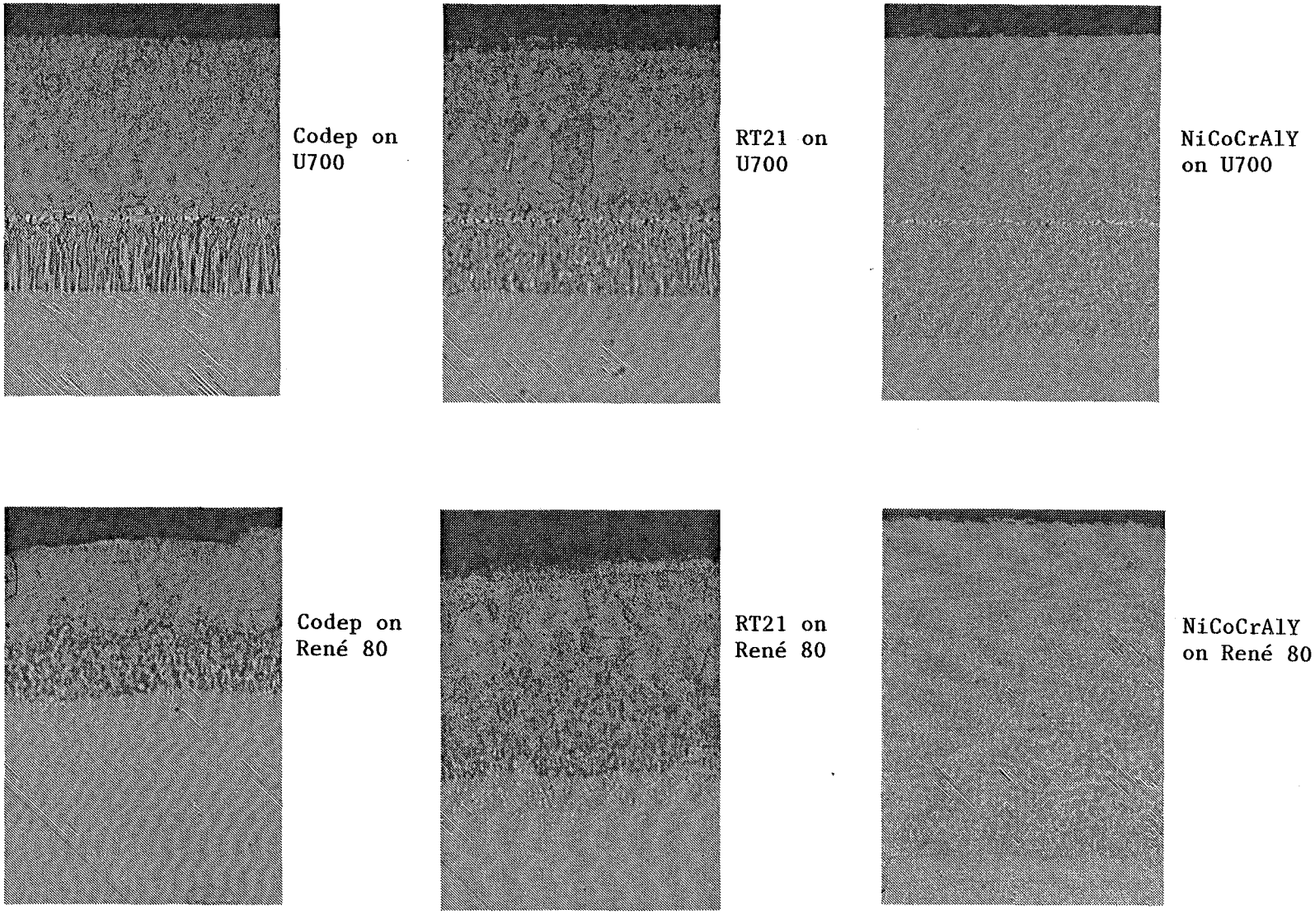

Figure 15. Microstructures of Codep, RT21, and Plasma-Sprayed NiCoCrAlY Coatings on U700 and René 80 (500×).

additive layer is substantial, atomic ratios of Co + Ni/Al were calculated. This ratio averaged approximately 0.80 for the four systems at the outer surface and increased to approximately 0.95 near the diffusion zone.

The above was recorded as baseline information and was available for comparison with EMP measurements on tested specimens.

Burner rigs with rotating specimen holders in test are shown in Figure 16. Testing was performed under the conditions listed in Table IV. Jet A fuel was used with a sulfur content 0.055%, adjusted by addition of ditertiary butyl sulfide. Burner pressure and the throat diameter requirements were achieved by fitting the burners with the specially designed exhaust nozzles shown in Figure 17. These are the same as used in the burner rigs at NASA Lewis in Cleveland, Ohio. The test cycle consisted of 1 hour at temperature followed by a minimum of 6 minutes of forced cooling to ambient temperature.

Table IV. Burner Rig Operating Conditions.

Specimen Temperature	900° C ± 9° C
Test Cycle	1 hour at temperature followed by 6 minutes of forced air cooling
Sodium Concentration	0.5 ppm sodium (± 10%) introduced in the combustion gases as aqueous NaCl
Combustion Air Preheat Temperature	232° C ± 10° C
Specimens	Eight positioned equally on a 4.2 cm (1.64 inch) diameter circle of holder rotating at 600 rpm
Burner Nozzle Throat Diameter	2.54 cm (1.0 inch)
Burner Pressure	1.0 psig
Nozzle Throat to Nearest Specimen	4.45 cm (1.75 inch)

Pertinent burner rig operating parameters were recorded at least twice during each test interval (nominally 20 cycles between inspections). Typical flow rates from combustion air and fuel were 0.91-0.96 standard m^3/minute (32-34 ft^3/minute) and 0.004-0.005 m^3/hr (1.3-1.5 gal/hour) respectively. To ensure continued reliability of the optical pyrometers used for specimen temperature control, specimen temperature was independently measured with a hand-held optical pyrometer. This independent temperature check was used as a rough indicator of gross deviation in calibration of the control optical pyrometer. The control pyrometers were calibrated with the optical pyrometer

1. Burner
2. Specimens on Holder Rotating at 600 RPM
3. Optical Pyrometer
4. Preheated Combustion Air
5. Salt Solution Spray Nozzle

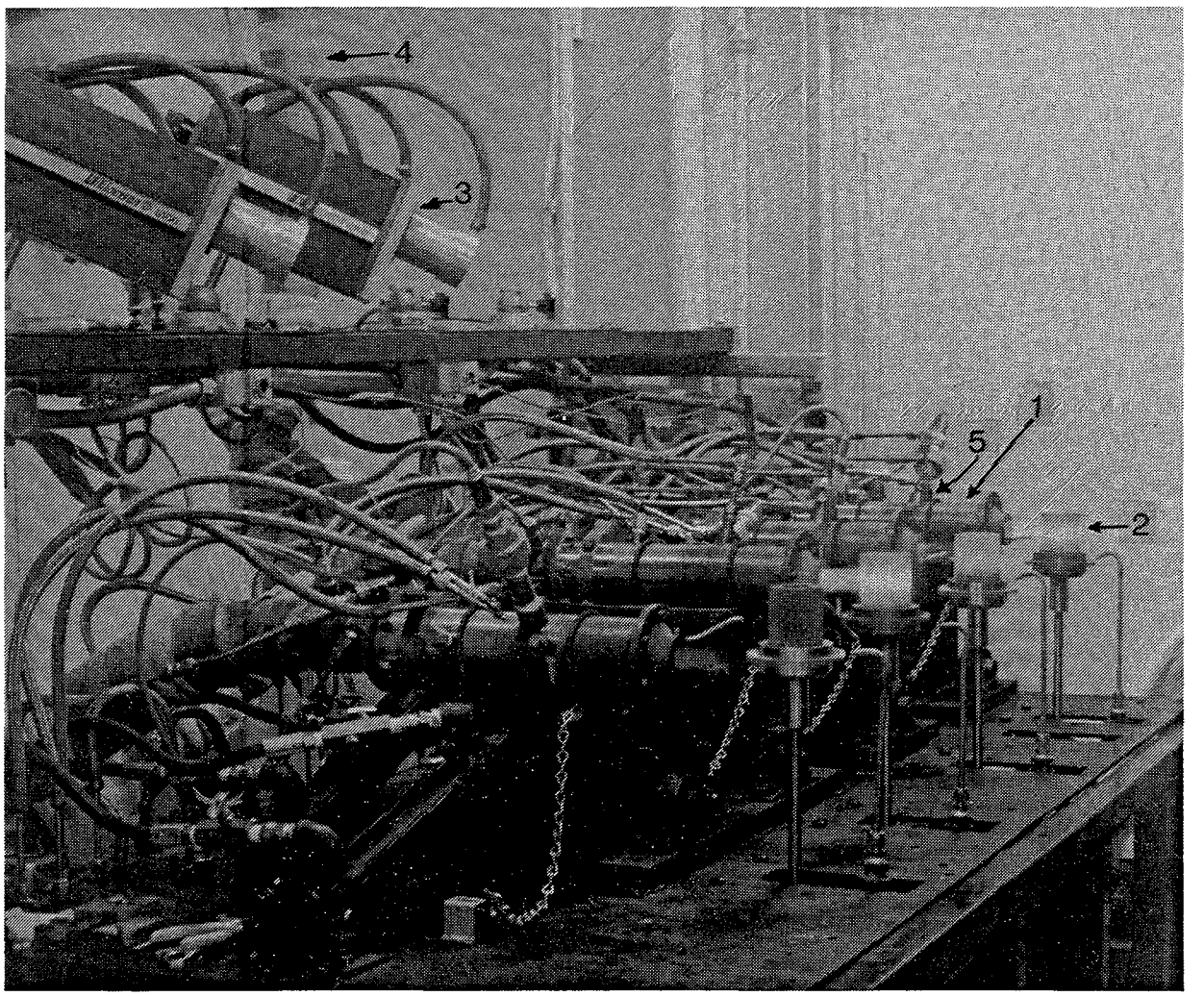

Figure 16. Corrosion Rig Setup.

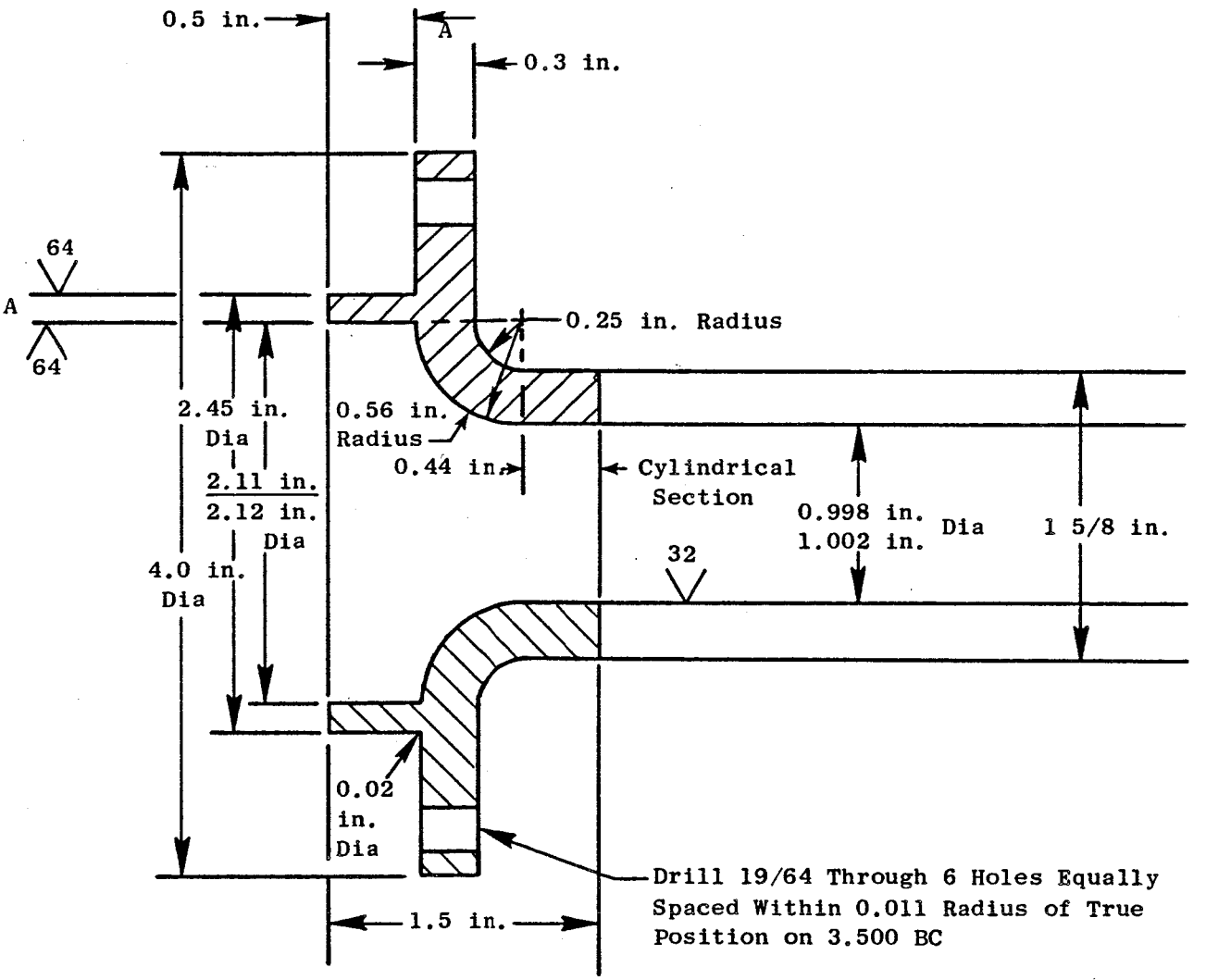

Figure 17. Thin-Wall Convergent Burner Nozzle (MAR-M-302).

calibration setup at NASA Lewis in Cleveland, Ohio. The calibration involved a slip-ring thermocouple arrangement attached to a specimen in a rotating holder.

The sodium in the combustion air was maintained at the specified level of 0.5 ppm by adding salt-water solution in the combustion products. The solution was introduced in the combustion air in the form of atomized spray. Figure 18 shows the salt solution spray nozzle.

The test plan included duplicate specimens, randomly distributed between two burner rigs, of U700 and René 80 uncoated and coated with RT21, Codep, or NiCoCrAlY. Specimens were removed at approximately 20-cycle intervals for inspection (in practice about 18 to 24 cycles). When visual evidence of hot corrosion was apparent at three successive inspections, the testing of that specimen was discontinued. Each specimen was photographed at each inspection. The plan also included testing of single specimens of each material for time periods of 100, 300, and 500 hours, if these time periods did not exceed 2/3 the time the original specimens of the same material were exposed. Thus, for a material that was not removed until at least 750 hours for visual reasons, the test provided evaluation of the extent of corrosion at four different time intervals.

Posttest specimens were evaluated by means of traditional destructive techniques used in Task I. In addition, this program provided an opportunity to extend the pioneering studies at NASA Lewis Research Center in which the progress of hot corrosion (or oxidation) is monitored, nondestructively, by measuring at each inspection interval the high-frequency inductance of a coil with the subject test specimen at the core (Reference 3).

Under carefully controlled conditions, noting that at high frequencies only the outer surface of the metallic core will influence the measurement, coil inductance can respond either to a change in metallic core volume (metal converted to oxide scale) or to a change in the composition of the metallic surface (formation of a depletion zone within the alloy as scale forms). In either event, results from such measurements afford high sensitivity in non-destructively following changes that occur during environmental degradation.

Coil inductance measurements were made with the burner rig specimens positioned in a coil (Figure 19) such that the center of the flame impingement zone, 2.5 cm from the top of the specimen, was in the center of the coil. Measurements were made in series mode with a multifrequency LCR meter (Figure 20) at a frequency of 10 MHz. At least two measurements were taken with each specimen core. For each measurement, the specimen was removed from the coil and replaced randomly to average the core/coil axial alignment.

Results

Test information and the metallographic measurements are summarized in Table V. Of the seven specimens that were in test for the full 1000 hours, the two that exhibited breach of coating did not in fact show visual evidence

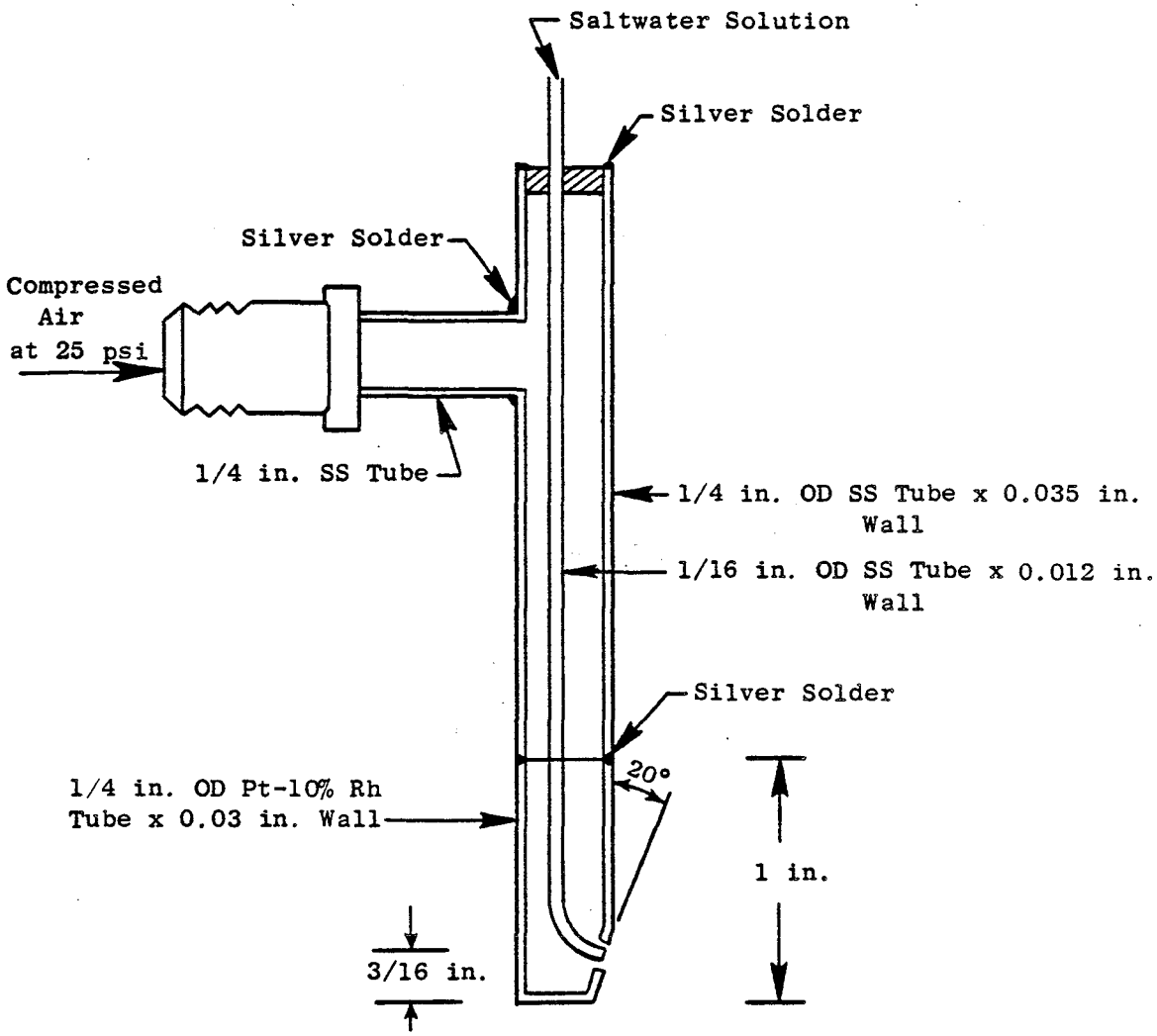

Figure 18. Salt Solution Spray Nozzle.

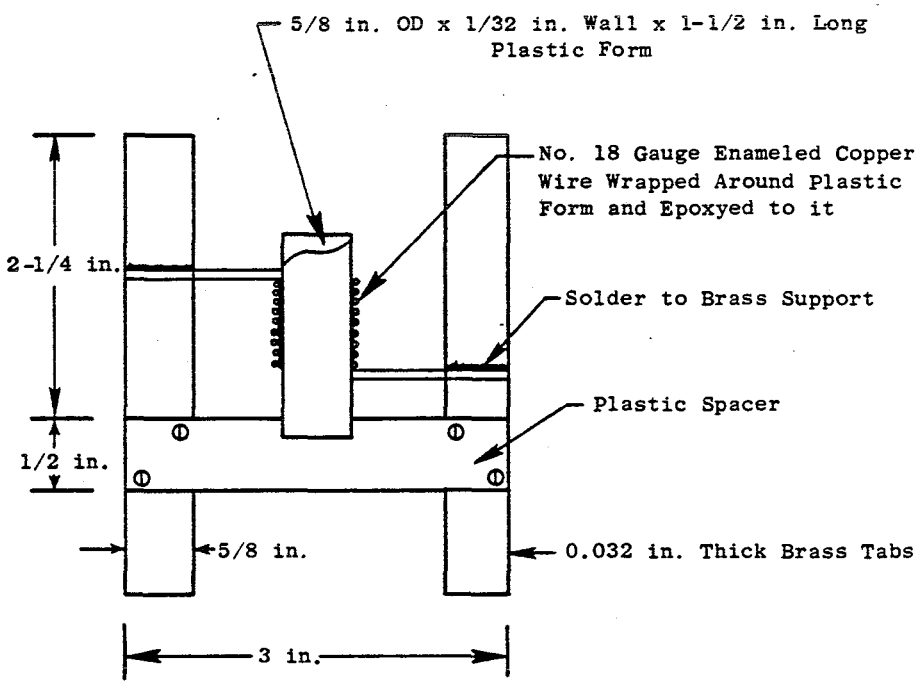

Figure 19. Inductance Coil and Support.

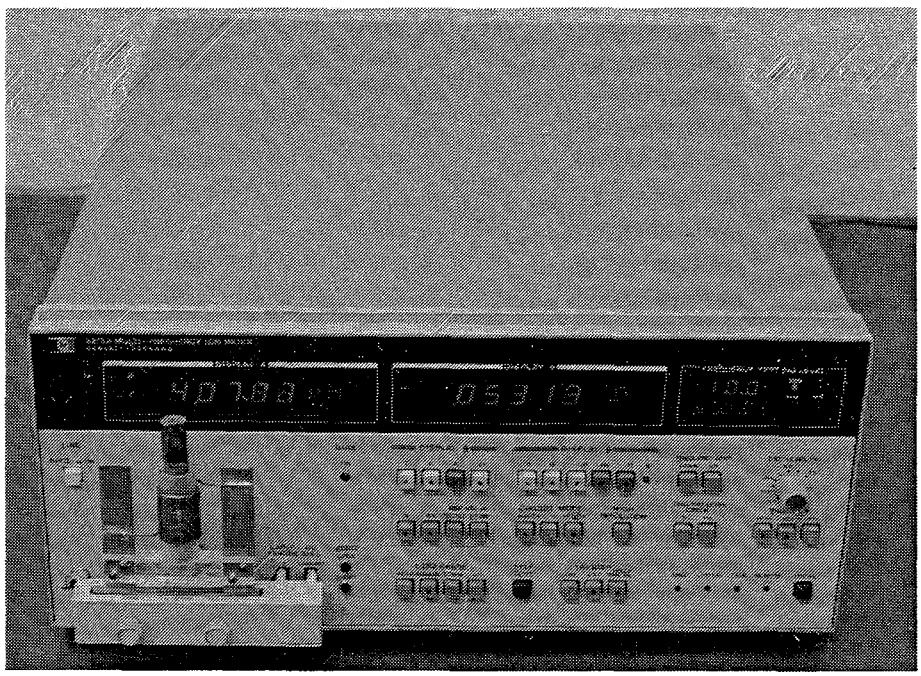

Figure 20. Inductance Rig/Coil with Specimen Core.

Table V. Test Information and Metallographic Measurements for Specimens Removed from Task II Burner Rig Hot Corrosion Test.

Code*	Alloy	Coating	Hours	Initial Coating Thickness, μm	Coil Inductance Change, μH	Maximum Corrosion Attack, μm
X3	U700		143		0.315	**
X19	U700		158		0.259	**
X108	U700		106		0.230	**
						(See Table VI)
L54	René 80		163		0.204	**
L77	René 80		168		0.186	**
L99	René 80		104		0.087	**
X14	U700	Codep	602	84	0.012	285**
X8	U700	Codep	425	84	0.017	40**
X22	U700	Codep	299	84	0.007	235**
X50	U700	Codep	99	84	-0.005	30
L3	René 80	Codep	528	50	0.034	250**
L7	René 80	Codep	439	50	0.023	40**
L12	René 80	Codep	297	50	0.022	130**
L110	René 80	Codep	103	50	0.016	25
X73	U700	RT21	1005	79	-0.005	95
X66	U700	RT21	997	79	0.000	10**
X104	U700	RT21	296	79	-0.001	15
X114	U700	RT21	97	79	-0.004	10
L36	René 80	RT21	1005	81	0.016	20**
L44	René 80	RT21	697	81	0.012	180**
L8	René 80	RT21	300	81	-0.020	10
L106	René 80	RT21	101	81	-0.017	10
X56	U700	NiCoCrAlY	1005	98	0.005	70
X30	U700	NiCoCrAlY	997	98	0.010	100
X79	U700	NiCoCrAlY	471	98	0.003	10
X65	U700	NiCoCrAlY	299	98	0.002	10
X131	U700	NiCoCrAlY	139	98	0.006	10
L41	René 80	NiCoCrAlY	1005	98	0.002	35**
L9	René 80	NiCoCrAlY	997	98	0.004	70
L49	René 80	NiCoCrAlY	528	98	0.006	30
L128	René 80	NiCoCrAlY	153	98	0.005	25
L133	René 80	NiCoCrAlY	101	98	0.002	20

* The first two entries for each materials system were tested to full term: two 20-hour cycles after first visual evidence of corrosion (or 1000 hours). Other specimens were tested for fractional times.

** Visual evidence of hot corrosion.

of hot corrosion. Of the other five not showing breach of coating, three had been visually judged as indicating hot corrosion. These discrepancies point up the dual problem in evaluation, particularly for coated specimens for which corrosion is frequently localized:

- It is difficult to capture localized pits in a single planar section. Conceivably, specimens that show visual evidence of hot corrosion have sites elsewhere where pitting has taken place down to the coating/substrate interface.

- Visual evidence of hot corrosion of a coated specimen generally is not apparent until the more rapidly corroding substrate at the site of a pit causes an eruption of scale.

Note that for several Codep-coated and RT21-coated specimens corrosion proceeded considerably into the substrate alloy (see Table V). This is a consequence, in part, of the criterion that a specimen be tested for two more 20-cycle periods after visual evidence of corrosion is detected. For coated specimens, visual evidence nominally coincides with coating penetration.

These uncertainties, of course, also apply to the other coated specimens. Nevertheless, it is clear that the RT21-coated specimens on average performed better than the Codep-coated specimens. Based on EMP analyses and additional evaluation, no significant compositional differences exist between the two coatings, and both have the structural features of inward aluminide coatings. On the other hand, the RT21 coating shows evidence of entrapment of small oxide particles in the outer 5 μm, while the Codep coating does not. Whether this is the cause of differences in hot corrosion lives cannot be concluded with certainty, but it may be noted in anticipation of results from Task IV testing that no consistent difference exists for specimens preaged at 1100° C.

Figure 21 indicates another difference between these two coatings. The accumulative coil-inductance changes for seven individual Codep-coated and RT21-coated specimens are shown, together with an average curve for four specimens coated with NiCoCrAlY. The time scale below 200 hours is expanded to show clearly the negative changes that appeared at the first inspection for the aluminide-coated specimens. These are considered real, inasmuch as the NiCoCrAlY-coated specimens showed a much smaller change; for these, the small changes as a function of time may represent normal scatter in measurements. Note that all four of the Codep-coated specimens show greater and faster increases which parallel the metallographic observations.

In all instances, Type 1 sulfidation was clearly present in RT21-coated or Codep-coated specimens, either within the coating or in a γ'-depleted region in the underlying alloy where the coating was breached. Typical microstructures are shown in Figure 22. X-ray oscillographs on several specimens showed the oxide scale to be aluminum rich with lesser amounts of Cr and Ti nonuniformly distributed.

The NiCoCrAlY coating is considerably more resistant to hot corrosion. Complete penetration was noted in only one of the four full term 1000-hour

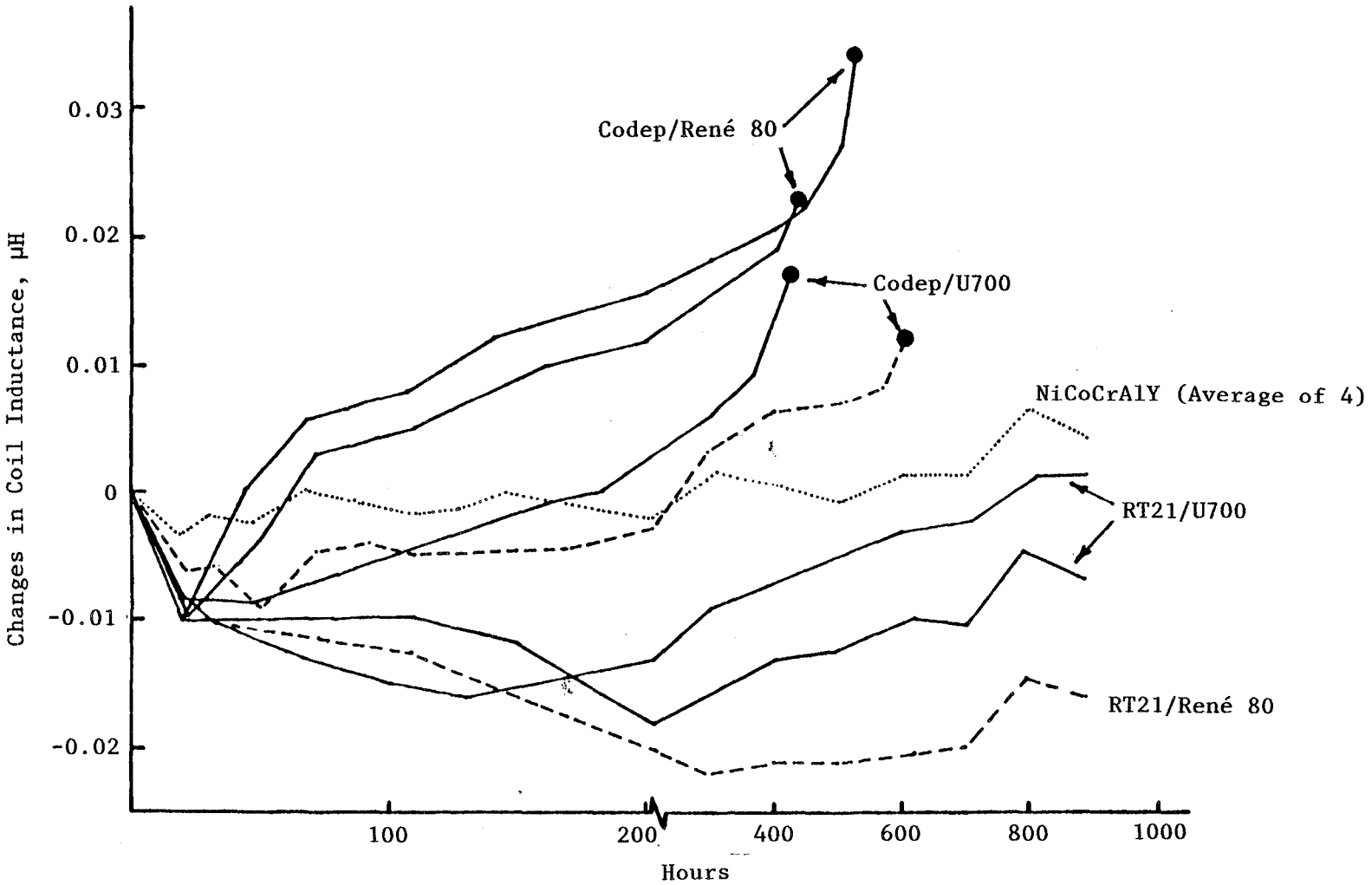

Figure 21. Changes in Coil Inductance with Hot Corrosion at 900° C, Cyclic Exposure.

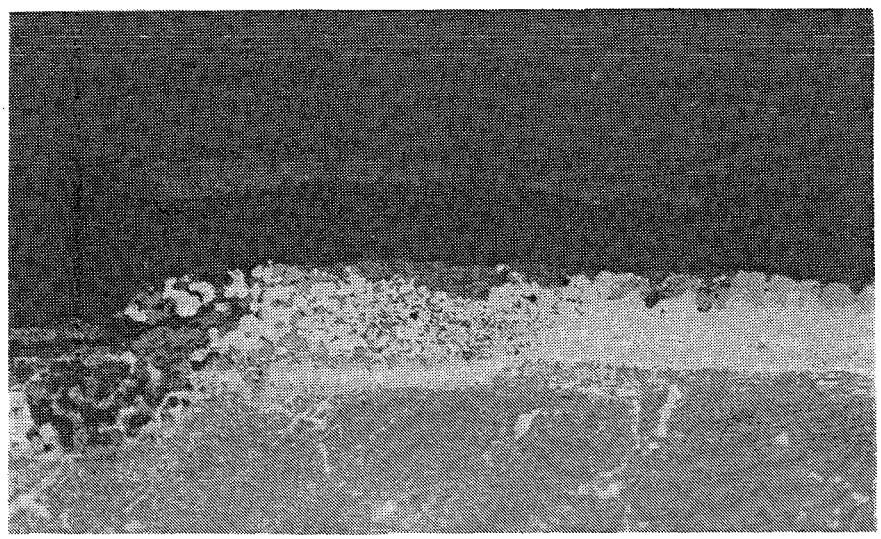

RT21/René 80, 697 Hours

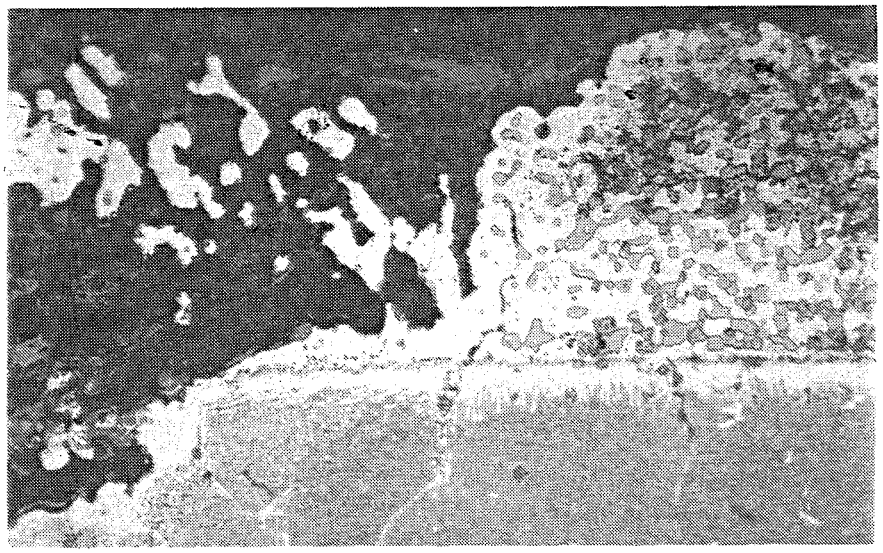

Codep/U700, 602 Hours

Figure 22. Photomicrographs from Burner Rig Hot Corrosion Tests at 900° C; Type 1 Sulfides are Present (Etched, 200×).

specimens. A series of three typical microstructures, depicting the progress of hot corrosion with time, is shown in Figure 23. The development of a substantial depleted layer at full term is shown, determined by EMP analysis to be primarily a loss of Cr down to about half of the nominal 18%. There was a corresponding increase in Ni but only a small decrease in Al. Type 1 sulfides could not be visually identified in the depletion zone as might have been expected, and this was confirmed by X-ray oscillographs. However, sulfur was found in local regions of scale deep within pits, primarily associated with Cr. Most of the scale was Al and Ti rich and devoid of sulfur.

With respect to uncoated specimens, corrosive attack is generally deeper than with coated specimens and is not localized; that is, corrosion occurs continuously around the entire circumference. Thus, the location of the original surface cannot be identified, which means that a reliable measurement of "maximum depth of penetration" is not possible. As an alternative, area measurements with the Leitz TAS-Plus Image Analyzer were used for these specimens. For each specimen, two measurements were made on etched mounts:

- Area of unaffected metal (base of the γ'-depleted layer).
- Area at the metal/scale interface.

These measurements were converted to average radius values and compared with pretest dimensions (see Table VI). Although these average values represent nonuniform corrosion, comparison with coil-inductance changes is appropriate. A real correlation is difficult for the following three reasons:

1. Coil inductance changes reflect compositional changes in the outer layer of metal as well as cross section changes.
2. Neither coil-inductance change nor corrosion is a linear function of time; a substantial fraction of the total coil-inductance change occurs during the corrosion incubation period (Figure 24).
3. The extent of corrosion observed metallographically is measured in a plane, but the coil inductance reflects total corrosion over the length of the specimen within the coil.

The extent of corrosion increases with time, as expected, and René 80 is about twice as resistant to corrosion as U700, also predictable from previous extensive burner rig studies and field experience. The depletion zone in all specimens showed expected Type 1 sulfidation (Figure 25), amply demonstrated with X-ray oscillographs. Scales were typically Al rich with lesser amounts of Ti and Cr.

As further documentation of these burner rig tests, salt accumulation (Na_2SO_4) was measured on several specimens. Results are given in Table VII. Rate of accumulation is essentially constant to 439 hours but is less for the 1004-hour specimens. This may reflect mechanical instability of the salt deposit (spallation) above a certain thickness. The alternate explanation

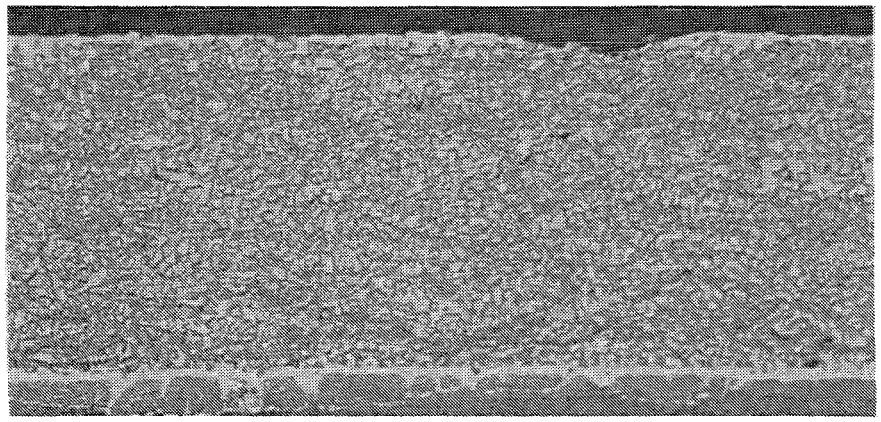

U700, 299 Hours

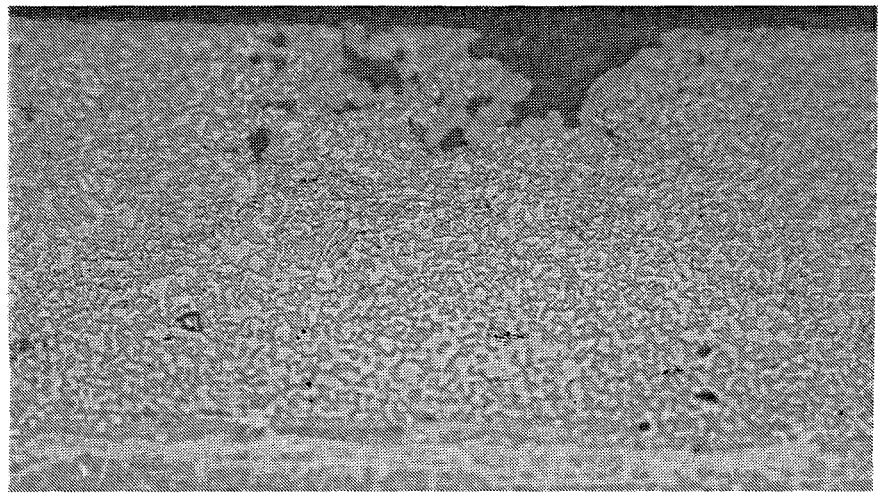

René 80, 528 Hours

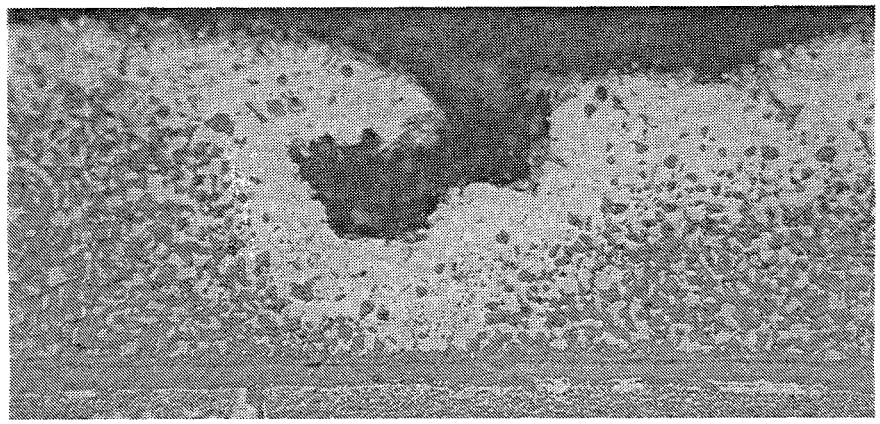

U700, 997 Hours

Figure 23. Photomicrographs of NiCoCrAlY Coated Specimens from Hot Corrosion Burner Rig Test at 900° C Showing Progressive Degradation with Time (Etched, 500×).

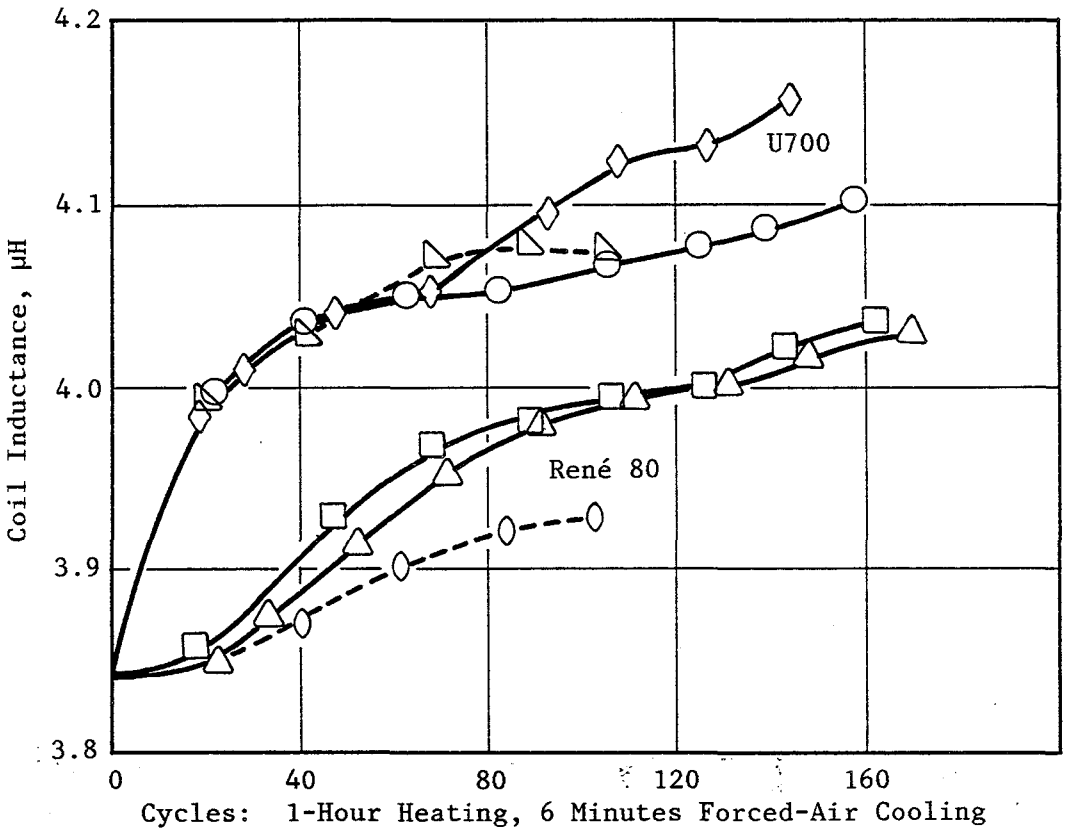

Figure 24. Uncoated Alloy Coil Inductance Changes with Hot Corrosion at 900° C, Cyclic Exposure.

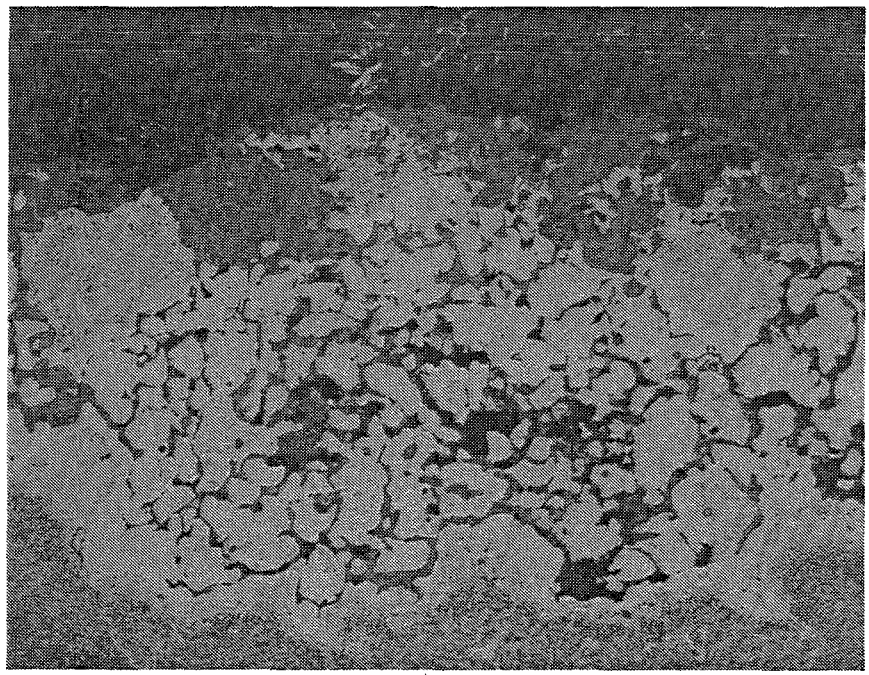

U700, 143 Hours

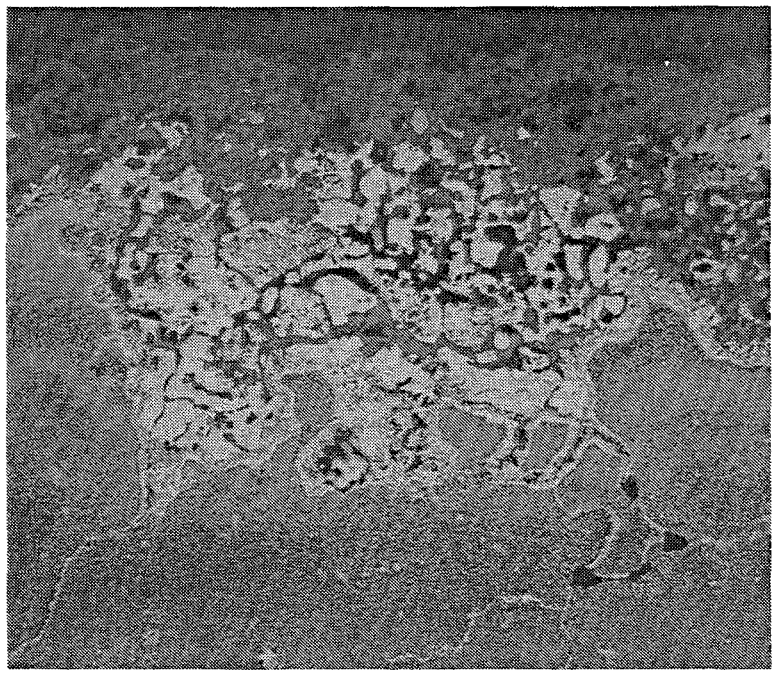

René 80, 168 Hours

Figure 25. Photomicrographs of Specimen from Burner Rig Tests; Type 1 Sulfides are Present (Etched, 200×).

Table VI. Average Corrosion (μm) of Uncoated Specimens from Task II Burner Rig Tests Based on Cross Section Area Measurements.

Code	Alloy	Hours	Coil Inductance Change, μH	Metal Loss	Depletion Zone	Total Affected Metal
X19	U700	158	0.259	310	45	355
X21*	U700	148	0.270	360	80	440
X3	U700	143	0.315	265	100	365
X108	U700	106	0.230	100	50	150
L77	René 80	168	0.186	100	80	180
L54	René 80	163	0.204	110	90	200
L99	René 80	104	0.087	40	35	75

* Dummy specimen, not in original test plan.

Table VII. Na_2SO_4 Accumulation on Task II Burner Rig Test Specimens.

Specimen Number	Test Time, Hours	Na, mg	Na_2SO_4	
			mg/cm^2	mg/cm^2 100 Hours
L77	168	8.3	1.28	0.76
X19	158	7.9	1.22	0.78
L7	439	22.8	3.51	0.80
X8	425	20.9	3.22	0.76
X73	1005	27.9	4.30	0.43
L36	1005	27.7	4.28	0.43
L41	1005	23.9	3.69	0.37

that the salt flux was lower in the latter part of the test may be discarded since several short-term dummy specimens exposed at various times after the initial 438-hour point exhibited deposition rates typical of the earlier specimens.

TASK III - AGING TREATMENTS

Treatment

The purpose of this Task was to prepare specimens for subsequent hot corrosion testing (Task IV) in which the coating composition had been altered by heat treatment at 1100° C in either inert or oxidizing environments. This induces coating/substrate interdiffusion with and without surface oxidation. Each treatment was employed on triplicate specimens of all six coating/substrate systems tested in Task II. Cyclic treatments involved 1-hour cycles with inspection at 20-cycle intervals. Treatment conditions were as follows:

- Cyclic, Static Air — 100 hours
- Cyclic, Burner Rig — 100, 300, 600 hours
- Isothermal, Static Air — 100, 300, 600 hours
- Isothermal, Vacuum — 100 hours

For the burner rig exposures, specimens were randomly distributed among four rigs. Weight and coil-inductance measurements were made before and after heat treatment and at intermediate inspections for cyclic exposures. One of each group of three was sectioned for metallographic measurement; the other two were retained for hot corrosion testing in Task IV.

Results

There were two somewhat unexpected results:

1. The vacuum heat treatment caused substantial weight losses, suggesting volatilization (presented in Table VIII). These losses were selective, as confirmed by the appearance of a thin layer (5-10 μm) in the sectioned NiCoCrAlY-coated specimens in which Cr was down to 7% from the nominal 18%.

2. In the burner rig exposures, very localized pitting on the back side of the NiCoCrAlY-coated specimens developed; consequently, those intended for 600-hour exposures were removed at times ranging from 352 to 420 hours when visual examination suggested coating penetration. Figure 26 is a photomicrograph showing the localized features of this degradation. Another specimen that showed coating penetration (U700, 380 hours) was carefully examined for sulfides as an indication of salt contamination; none were found. Also, if the temperature was significantly higher on the back side, the Codep and RT21 coatings presumably would have failed locally; this did not happen. There is as yet no explanation why the NiCoCrAlY coatings exhibited such nonuniform oxidation in contrast to Codep and RT21. (Note the NiCoCrAlY-coated specimens exposed for the full 600 hours under static conditions showed a very thin, coherent, alumina scale but essentially no metal loss. See Figure 27).

Table VIII. Weight Changes and Coil Inductance Changes for Task III Specimens.

Material	Test Condition	100 Hours		300 Hours		600 Hours	
		mg	μH	mg	μH	mg	μH
Codep/U700	One-hour cyclic	12 (99) *	0.0200	16 (306)	0.0280	12 (477)	0.0265
RT21/U700	burner rig results	12 (99)	0.0192	12 (306)	0.0347	5 (482)	0.0275
NiCoCrAlY/U700	for single speci-	12 (99)	0.0042	-17 (291)	0.0116	2 (380)	0.0106
Codep/René 80	mens selected for	13 (99)	0.0246	14 (306)	0.0264	1 (357)	0.0316
RT21/René 80	metallographic	12 (99)	0.0106	14 (306)	0.0197	7 (482)	0.0216
NiCoCrAlY/René 80	evaluation.	14 (99)	0.0084	12 (291)	0.0086	16 (420)	0.0093
Codep/U700	Isothermal furnace	9	0.0174	36	0.0227	37	0.0290
RT21/U700	oxidation, average	8	0.0173	27	0.0204	27	0.0310
NiCoCrAlY/U700	results for	10	0.0017	7	0.0056	21	0.0096
Codep/René 80	triplicate	16	0.0212	25	0.0266	27	0.0347
RT21/René 80	specimens.	10	0.0059	25	0.0161	19	0.0241
NiCoCrAlY/René 80		14	0.0021	-27	0.0064	-93	0.0107
Codep/U700	One-hour cyclic	15	0.0229				
RT21/U700	furnace oxidation,	13	0.0225				
NiCoCrAlY/U700	average results	9	0.0058				
Codep/René 80	for triplicate	26	0.0264				
RT21/René 80	specimens.	15	0.0236				
NiCoCrAlY/René 80		-2	0.0059				
Codep/U700	Isothermal vacuum,	-41	0.0190				
RT21/U700	average results	-57	0.0170				
NiCoCrAlY/U700	for triplicate	-84	0.0017				
Codep/René 80	specimens.	-107	0.0211				
RT21/René 80		-89	0.0154				
NiCoCrAlY/René 80		-105	0.0051				

* ( ) = Actual test hours.

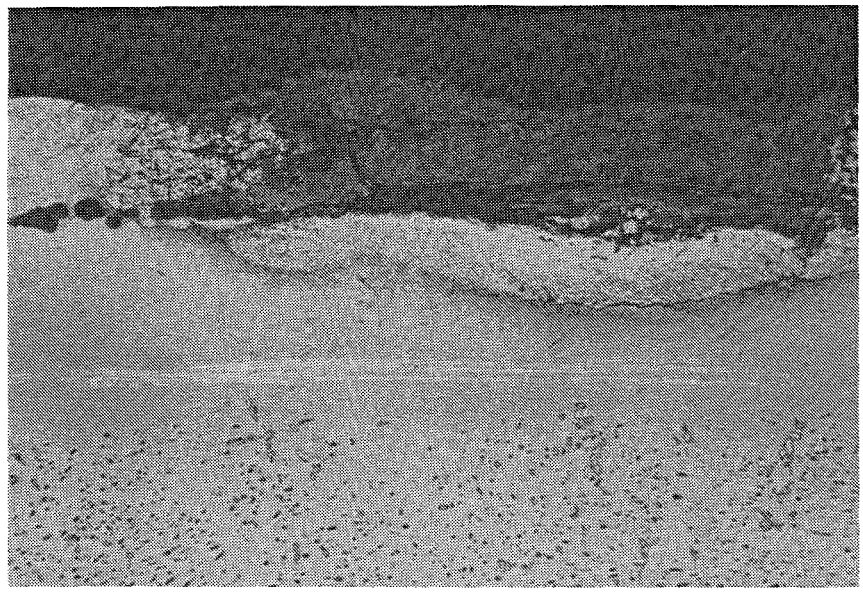

Figure 26. NiCoCrAlY Coated U700 Specimen Showing Localized Attack on Back Side after 291 Hours at 1100° C Burner Rig Cyclic Oxidation (200×).

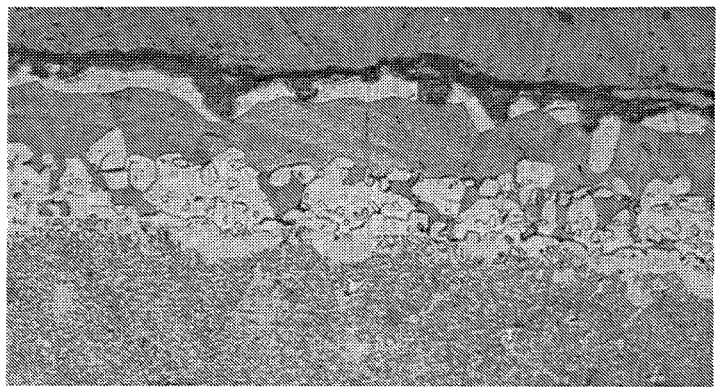

RT21/René 80

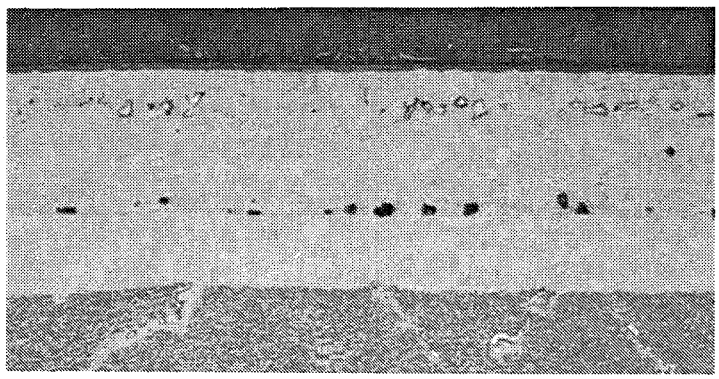

NiCoCrAlY/René 80

Figure 27. RT21 and NiCoCrAlY Coatings after 600 Hours of Isothermal Oxidation at 1100° C (Etched, 200×).

The Codep-coated and RT21-coated specimens also showed visual evidence of coating penetration at far less than 600 hours in the burner rig, and those planned for the full exposure were removed at times ranging from 357 to 488 hours. However, the site of initial failure was at the back of the specimen in only a few instances.

In general, oxidation was fairly uniform around the circumference, rather scalloped, though somewhat more on the back side. Typical microstructures are shown in Figure 28. In one instance, local coating failure was confirmed in only 99 hours for a RT21-coated René 80 specimen (Figure 29). Although this failure occurred on the back side of the specimen, it was considerably removed from the 180° location at or near which all of the NiCoCrAlY-coated specimens showed localized degradation.

Even for specimens aged in static air, there was evidence of occasional localized degradation for all three coatings. Specific observations and maximum-penetration measurements for all sectioned specimens are deferred to the Task IV discussion since this information directly relates to coating life in the subsequent hot corrosion test. Typical microstructures for the RT21 and NiCoCrAlY coatings after 600 hours of isothermal oxidation at 1100° C are shown in Figure 27 for typical regions. For the RT21 coating, the scattered, light phase at the outer surface is γ' resulting from decreased Al content. In the diffusion zone, separation of carbides and/or intermetallics has occurred. These changes are visible but much less so after 100 and 300 hours. The voids shown at the NiCoCrAlY/substrate interface are typical of all the aged specimens with this coating.

Also of use in Task IV are the results of electron microprobe (EMP) examination. Selected quantitative analyses are summarized in Table IX together with X-ray oscillograph observations on several scales. Included for comparison are results obtained previously for as-fabricated specimens. All of these values are averages of several analyses at different depths within the bulk coating, that is, neglecting the diffusion zone and the region near the outer surface. (For three NiCoCrAlY-coated specimens, analyses for Cr and Al just beneath the scale are included.) Composition changes are substantial, notably caused by inward diffusion of Al and outward diffusion of substrate elements. Of particular interest is the similarity of air and vacuum exposed specimens; composition changes due to interdiffusion dominate over those resulting from oxidation.

In addition to the above metallographic and EMP observations, weight changes and coil-inductance changes were recorded. These are summarized in Table VIII. The latter for cyclic exposure, both in the burner rig and under static conditions, are shown in Figures 30 and 31. There were no negative changes at the first inspection as previously noted for coated specimens in the Task II hot corrosion test at 900° C (Figure 21).

Further comments are required with respect to the weight changes in Table VIII. Since Codep and RT21 are pack cementation coatings, they covered the entire surface of the specimen. For these specimens, weight changes were progressively positive with time and did not suggest scale spallation except

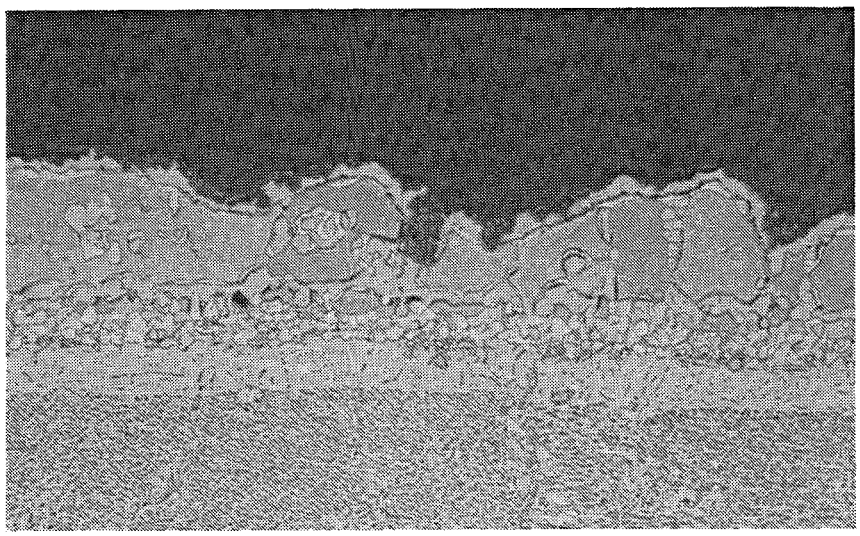

200×

Note local irregularities but generally uniform degradation.

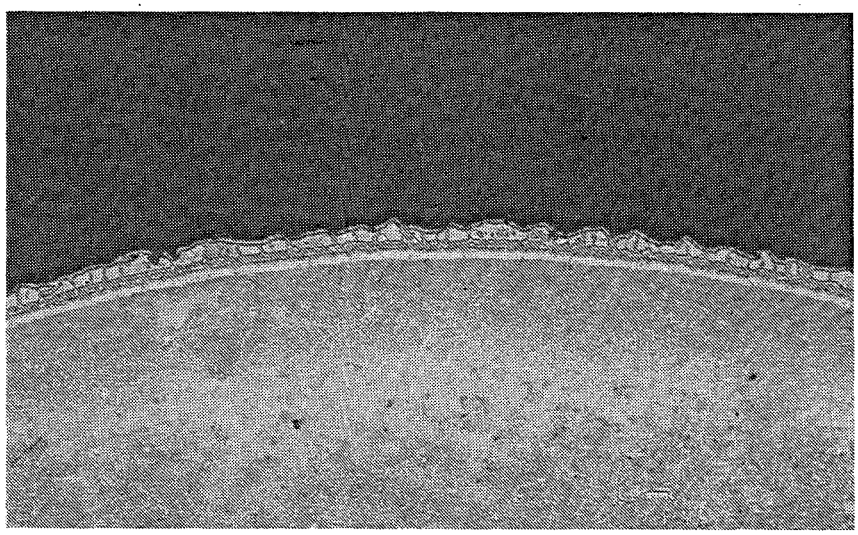

32×

Figure 28. Codep Coated U700 Specimen after 477 Hours at 1100° C in Burner Rig Cyclic Oxidation.

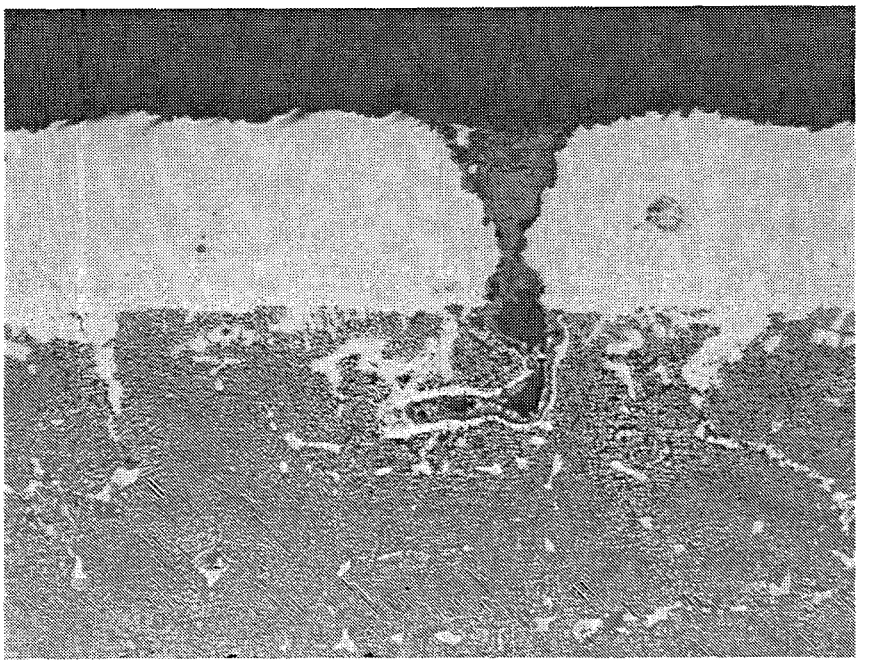

Figure 29. RT21 Coated René 80 Specimen Showing Localized Coating Failure after 99 Hours at 1100° C in Burner Rig Cyclic Oxidation (Etched, 200×).

Table IX. Electron Microprobe Analyses of Coatings Before and After Various Aging Treatments at 1100° C.

Code	Alloy	Coating	Aging Conditions	Weight Percent									
				Bulk Coating							Outer Layer		
				Ti	Cr	Co	Ni	W	Al	Mo	Al	Cr	Scale
L96	René 80	Codep	None	0.7	5.0	6.5	52.0	0.9	32.0	0.8			
L101	René 80	RT21	None	0.4	3.5	6.0	52.0	0.0	32.0	0.4			
L103	René 80	RT21	100 Hour Vacuum	4.0	7.5	9.3	61.0	0.1	18.0	0.3			
L94	René 80	Codep	100 Hour Vacuum	3.7	6.5	9.4	64.0	0.1	17.0	0.4			
L125	René 80	Codep	100 Hour Cyclic	3.6	6.3	8.5	63.0	0.5	17.0	0.3			(1)
X26	U700	Codep	None	0.8	3.8	10.6	52.0	---	32.0	0.6			
X113	U700	RT21	None	0.5	3.0	10.4	50.0	---	31.0	0.3			
X123	U700	RT21	100 Hour Vacuum	3.1	6.7	12.4	61.0	---	17.0	0.6			
X130	U700	Codep	100 Hour Cyclic	2.5	6.7	11.0	61.0	---	18.0	0.5			(1)
X87	U700	RT21	99 Hour Burner Rig	3.0	7.7	11.8	60.0	---	17.0	1.0			
L88	René 80	NiCoCrAlY	None	0.2	20.1	18.8	43.0	---	13.0	---			
L111	René 80	NiCoCrAlY	100 Hour Vacuum	1.7	14.4	18.7	53.0	0.4	11.0	0.7	17	7	
L37	René 80	NiCoCrAlY	100 Hour Cyclic	1.8	15.4	17.4	55.0	0.5	12.0	0.0			(2)
L57	René 80	NiCoCrAlY	600 Hour Isothermal	2.5	18.8	16.1	54.0	1.2	7.8	1.3			(2)
L5	René 80	NiCoCrAlY	99 Hour Burner Rig	1.8	16.2	17.2	54.0	0.6	10.7	1.2	9	21	(2)
X39	U700	NiCoCrAlY	None	0.4	20.0	20.9	44.0	---	12.0	---			
X34	U700	NiCoCrAlY	100 Hour Cylic	1.4	15.6	19.4	54.0	---	14.0	0.2			(2)
X48	U700	NiCoCrAlY	600 Hour Isothermal	2.2	16.7	18.6	54.0	---	7.5	1.9			(2)
X13	U700	NiCoCrAlY	99 Hour Burner Rig	1.8	15.1	18.6	54.0	---	11.6	0.4	9	18	(2)
X15	U700	NiCoCrAlY	291 Hour Burner Rig	2.6	17.1	18.9	55.0	---	7.4	1.9			(3)

(1) Coherent Al_2O_3 scale with scattered Ti, especially at pits.
(2) Coherent Al_2O_3, no Ti.
(3) In pit, high Al, Ti with scattered Cr, Y.

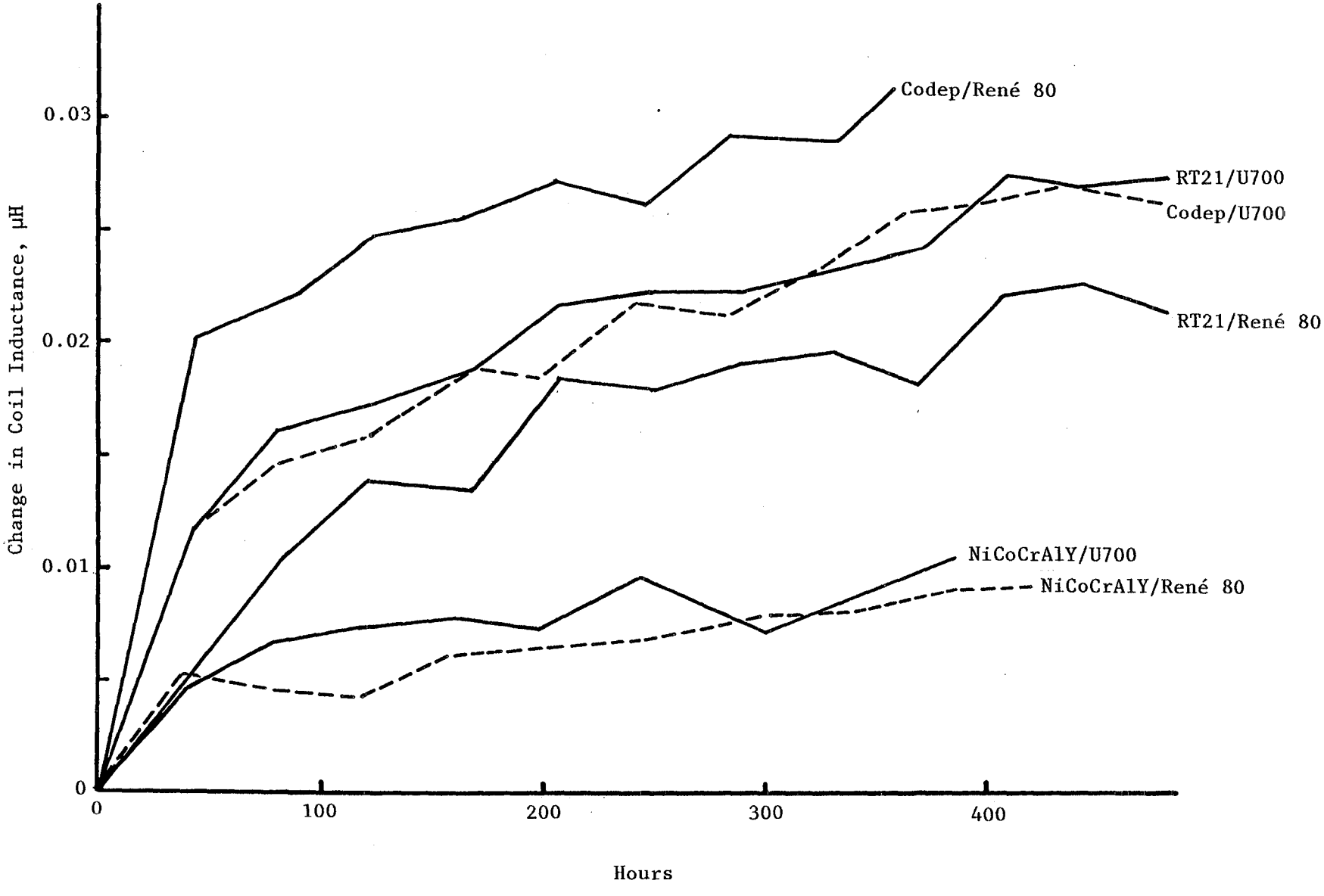

Figure 30. Changes in Coil Inductance with Oxidation at 1100° C Cyclic Exposure in Burner Rig.

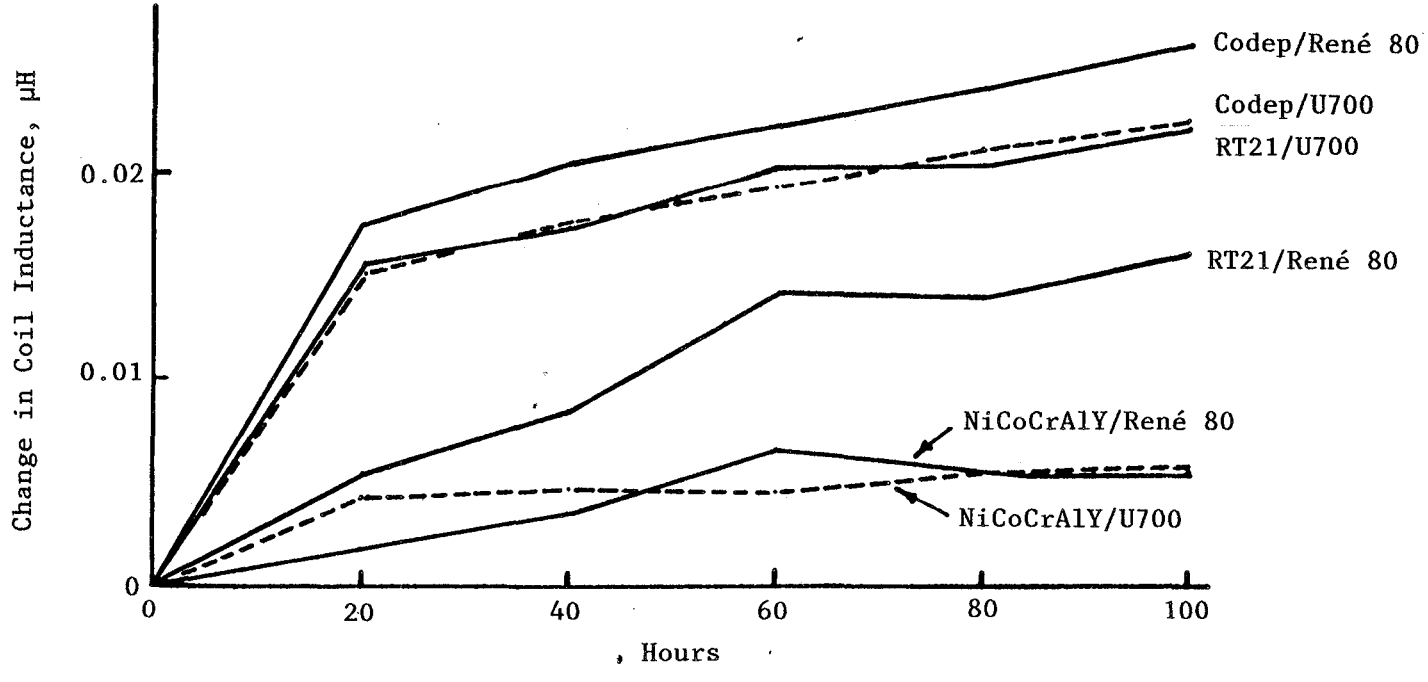

Figure 31. Changes in Coil Inductance in Static Oxidation at 1100° C Cyclic Exposure.

for the longest burner rig exposures for which localized blistering (and probably spalling) occurred, as discussed above.

On the other hand, the NiCoCrAlY coating was plasma sprayed, leaving the bottom end of the specimens uncoated. These uncoated ends were given some protection with a slurry aluminide coating to prevent gross degradation in the long-term aging treatments. This protection was adequate yet only marginal as indicated by the significant weight losses of several of these specimens when aged for 300 hours or more.

TASK IV - HOT CORROSION TESTS OF AGED SPECIMENS

Testing

This hot corrosion test included a total of 96 specimens, duplicates of six coating/alloy systems representing eight aging conditions. The specimens were randomly distributed among four burner rigs. All specimens were exposed to coating failure or 1000 hours, whichever occurred first. As in Task II, specimens were removed after the first visual evidence of hot corrosion plus two additional 20-hour cyclic exposures. Test conditions were the same as in Task II.

Results

Table X includes aging history, hot corrosion test time, coil inductance changes separately for the aging and hot corrosion exposures, and maximum metal degradation. Coating integrity for the five NiCoCrAlY specimens marked "not failed" after the full 1000 hours of testing was metallographically confirmed; localized corrosion to a depth of less than half the initial coating thickness of 98 μm was observed. Evidence for Type 1 hot corrosion was consistently observed.

For the ≧300-hour burner rig and 600-hour isothermal aging, most of the specimens exhibited a coating hot corrosion life of less than 100 hours. Noting that the criterion for specimen removal was exposure for two 20-hour cycles after first visual evidence of corrosion, it is clear that the coating was essentially failed at the beginning of the hot corrosion test. Thus, these results are of minimal use in evaluating the effect of aging on hot corrosion life. This comment is particularly valid for NiCoCrAlY-coated specimens aged in the burner rig; as discussed previously, these exhibited extreme localized degradation on the back side away from the flame. For these, hot corrosion life was shorter than for the RT21-coated and Codep-coated specimens.

In most other instances, coating lives for duplicate specimens were in good agreement. For those few cases where this was not true, significant differences between burner rigs in operating parameters have been ruled out. Rather, differences are believed to be largely caused by relatively nonuniform degradation during the aging treatment. Figure 32 shows typical specimens.

Table XI presents metallographic observations from the aging treatments vis-a-vis visual observations from the subsequent hot corrosion test. The hot corrosion coating failures do not necessarily correspond to the locations of coating "weak spots" developed in the prior aging; the two specimens of each coating/alloy system tested in hot corrosion may be either more or less degraded, and in different locations, than the Task III control specimen.

In spite of the above uncertainties, several observations may be made. Figure 33 and Figure 34 show averages for duplicate specimens, except for two

Table X. Specimens Removed From Task IV Burner Rig Test.

Code	Alloy	Coating	Task III Exposure	Change in Coil Inductance, μm	Task IV Rig No.	Task IV Hours	Change in Coil Inductance, μH	Initial Coating Thickness, μm	Maximum Corrosion Attack, μm
X119	U700	Codep	100 Hours Vacuum	0.0179	1	119	0.0233	84	85
X103	U700	Codep	100 Hours Vacuum	0.0220	2	140	0.0124	84	130
X126	U700	RT21	100 Hours Vacuum	0.0181	3	140	0.0108	79	80
X90	U700	RT21	100 Hours Vacuum	0.0102	4	140	0.0177	79	230
X74	U700	NiCoCrAlY	100 Hours Vacuum	0.0026	1	997*	0.0178	98	40
X60	U700	NiCoCrAlY	100 Hours Vacuum	0.0003	2	893	0.0277	98	200
L71	René 80	Codep	100 Hours Vacuum	0.0244	3	200	0.0540	50	175
L100	René 80	Codep	100 Hours Vacuum	0.0174	4	200	0.0289	50	200
L108	René 80	RT21	100 Hours Vacuum	0.0183	1	353	0.0145	81	300
L117	René 80	RT21	100 Hours Vacuum	0.0189	2	564	0.0452	81	380
L104	René 80	NiCoCrAlY	100 Hours Vacuum	0.0055	1	997*	0.0110	98	40
L92	René 80	NiCoCrAlY	100 Hours Vacuum	0.0047	2	1000*	0.0107	98	35
X105	U700	Codep	100 Hours Cyclic	0.0226	1	200	0.0188	84	180
X71	U700	Codep	100 Hours Cyclic	0.0235	3	200	0.0063	84	75
X127	U700	RT21	100 Hours Cyclic	0.0243	2	283	0.0180	79	430
X134	U700	RT21	100 Hours Cyclic	0.0227	4	200	0.0081	79	100
X35	U700	NiCoCrAlY	100 Hours Cyclic	0.0048	3	524	0.0342	98	400
X37	U700	NiCoCrAlY	100 Hours Cyclic	0.0070	4	606	0.0495	98	190
L102	René 80	Codep	100 Hours Cyclic	0.0260	2	765	0.0392	50	250
L105	René 80	Codep	100 Hours Cyclic	0.0258	4	524	0.0533	50	220
L109	René 80	RT21	100 Hours Cyclic	0.0115	1	556	0.0204	81	80
L127	René 80	RT21	100 Hours Cyclic	0.0180	3	483	0.0578	81	250
L42	René 80	NiCoCrAlY	100 Hours Cyclic	0.0077	3	1003	0.0710	98	250
L45	René 80	NiCoCrAlY	100 Hours Cyclic	0.0038	4	920	0.0740	98	330
X32	U700	Codep	100 Hours Isothermal	0.0174	1	140	0.0051	84	75
X54	U700	Codep	100 Hours Isothermal	0.0192	2	88	0.0295	84	85
X81	U700	RT21	100 Hours Isothermal	0.0174	3	100	0.0315	79	80
X86	U700	RT21	100 Hours Isothermal	0.0162	4	121	0.0365	79	75
X53	U700	NiCoCrAlY	100 Hours Isothermal	0.0022	1	179	0.0218	98	80
X59	U700	NiCoCrAlY	100 Hours Isothermal	0.0023	2	1000	0.0169	98	74
L21	René 80	Codep	100 Hours Isothermal	0.0203	3	525	0.0433	50	200
L25	René 80	Codep	100 Hours Isothermal	0.0226	4	505	0.0352	50	200
L59	René 80	RT21	100 Hours Isothermal	0.0047	1	203	0.0115	81	230
L74	René 80	RT21	100 Hours Isothermal	0.0070	2	189	0.0169	81	230
L63	René 80	NiCoCrAlY	100 Hours Isothermal	0.0018	3	1003*	0.0161	98	25
L72	René 80	NiCoCrAlY	100 Hours Isothermal	0.0021	4	1001*	0.0177	98	45
X122	U700	Codep	300 Hours Isothermal	0.0246	1	80	0.1229	84	330
X98	U700	Codep	300 Hours Isothermal	0.0214	2	242	0.0302	84	130
X100	U700	RT21	300 Hours Isothermal	0.0226	1	80	0.0453	79	80
X111	U700	RT21	300 Hours Isothermal	0.0209	2	121	0.0101		
X125	U700	NiCoCrAlY	300 Hours Isothermal	0.0088	3	384	0.0804		
X84	U700	NiCoCrAlY	300 Hours Isothermal	0.0053	4	384	0.0987		
L87	René 80	Codep	300 Hours Isothermal	0.0216	1	356	0.0658		
L70	René 80	Codep	300 Hours Isothermal	0.0286	2	334	0.1131		
L124	René 80	RT21	300 Hours Isothermal	0.0177	1	161	0.0150	81	80
L85	René 80	RT21	300 Hours Isothermal	0.0189	2	233	0.0537		
L90	René 80	NiCoCrAlY	300 Hours Isothermal	0.0052	1	755	0.0459	98	100
L89	René 80	NiCoCrAlY	300 Hours Isothermal	0.0077	2	625	0.0469		

* Based on visual appearance, coating not failed.

Table X. Specimens Removed From Task IV Burner Rig Test (Concluded).

Code	Alloy	Coating	Task III Exposure	Change in Coil Inductance, μm	Task IV		Change in Coil Inductance, μH	Initial Coating Thickness, μm	Maximum Corrosion Attack, μm
					Rig No.	Hours			
X18	U700	Codep	600 Hours Isothermal	0.0314	1	80	0.1468		
X20	U700	Codep	600 Hours Isothermal	0.0317	2	80	0.1383	84	280
X67	U700	RT21	600 Hours Isothermal	0.0329	1	72	0.0844		
X80	U700	RT21	600 Hours Isothermal	0.0304	2	85	0.1478		
X52	U700	NiCoCrAlY	600 Hours Isothermal	0.0078	1	183	0.1475	79	180
X47	U700	NiCoCrAlY	600 Hours Isothermal	0.0084	2	181	0.2183	98	220
L16	René 80	Codep	600 Hours Isothermal	0.0339	1	72	0.1077		
L19	René 80	Codep	600 Hours Isothermal	0.0355	2	60	0.1194	50	100
L20	René 80	RT21	600 Hours Isothermal	0.0244	1	130	0.0514	81	180
L10	René 80	RT21	600 Hours Isothermal	0.0228	2	120	0.0808		
L56	René 80	NiCoCrAlY	600 Hours Isothermal	0.0118	3	445	0.1312		
L60	René 80	NiCoCrAlY	600 Hours Isothermal	0.0096	4	525	0.1430	98	350
X23	U700	Codep	103 Hours Burner Rig	0.0213	1	115	0.0090	84	175
X36	U700	Codep	107 Hours Burner Rig	0.0240	3	121	0.0650	84	280
X69	U700	RT21	103 Hours Burner Rig	0.0207	2	112	0.0226	79	175
X85	U700	RT21	107 Hours Burner Rig	0.0194	4	140	0.0548	79	280
X11	U700	NiCoCrAlY	103 Hours Burner Rig	0.0079	1	179	0.0327	98	300
X12	U700	NiCoCrAlY	107 Hours Burner Rig	0.0068	2	825	0.0666	98	350
L33	René 80	Codep	103 Hours Burner Rig	0.0238	2	278	0.0629	50	250
L52	René 80	Codep	107 Hours Burner Rig	0.0276	4	159	0.0352	50	160
L22	René 80	RT21	103 Hours Burner Rig	0.0140	1	377	0.0360	81	280
L27	René 80	RT21	107 Hours Burner Rig	0.0143	3	221	0.0468	81	280
L1	René 80	NiCoCrAlY	103 Hours Burner Rig	0.0082	3	766	0.0811	98	350
L2	René 80	NiCoCrAlY	107 Hours Burner Rig	0.0046	4	746	0.0687	98	300
X45	U700	Codep	304 Hours Burner Rig	0.0281	3	75	0.1214		
X51	U700	Codep	298 Hours Burner Rig	0.0302	3	75	0.0836		
X95	U700	RT21	304 Hours Burner Rig	0.0231	3	75	0.0737		
X96	U700	RT21	298 Hours Burner Rig	0.0223	4	81	0.0323		
X24	U700	NiCoCrAlY	289 Hours Burner Rig	0.0077	3	60	0.0937		
X28	U700	NiCoCrAlY	293 Hours Burner Rig	0.0037	3	60	0.1011		
L66	René 80	Codep	304 Hours Burner Rig	0.0312	4	150	0.0456		
L69	René 80	Codep	298 Hours Burner Rig	0.0282	4	143	0.0641		
L39	René 80	RT21	304 Hours Burner Rig	0.0182	3	95	0.0563		
L50	René 80	RT21	298 Hours Burner Rig	0.0174	3	115	0.0583		
L13	René 80	NiCoCrAlY	289 Hours Burner Rig	0.0083	3	60	0.0268		
L15	René 80	NiCoCrAlY	293 Hours Burner Rig	0.0048	4	69	0.0492		
X61	U700	Codep	480 Hours Burner Rig	0.0383	4	69	0.0627		
X89	U700	Codep	488 Hours Burner Rig	0.0367	4	69	0.0667		
X101	U700	RT21	485 Hours Burner Rig	0.0323	4	81	0.0782		
X118	U700	RT21	477 Hours Burner Rig	0.0288	4	81	0.0935		
X29	U700	NiCoCrAlY	375 Hours Burner Rig	0.0094	3	60	0.1041		
X31	U700	NiCoCrAlY	381 Hours Burner Rig	0.0114	4	69	0.1214		
L95	René 80	Codep	477 Hours Burner Rig	0.0515	4	109	0.0814		
L98	René 80	Codep	383 Hours Burner Rig	0.0299	3	115	0.1100		
L51	René 80	RT21	485 Hours Burner Rig	0.0197	4	101	0.0388		
L55	René 80	RT21	477 Hours Burner Rig	0.0205	4	101	0.0150		
L18	René 80	NiCoCrAlY	353 Hours Burner Rig	0.0134	3	60	0.0441		
L24	René 80	NiCoCrAlY	415 Hours Burner Rig	0.0108	3	60	0.0424		

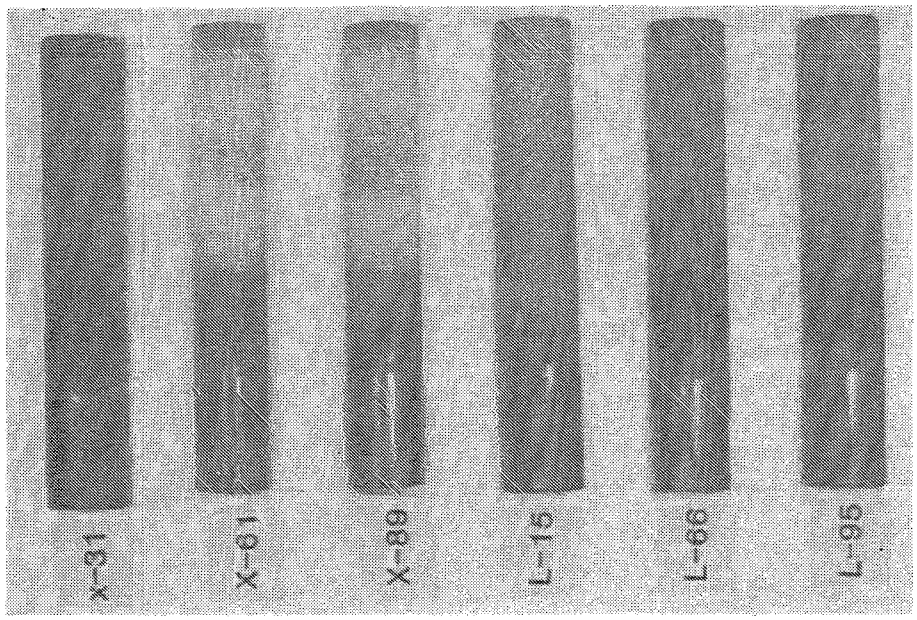

From Left to Right:
NiCoCrAlY Coated U700
Codep Coated U700
Codep Coated U700
NiCoCrAlY Coated René 80
Codep Coated René 80
Codep Coated René 80

Top: After Task III Aging

Bottom: After 69 Hours of Task IV Hot Corrosion Testing

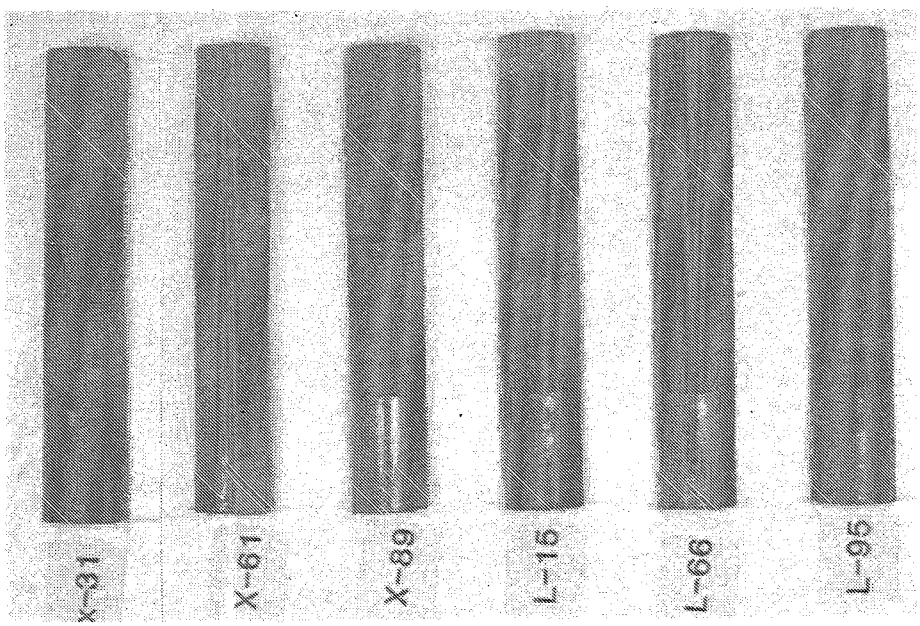

Figure 32. Rear View of Burner Rig Specimens.

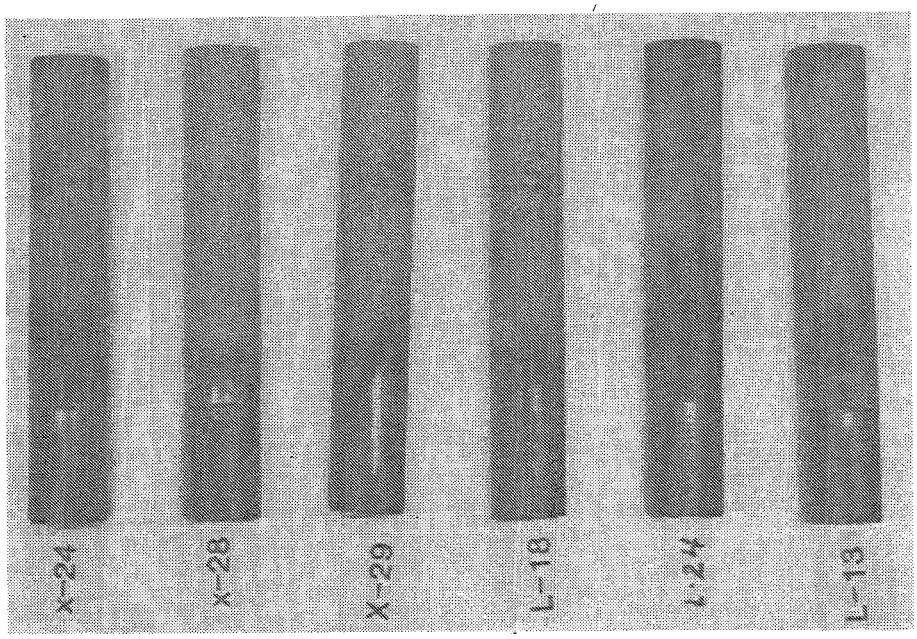

Top: After Task III Aging

Bottom: After 60 Hours of Task IV Hot Corrosion Testing

From Left to Right:
NiCoCrAlY Coated U700
NiCoCrAlY Coated U700
NiCoCrAlY Coated U700
NiCoCrAlY Coated René 80
NiCoCrAlY Coated René 80
NiCoCrAlY Coated René 80

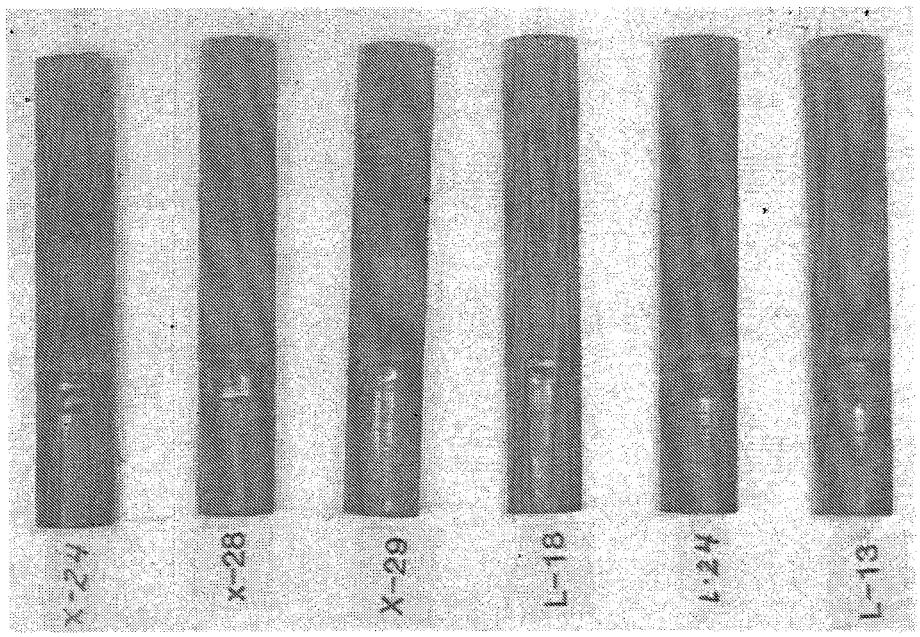

Figure 32. Rear View of Burner Rig Specimens (Concluded).

Table XI. Metallographic Evaluations of Task III Control Specimens (1100° C Aging) and Visual Observations of Degradation in Subsequent Task IV Hot Corrosion Tests (900° C).

Task III Conditions	U700		René 80	
	Task III Degradation, μm	Task IV Visual Observations *	Task III Degradation, μm	Task IV Visual Observations *
100 Hour Vacuum				
Codep	nil	d	nil	d
RT21	nil	a	nil	d
NiCoCrAlY	nil	a,c	nil	a
100 Hour Cyclic				
Codep	15	c	25	c,d
RT21	50 (local)	d	50 (local)	d
NiCoCrAlY	nil	d	nil	b,d
100 Hour Isothermal				
Codep	nil	b	25	b
RT21	nil	b,d	20	d
NiCoCrAlY	10 (local)	a,d	30 (local)	a
300 Hour Isothermal				
Codep	35 (local)	c	50	b
RT21	20	c	25	b
NiCoCrAlY	nil	d	30 (local)	a,b
600 Hour Isothermal				
Codep	35 (few)	b,c	25	c
RT21	35 (few)	c	35 (few)	b
NiCoCrAlY	nil	b	nil	d
100 Hour Burner Rig				
Codep	70 (local)	c	50	b
RT21	nil	c	80	b
NiCoCrAlY	20 (back)	d	35 (local)	b
300 Hour Burner Rig				
Codep	45	c	20	d
RT21	40	b	45	b
NiCoCrAlY	100 (back)	a	70 (back)	b
>300 Hour Burner Rig				
Codep	50	b	50	a,b
RT21	50	c	25	b
NiCoCrAlY	100 (back)	b	50 (back)	a,b

* Entries in this column are coded as follows:

a - Relatively local attack on back of specimen.
b - General attack on back half of specimen.
c - General attack, essentially all around.
d - Relatively local attack in second and/or third quadrants from front (not in back).

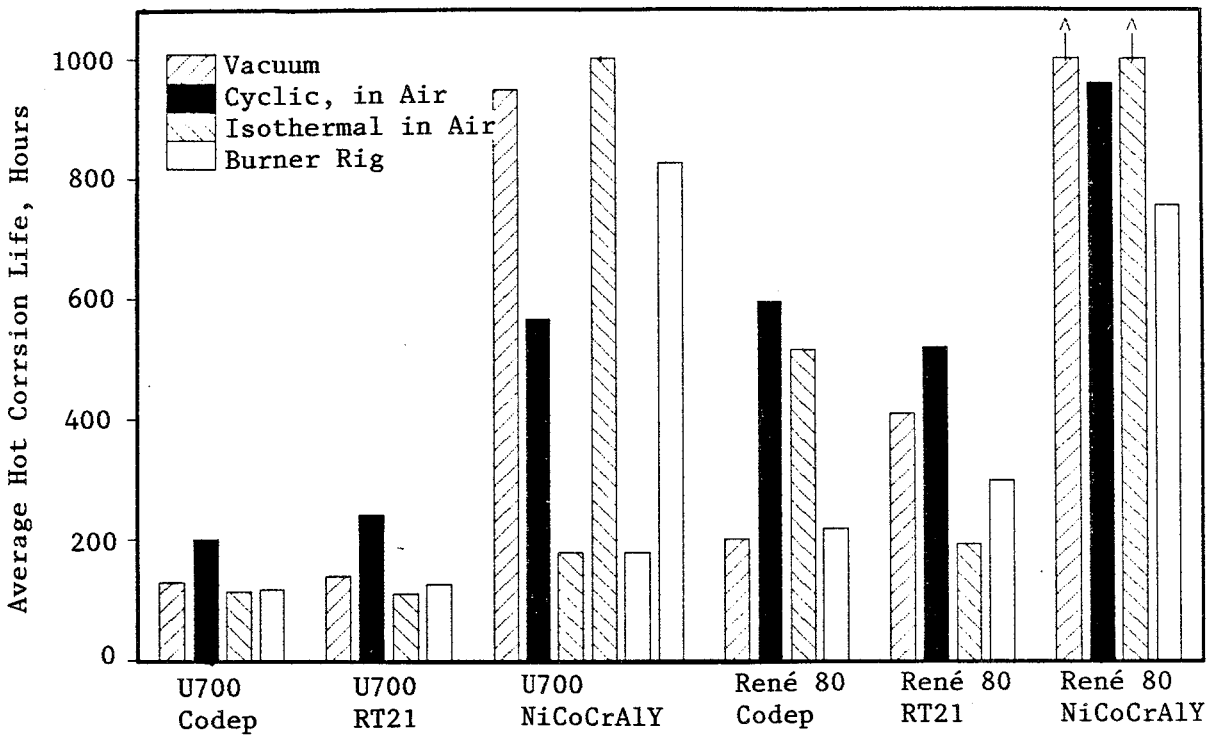

Figure 33. Task IV Results, 100 Hours of Preaging.

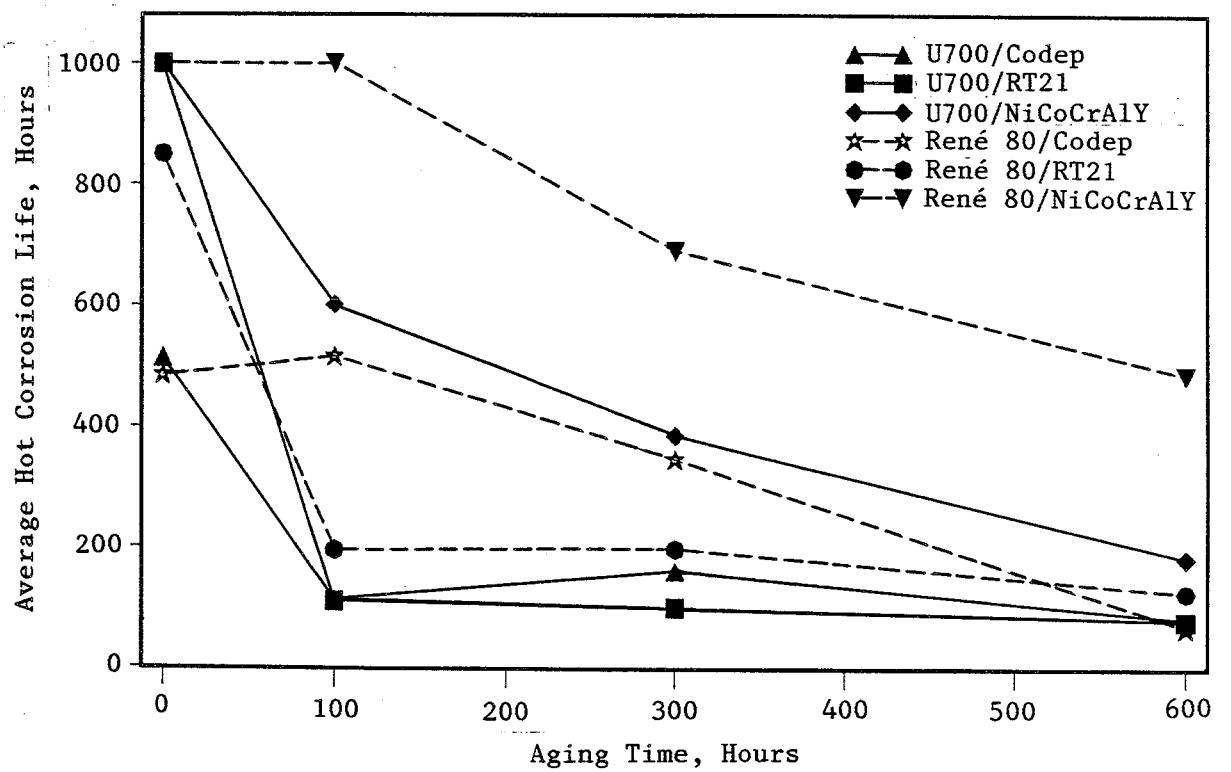

Figure 34. Hot Corrosion Life Versus Isothermal Aging.

instances in Figure 33 for which widely disparate coating lives were observed. (U700/NiCoCrAlY, isothermal and burner rig preoxidation).

1. For most of aging conditions, Codep and RT21 coatings exhibit considerably lower lives than were observed in Task II. This reflects, in part, compositional changes (that is, lower Al content caused by the substantial interdiffusion in the 1100° C aging treatment in vacuum, see Table IX). The shorter lives for those specimens aged under cyclic oxidation conditions may include the effect of a measurable loss in coating thickness during aging. However, comparable removal times for specimens aged in vacuum versus air suggest that the bulk compositional change is the overriding factor in decreasing coating life.

2. On average, the lives of the RT21 and Codep coatings are in the same range, in contrast to the substantial differences observed in Task II. Whatever minor differences exist in these coatings in the as-processed condition are apparently erased by heat treatment at 1100° C in either inert or oxidizing environment.

3. For NiCoCrAlY-coated specimens, there are parallel but less extreme decreases in hot corrosion life caused by the 1100° C aging. As shown in Table IX, there were decreases in coating Al content at 1100° C but less dramatic and slower than in the Codep and RT21 coatings.

4. The most striking observation is that, for all three coatings, the corrosion life decrease, relative to Task II results, is far greater for U700 substrates than for René 80 substrates. The EMP results in Table IV do not show any major differences in bulk coating compositions of the two substrate systems, although U700 and René 80 differ appreciably in content of several minor elements. This may lead to significant differences between the two systems in the amount and composition of various carbide and intermetallic phases that develop during aging at 1100° C.

5. The results in Figure 34 demonstrate that for some coating/substrate systems coating lives degrade progressively from 100 to 600 hours preoxidation; in other systems maximum degradation has occurred in 100 hours preoxidation.

In addition to these observations based on the information in Table X and metallographic evaluations, selected coil-inductance changes are shown in Figures 35 and 36. The offset at zero time indicates the change that occurred during the prior aging treatment.

The data shown in Figure 35 further reinforce the observation that RT21 and NiCoCrAlY coatings both exhibit a much shorter life on U700 than on René 80. The same is true for Codep-coated specimens (See Table X). For the RT21 coated specimens, the magnitude of the coil-inductance changes is much greater

——— Aged 600 Hours, Isothermal Oxidation at 1100° C, RT21 Coating.

– – – – – Aged 100 Hours, Cyclic Furnace Oxidation at 1100° C, NiCoCrAlY Coating

Open Symbols Represent U700, Solid are René 80

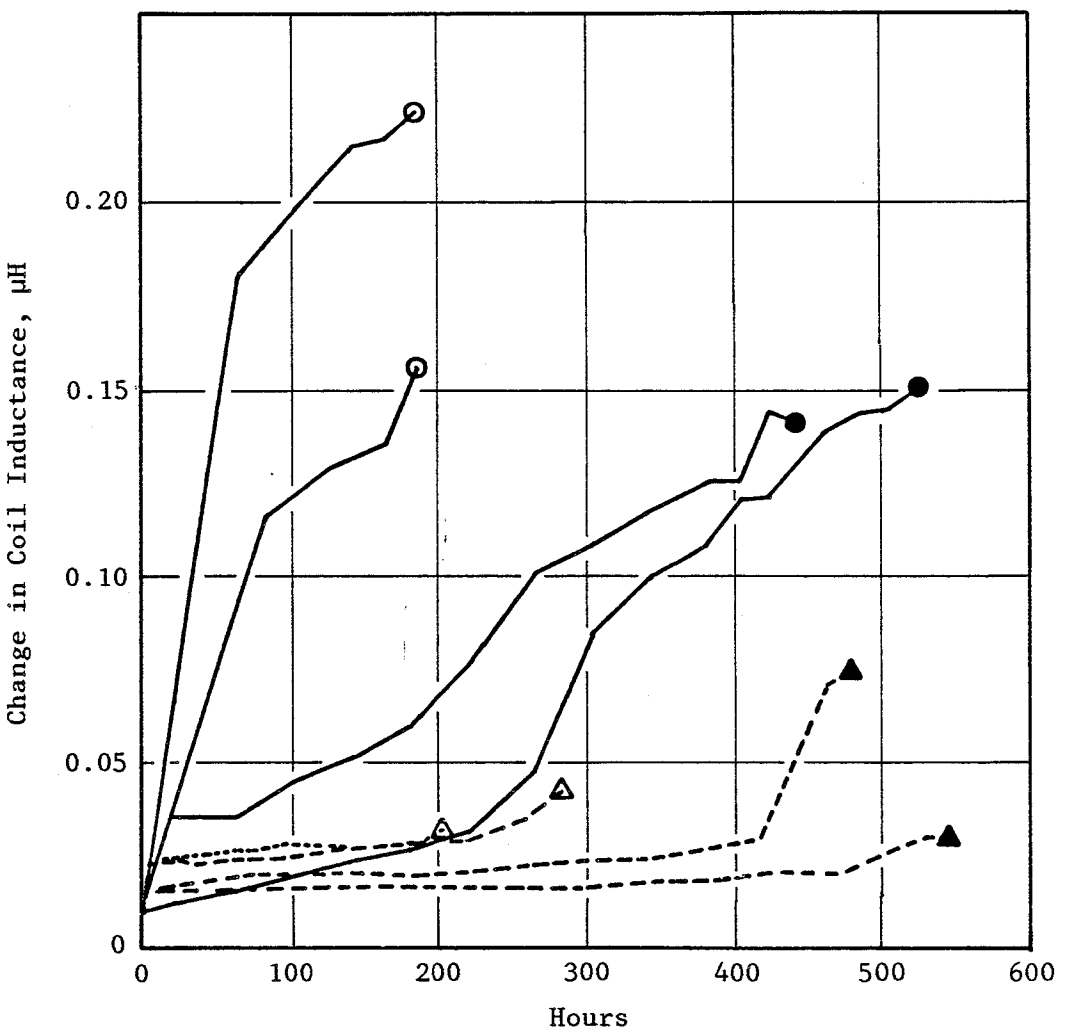

Figure 35. Change in Coil Inductance of Aged and Coated Specimens with Hot Corrosion at 900° C.

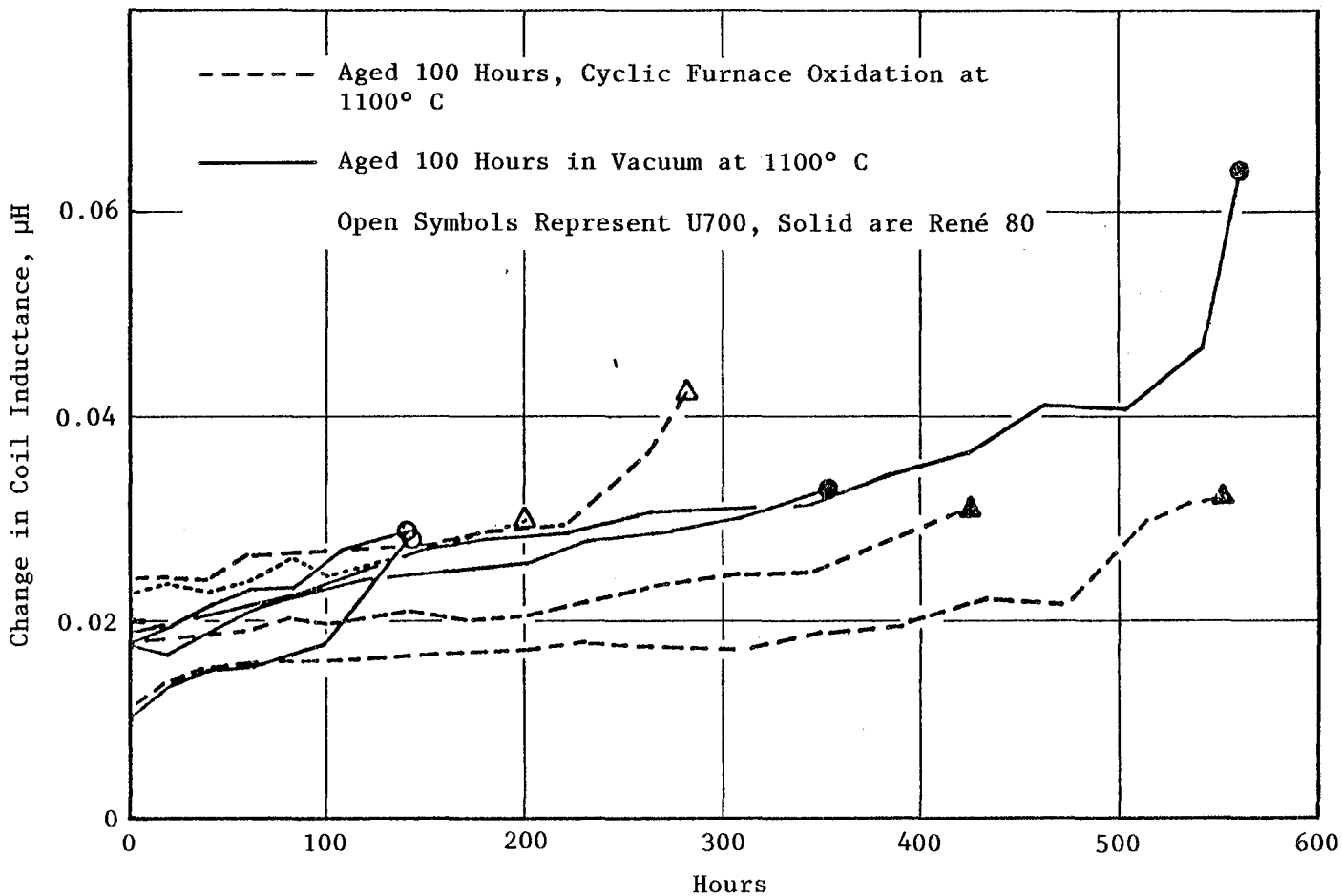

Figure 36. Change in Coil Inductance of Aged RT21 Coated Specimens with Hot Corrosion at 900° C.

than for their analogs tested in Task II in the as-fabricated condition (see Figure 21). This could indicate degradation of a greater fraction of the surface of aged specimens.

The small changes in Figure 36 do not suggest a consistent difference between vacuum and oxidizing aging treatments. This reinforces the comment, made earlier, that compositional changes caused by coating/substrate interdiffusion are more important in decreasing coating life than are compositional changes involved in oxide scale formation.

Salt accumulation (Na_2SO_4) was measured on 12 specimens. Results are given in Table XII. These accumulation rates are higher and more variable than was observed in Task II (Table VII) and may be a consequence of rougher specimen surfaces formed in the prior 1100° C aging. Thorough checking of burner rig operating conditions did not reveal any discrepancies. The higher salt-accumulation rates may contribute to higher corrosion rates; however, such an effect is not considered a major one since coating lives of duplicate specimens (Table X) were generally in agreement.

Table XII. Na_2SO_4 Accumulation on Task IV Burner Rig Test Specimen.

Specimen Number	Test Time, Hours	Na, mg	Na_2SO_4	
			mg/cm^2	mg/cm^2 100 hours
L71	200	24.0	3.71	1.85
L100	200	34.4	5.30	2.65
X103	140	39.0	6.02	4.29
X119	119	25.3	3.90	3.27
L59	203	12.3	1.90	0.93
X47	181	11.2	1.73	0.95
L33	278	27.1	4.18	1.50
L69	143	13.1	2.02	1.41
L50	115	17.6	2.71	2.35
L74	189	26.9	4.15	2.19
L70	334	24.9	3.84	1.15
X81	100	16.6	2.57	2.57

LIFE PREDICTION MODELING

Operation of an aircraft engine encompasses a broad range of turbine temperature and gas pressure in the sequence of taxi, takeoff, climb, cruise, descent, thrust reverse, and taxi. Superimposed is an equally broad range of possible contaminant ingestion - substantial yet indeterminate at and near ground level and negligible at high altitude. The implication of such extreme variation is that corrosive deposits may collect on airfoil surfaces during low-altitude portions of a mission at a rate influenced by turbine temperature and pressure, contaminant flux, and aerodynamic aspects of a particular engine design. During high-altitude operation, the deposits may evaporate. Thus, corrosive degradation is, not surprisingly, determined in part by the fraction of operating time spent at low altitudes - as shown in Figure 7.

Nonetheless, it is useful to consider life prediction in terms of average contaminant deposits and to incorporate new information obtained in this study on aging effects. As background information, General Electric corrosion life experience is available for LM2500 engines operated in a marine environment. These engines, derivatives of the TF39/CF6-6 family, have been in place on the cargo ship Admiral William M. Callaghan operated under sponsorship of the U.S. Navy. Although the turbine coatings are designed for marine environments and hence are not directly applicable to airborne jet engines, the 180,000 engine hours accumulated to date provide considerable insight into environmental effects, particularly since most of this operation has been under conditions of programmed and documented power profiles and with reasonably well-known and continuous sea salt ingestion via filtered inlet air. Three salient observations have been made pertinent to modeling and predicting corrosion life for aircraft engines.

1. The two LM2500 engines on the Admiral Callaghan have separate air inlets with filtration systems that differ by about a factor of 4 in the flux of sea salt passed to the engine. This difference, confirmed by measurement of Na_2SO_4 accumulation rates on turbine airfoils, is manifested in much lower rates of corrosion for the cleaner environment (Reference 4).

2. At steady-state, high-power operation, surfaces such as the leading edge of the first-stage HPT blade will be too hot to collect corrosive salts at the levels ingested. However, in cyclic operation, this leading-edge temperature will oscillate below and above the Na_2SO_4 dewpoint. A deposition/evaporation syndrome thus poses a problem in interpretation since corrosion can and does occur during evaporation and appreciably after evaporation is complete. In one instance, this "memory effect" has been estimated as about 7 hours, at about 925° C (Reference 5). For aircraft, a similar deposition/evaporation cycle is possible for a different reason. Contaminant ingestion will occur primarily during takeoff and landing; at higher flight altitudes many deposited mineral salts, including Na_2SO_4, will evaporate.

3. Under certain modes of cyclic operation, both Type 1 and Type 2 corrosion mechanisms have been observed. Type 1 is a function of salt flux, as mentioned above, and Type 2 is sensitive to the flux of sulfur oxides as well. Type 2 hot corrosion is, however, uncommon on aircraft HPT components (see Task I) and is not considered in the following discussion.

With the above as background information for gas turbines operating in a marine environment, the following are proposed as two separate and unrelated phenomena that determine life-limiting aspects of aircraft turbine airfoil coatings and, hence, set the stage for life prediction capability.

The first is a well-known environmental effect: hot corrosion rate is a function of the total amount of corrosive contaminant (usually Na_2SO_4). This total amount is usually defined as the flux in the ingested air, sometimes also including salts in the fuel, but more properly should be defined as salt-deposit film thickness on an airfoil surface. This may be expressed as

$$\text{Corrosion Rate} = Ct^n e^{-Q/RT} \text{ (kelvins)}$$

for Type 1 hot corrosion. In controlled laboratory tests, Fang and Shores (Reference 6) have demonstrated a monotonic increase in corrosion rates with Na_2SO_4 film thickness over the range of interest and up to about 1.5 mg/cm^2 of surface. Although their data are sparse, further measurements should permit establishing the exponent n for film thickness t in the proposed expression. Application of this equation to an aircraft turbine involves, of course, the uncertainties of unknown and intermittent salt ingestion rates together with the "memory effect" described above. Further empirical correlations, as discussed in Task I, are needed to establish the validity of assumptions based on salt-deposit analyses and/or mission analyses.

The activation energy, Q, is also derivable from laboratory studies. Various estimates in the range 125-146 kJ/mole (30-35 kcal/mole) exist in the literature for the Type 1 hot corrosion of coatings and alloys that form a protective film of alumina.

A major caution in interpreting contaminant levels is that deposit film thickness is the key variable, but the estimated flux in the ingested air is frequently the only known quantity (Reference 4). The correlation between these two parameters is undoubtedly design sensitive, influenced for example by aerodynamic differences. Thus any model ultimately derived from further CF6-50 evaluations as described in Task I would have to be "recalibrated" in this respect to be applicable to another engine design.

The second phenomenon proposed as an important influence on hot corrosion life is airfoil coating/substrate interdiffusion (internal effects) at high temperatures encountered during aircraft takeoff; high temperatures may cause changes in the diffusion zone and severely degrade coating hot corrosion life. This phenomenon, not previously identified, was suggested by the results of Task IV. More detailed evaluation will be presented in Task V, but some important conclusions are as follows:

1. All three coatings in this study (Codep, RT21, and NiCoCrAlY) exhibit coating life degradation in the standard 900° C hot corrosion test after aging at 1100° C.

2. For all three coatings, life degradation is more severe on U700 than on René 80 substrates.

3. For a given 100-hour aging time, life degradation is similar whether the aging environment is air or vacuum. Thus, coating/substrate interdiffusion effects are far more important in determining hot corrosion life than are surface chemistry changes during oxidation.

The above conclusions, as supported by the results in Task IV, were exemplified in Figures 33 and 34. The importance of these observations is best described by the mission of an aircraft engine. A small percentage of time is spent at turbine temperatures considerably higher than cruise (takeoff and thrust reverse). Note the maximum temperature is 1090° C (Table II) for CF6-50 Stage 1 turbine blades; under this condition, coating/substrate interdiffusion will take place with consequent accumulative decrease in coating life. Remembering that coating life degradation caused by 1100° C aging depends on the identity of the substrate as well as the coating, it is clear that the behavior of the materials system must be understood. These results suggest that there is a materials-system-dependent temperature limit for accumulative high-temperature operation, and operation above that limit will penalize coating hot corrosion life. This temperature limit may be strongly dependent on the substrate as well as the coating. At lower maximum temperatures there are no corrosion life penalties. Clearly this interpretation, if vindicated by the results to be described in Task V, translate directly into correlation with turbine/mission operating parameters.

This two-part model, as stated, requires considerably more empirical data of the type presented in Task I - especially time/temperature relationships, and refined judgments regarding assumed average contaminant levels together with metallographic evaluations and analyses of flight patterns. In addition, several laboratory studies would be of considerable value in supporting the model and extending the range of usefulness. (These are described later.) At present, and with the additional information to be presented in Task V, the application is limited to Codep coatings on U700 or René 80 substrates.

To address some of the unanswered questions in the model, the following three burner rig hot corrosion tests were designed and performed in Task V. To have maximum opportunity to obtain detailed information within available resources, specimens were limited to Codep-coated U700 and Codep-coated René 80. All aging treatments were performed isothermally in static air.

Test No. 1

Objectives - Obtain further information between 0 and 100 hours aging per Figure 34.

- Perform detailed metallographic and EMP analyses for both materials systems as a function of aging times.

- Interpret differences in response of the two systems in hot corrosion.

Approach - Age duplicate specimens for 15 and for 25 hours.

- Hot corrosion test in burner rig at 900° C, ½ ppm Na as NaCl.

- Evaluate.

Test No. 2

Objective - Obtain hot corrosion Codep life information for different burner rig salt level and for various aging conditions.

Approach - Age duplicate specimens for 0, 15, and 25 hours.

- Hot corrosion test in burner rig at 900° C, ¼ ppm Na as NaCl.

- Evaluate.

Test No. 3

Objectives - Obtain additional results in support of Test No. 1.

- Age Codep/U700 specimens at lower than 1100° C to attempt to induce significant interdiffusion without degrading coating hot corrosion life.

- Age Codep/René 80 specimens at higher than 1100° C to attempt to induce more extensive changes in the diffusion zone and degrade coating hot corrosion life.

Approach - Age duplicate Codep/U700 specimens at 1100° C, 6 and 10 hours.

* - Age duplicate Codep/U700 specimens at 1050° C, 10 and 20 hours.

* - Age duplicate Codep/René 80 specimens at 1135° C for 15, 25, and 50 hours.

- Hot corrosion test in burner rig at 900° C, ½ ppm Na as NaCl.

- Evaluate.

* Conditions selected after aging spare specimens for various times/temperatures to obtain structures judged to satisfy the objectives of this test.

TASK V - HOT CORROSION TESTS TO VERIFY PROPOSED LIFE PREDICTION MODEL

Table XIII summarizes information for all three tests in Task V including specimen-aging conditions, coating life, and coil-inductance changes in the 900° C burner rig hot corrosion test. Accumulation of Na_2SO_4 deposits on selected specimens is recorded in Table XIV. Metallographic evaluations of all specimens confirmed Type 1 hot corrosion morphology, substrate sulfides, and coating penetration with additional distress of the substrate averaging about 150 μm in depth. Results of the tests will be discussed separately in the context of the objectives stated previously.

Test No. 1

Coatings lives are shown in Figure 37, together with results obtained for Task II and Task IV specimens (isothermal age only). The previously noted marked difference between the Codep/U700 and Codep/René 80 systems is further reinforced by the additional results. The convergence of the two lines in Figure 37 at longer aging times reflects, in part, significant metal recession that occurred in 300 and 600 hours.

A difference between the two systems is also apparent in coil-inductance measurements (Figures 38 and 39). For the Codep/U700 specimens, note that the change with time is faster as aging time increases, but that is not so for the Codep/René 80 specimens. Also, the small negative changes at short times, characteristic of unaged specimens (Figure 21), persists with aging time for Codep/René 80 specimens but not for Codep/U700 specimens. A possible follow-on study to the present program would be to study the subtle coil-inductance changes at short times in a hot corrosion environment and attempt to correlate life degradation as a function of preaging.

To attempt to explain the differences between the two coating substrate systems shown in Figure 37, extensive quantitative electronmicroprobe analyses have been performed for 0, 15, 25, and 100 hours aging (before hot corrosion testing). The results, presented in detail in the Appendix, include two types of information:

- For analysis of the additive layer and substrate immediately below the diffusion zone, an elongated rectangular raster was used, approximately 1 μm thick and 65 μm wide. This raster was oriented with the long axis parallel to the coating/substrate interface. A series of analyses was performed with the raster incrementally moved across the additive layer, and a single analysis was made in the substrate. This geometry of analysis area provides more reliable results than the usual spots for a material in which some localized segregation is possible.

- For analysis of precipitates in the diffusion zone and in the diffusion zone matrix between precipitate particles, spot areas were used. Precipitates were identified as either "blocky" or "acicular."

Table XIII. Test Information for Codep Coated Specimens Removed from Task V Burner Rig Hot Corrosion Tests.

Test	ppm Na	Code	Alloy	Aging		Change in Coil Inductance, μH	Hours
				Temperature	Hours		
1	½	X10	U700	1100° C	15	0.0173	199
		X27	U700	1100° C	15	0.0117	199
		X49	U700	1100° C	25	0.0291	179
		X55	U700	1100° C	25	0.0235	179
1	½	L83	René 80	1100° C	15	0.0432	420
		L93	René 80	1100° C	15	0.0393	461
		L23	René 80	1100° C	25	0.0448	502
		L120	René 80	1100° C	25	0.0555	522
2	¼	X9	U700	---	0	0.0474	440
		X75	U700	---	0	0.0230	893
		X16	U700	1100° C	15	0.0257	360
		X42	U700	1100° C	15	0.0271	301
		X57	U700	1100° C	25	0.0726	261
		X63	U700	1100° C	25	0.0697	301
2	¼	L78	René 80	---	0	0.0324	618
		L81	René 80	---	0	0.0733	440
		L114	René 80	1100° C	15	0.0391	790
		L115	René 80	1100° C	15	0.0282	577
		L29	René 80	1100° C	25	0.0365	719
		L121	René 80	1100° C	25		721
3	½	X4	U700	1100° C	6	0.0192	279
		X5	U700	1100° C	6	0.0439	180
		X68	U700	1100° C	10	0.0331	238
		X70	U700	1100° C	10	0.0734	160
3	½	X62	U700	1050° C	10	0.0571	299
		X102	U700	1050° C	10	0.0554	140
		X115	U700	1050° C	20	0.0620	299
		X120	U700	1050° C	20	0.0695	140
3	½	L53	René 80	1135° C *	15	0.0406	81
		L73	René 80	1135° C	15	0.0962	60
		L43	René 80	1135° C	25	0.1300	81
		L122	René 80	1135° C	25	0.1770	60
		L131	René 80	1135° C	50	0.1392	40
		L135	René 80	1135° C	50	0.2713	40

* To minimize surface oxidation, aging at 1135° C was performed in a sealed cannister containing 3-psia air.

Table XIV. Na_2SO_4 Accumulation on Task V Burner Rig Test Specimens.

Test	ppm Na	Specimen Number	Test Time, Hours	Na, mg	Na_2SO_4	
					mg/cm^2	mg/cm^2 100 hours
1	½	X10	199	23.0	3.05	1.53
		L83	420	25.0	3.93	0.93
		L120	522	25.0	3.93	0.75
2	¼	X57	261	12.3	1.90	0.73
		X16	360	12.1	1.87	0.52
		L29	719	17.2	2.65	0.37
3	½	X4	279	14.8	2.28	0.82
		X5	180	12.9	1.99	1.11
		X70	160	16.1	2.48	1.55

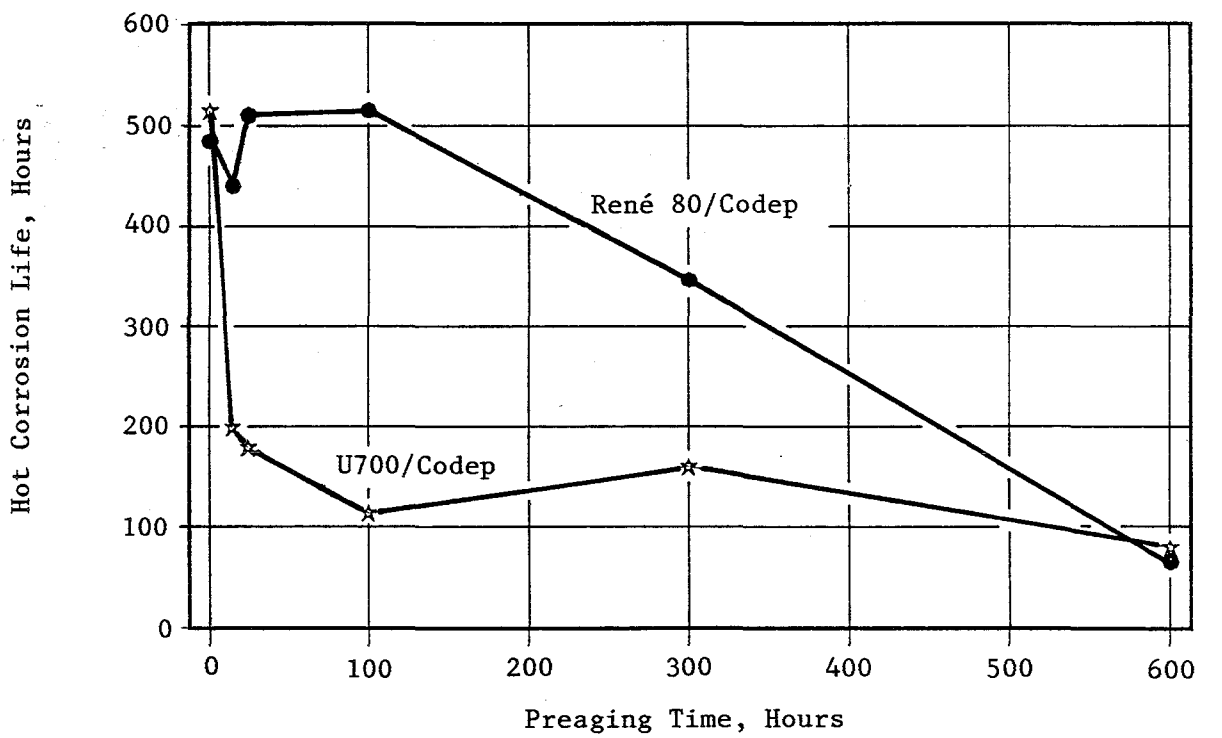

Figure 37. Hot Corrosion Codep Coating Life at 900° C as a Function of Isothermal Preaging at 1100° C.

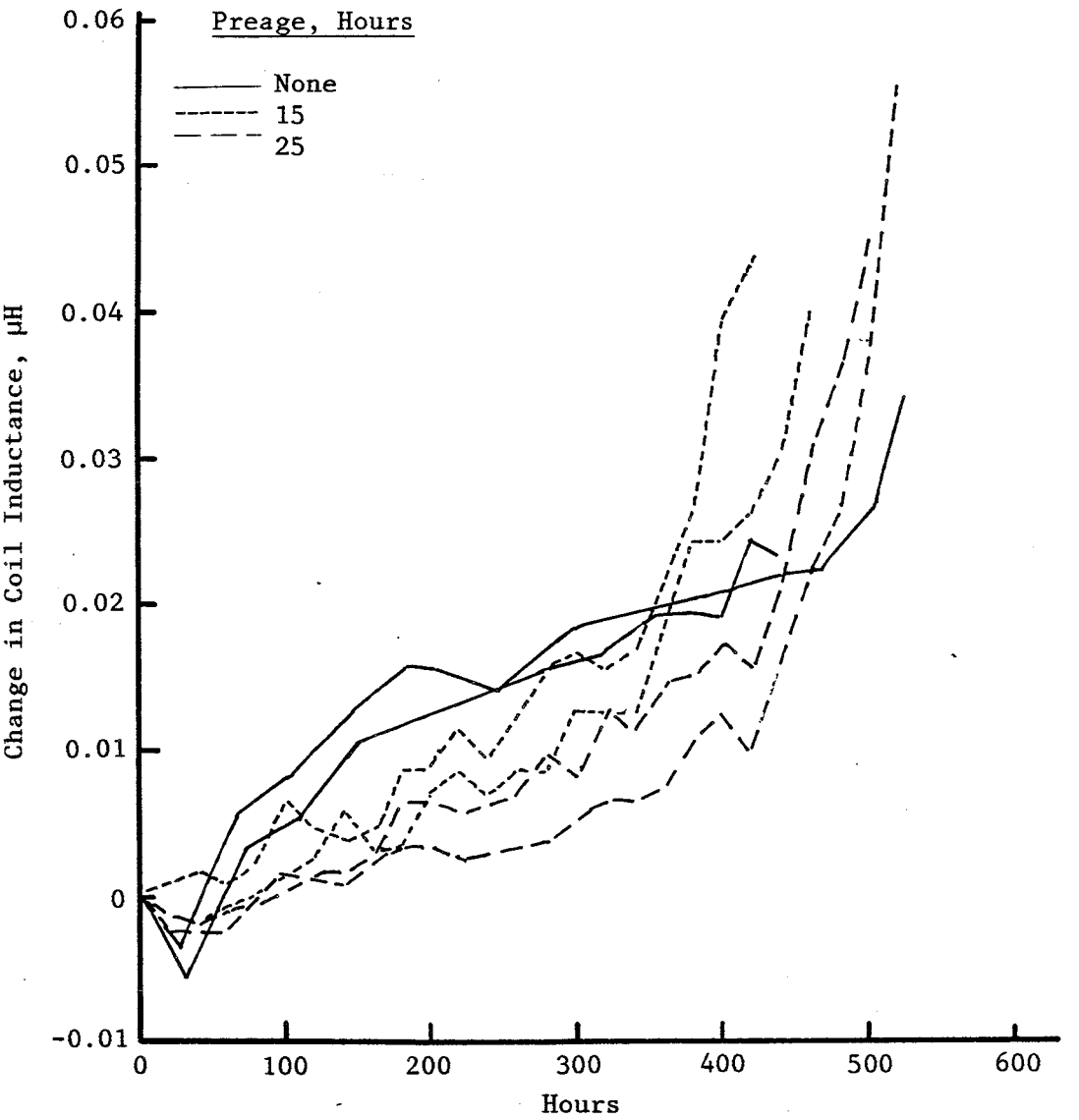

Figure 38. Changes in Coil Induction with Hot Corrosion at 900° C for Codep/René 80 Specimens.

Results obtained for aluminum and titanium in the coating additive layer are shown in Figure 40. Changes are similar for the two systems and in fact faster for Codep/René 80. These faster rates probably reflect higher Ti and lower Al in René 80 (that is, higher concentration gradients compared to the coating as-fabricated) and considerably strengthen the notion that composition changes in the additive layer are not in themselves responsible for the differences in the two systems indicated in Figure 37.

A similar conclusion appears unavoidable with respect to the other alloy elements in the systems, considered either singly or in combinations. Rather, attention is focused on precipitation phenomena in the diffusion zone. Note the microstructures in Figures 41 and 42. Visually, the diffusion zone in the as-fabricated condition is quite similar for the two systems: a close-spaced, needle-like phase in a β matrix, oriented normal to the surface. As aging at 1100° C progresses, this phase gradually disappears, and a blocky phase forms. The rate of this transformation is considerably faster for the U700 system and is nearly complete in 100 hours. In the René 80 system, a similar makeup of the diffusion zone is developed after 300 hours, but here there is the added complexity of the loss of much of the β structure caused by further loss of aluminum. As McCarron et al. have shown (Reference 7), γ' is considerably inferior to β in resistance to sulfidation.

The nature of the phases in the diffusion zone was well characterized by Redden's phase-extraction studies of Codep-coated U700 (Reference 8). He identified the needle-like phase as σ in the as-coated condition, with some carbides also present. The σ phase transforms on long-term heating at 982° C (1800° F) to $M_{23}C_6$ (presumably the blocky phase described above).

To complement Redden's observations, considerable information from spot analyses has been obtained for the needle-like phase, the blocky phase, and the diffusion-zone matrix. Although there is some data scatter, a number of qualitative comments may be made. Average numerical data are given in Table XV. Each entry tabulated for σ and blocky phases is an average of three or more particles. The diffusion zone matrix results are averages of two spots.

- Needle Phase (σ): High Cr, Ni, Mo, (W in René 80 system).
- Blocky Phase (Carbides): Essentially absent before aging. High Cr, Mo, (W in René 80 system). See Figure 43.
- Matrix: β NiAl with substantial Co and Ti that are essentially unchanged with aging time. Mo is low. Cr drops to a leveling-off value of about 8% in the first 15 hours of aging.

Additionally:

- Chromium partitions strongly to the blocky phase, some increase with aging time, range 53-69%. Prior to aging, essentially no blocky phase exists, and the β matrix contains more Cr (12-16%) than after aging (5-7% after 100 hours). The U700 and René 80 systems are similar.

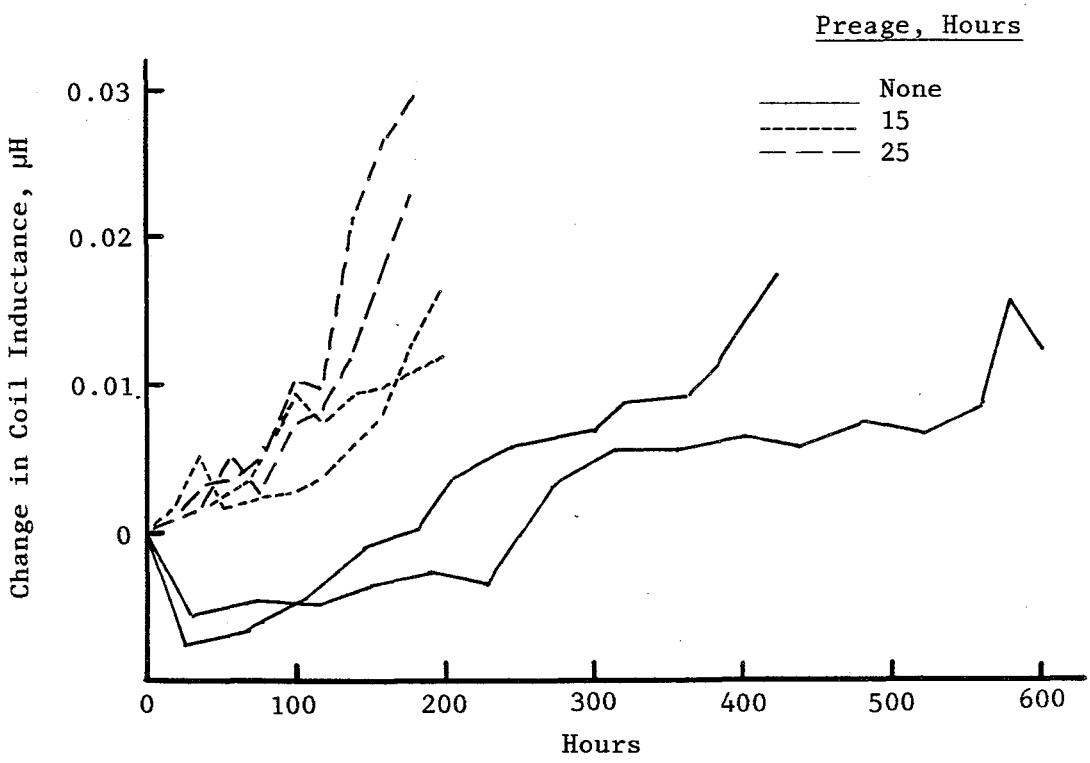

Figure 39. Changes in Coil Induction with Hot Corrosion at 900° C for Codep/U700 Specimens.

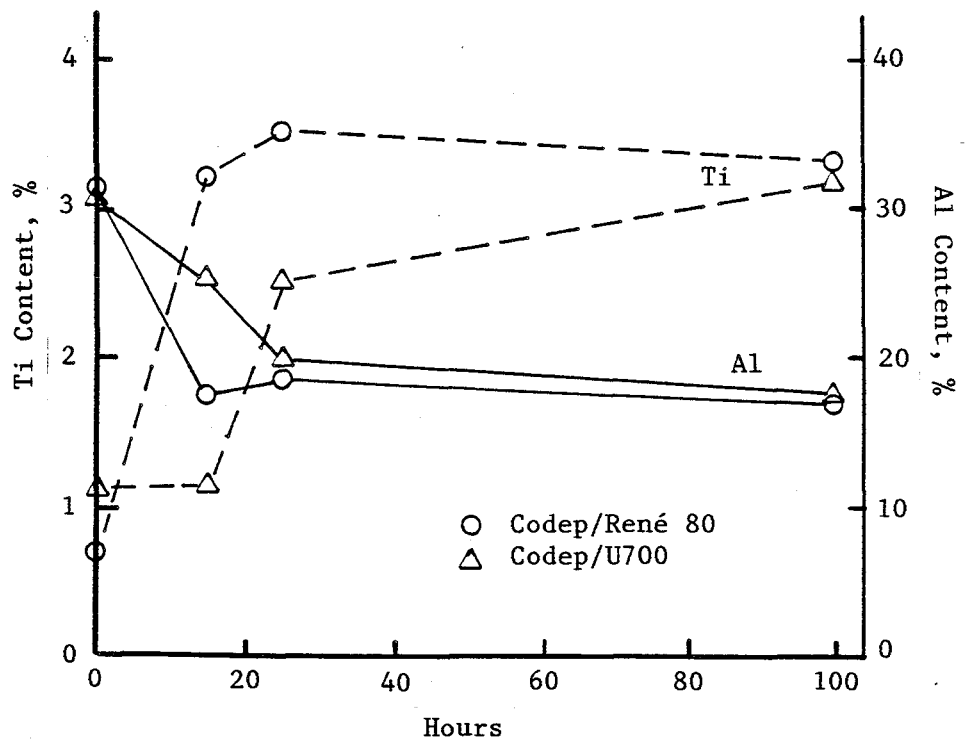

Figure 40. Average Al and Ti Contents in Coating Additive Layer as a Function of Aging at 1100° C.

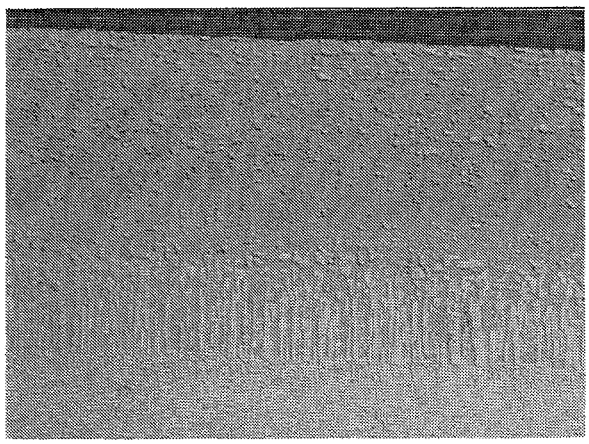

0 Hours

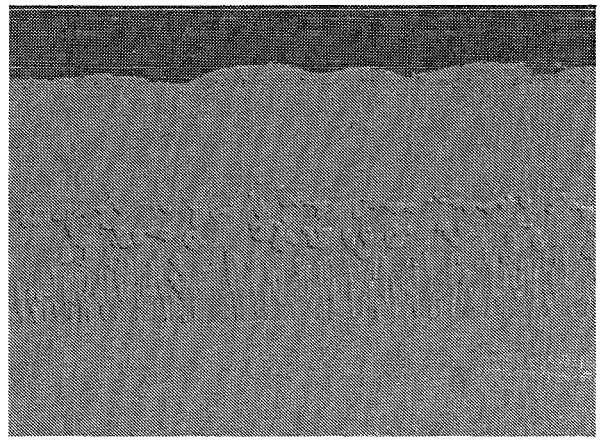

6 Hours

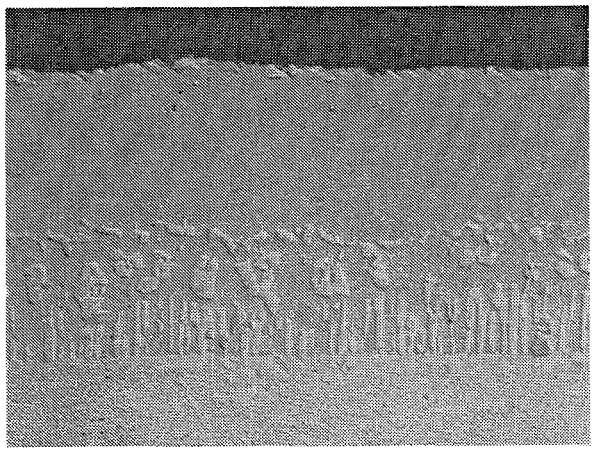

10 Hours

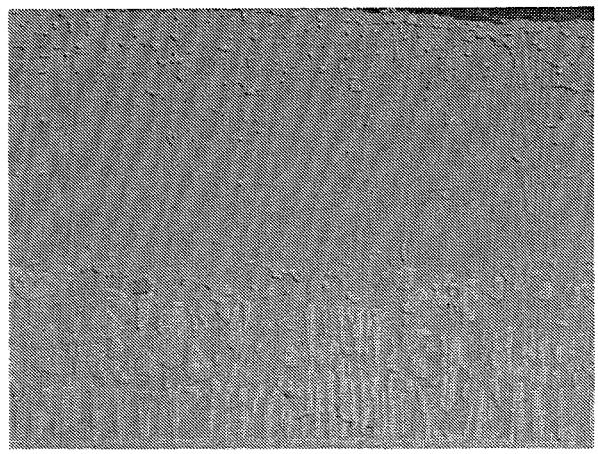

15 Hours

25 Hours

100 Hours

Figure 41. Codep Coated U700 after Isothermal Aging in Air at 1100° C (500×).

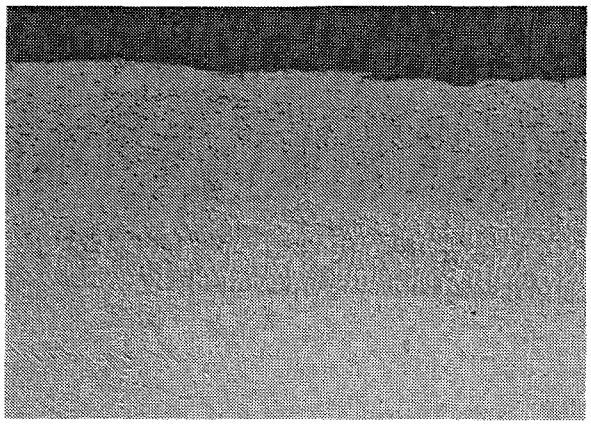

0 Hours

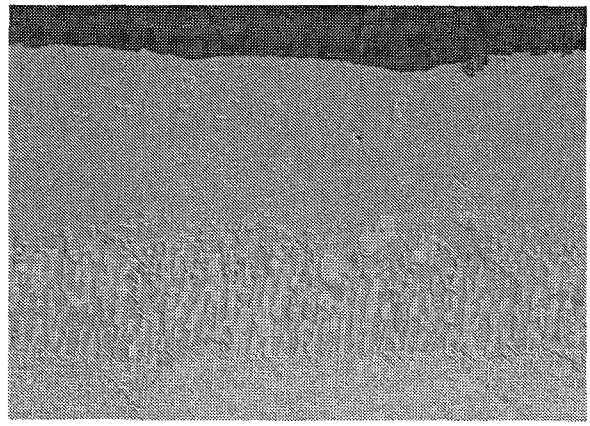

15 Hours

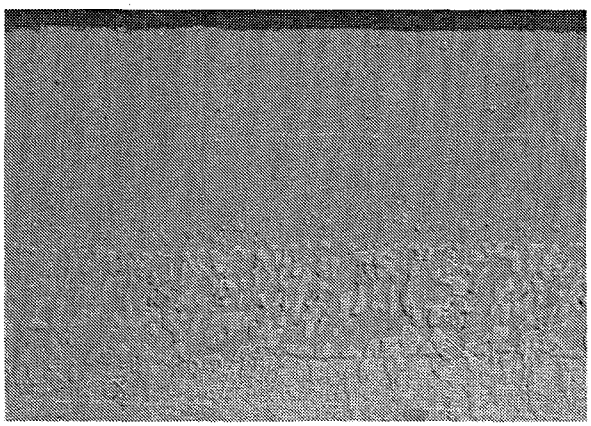

25 Hours

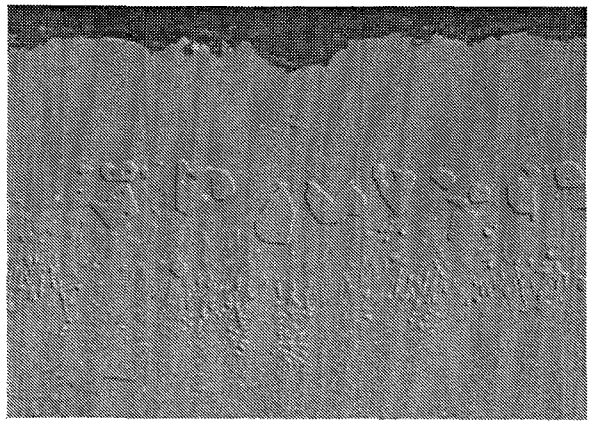

100 Hours

300 Hours

Figure 42. Codep Coated René 80 after Isothermal Aging in Air at 1100° C (500×).

Table XV. Composition of Diffusion Zone: Codep Coatings.

Alloy	1100° C Hours	Weight % Ti	Cr	Co	Ni	W	Al	Mo	
René 80	15	4	26	11	22	17	4	16	Acicular Percipitate
	100	5	13	8	25	23	2	23	
U700	0	3	26/60	14	12/36	--	7	12	
	15	3	18	13	43	--	10	5	
	25	3	19	15	44	--	11	7	
	100	3	21	4	15	--	3	51	
René 80	15	1	58	3	11	12	6	10	Blocky Percipitate
	25	1	25/65	2/12	5/20	11/31	4	11/25	
	100	2	63	2	5	10	5	11	
U700	15	2	53	6	15	--	7	12	
	25	1	69	4	6	--	6	14	
	100	1	69	4	4	--	6	15	
René 80	0	9	12	8	58	3	8	2	Matrix
	15	4	8	9	61	1	16	1	
	25	6	7	8	60	1	16	1	
	100	6	5	8	66	1	8/18	1	
U700	0	4	16	13	45	--	17	3	
	15	5	9	14	54	--	17	1	
	25	5	8	14	56	--	17	1	
	100	4	7	12	61	--	16	1	

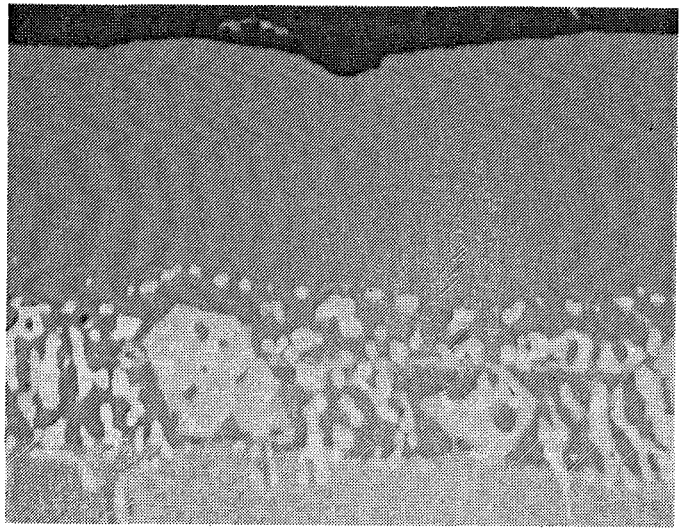

Backscatter Electron Image

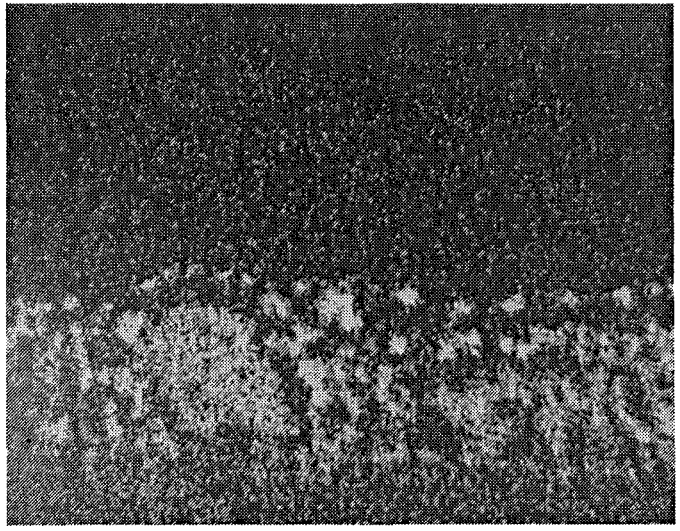

Tungsten

Carbon

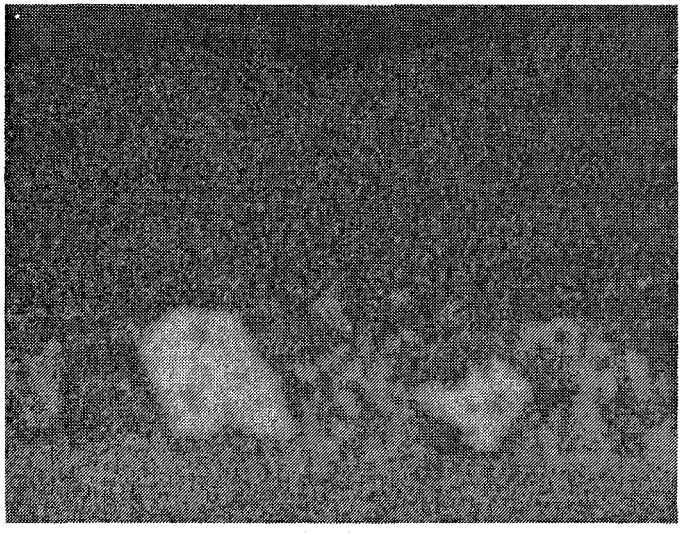

Chromium

Figure 43. X-Ray Oscillograms Showing Evidence of W, C, and Cr in Diffusion Zone Precipitates; Codep/René 80 after 15 Hours Aging at 1100° C (1000×).

- Ti and Co are deficient in the blocky phase, stable with aging time. Both are present at substantial levels in the blocky phase and matrix, again stable with aging time.

- Al is present in all three phases, individual particles varying considerably. In the matrix a higher, rather consistent 16-18% is present and is stable with aging time. U700 and René 80 systems are similar.

- W (René 80 only) is essentially absent in the matrix, about 10% in the blocky phase, and stable with time, appreciably more in the needle phase, but individual particles vary considerably.

- Mo is essentially absent in the matrix and quite high but erratically distributed in the other two phases.

In summary, these results indicate only one clear difference in diffusion zone makeup between the U700 and René 80 systems: the relative amounts of blocky and needle phases which change with aging time. The compositions of these particles are similar in the two systems within the limits of the data. There are some small differences in the two systems for certain elements in certain phases (such as the presence of W in the René 80 system); since these differences are apparently not influenced by aging, it is presumed they are not relevant to the Task II/Task IV differences in corrosion resistance.

A probable interpretation of the differences shown in Figure 37 involves the following scenario:

1. The sulfidation front moves relatively rapidly through the additive layers, then slows down upon arrival at the diffusion zone for unaged specimens in which this diffusion zone contains a closely spaced array of σ particles considerably higher in Cr than the surrounding matrix.

2. During 1100° C aging, these σ phases gradually transform to the larger, blocky phases (as shown in Figures 41 and 42). These blocky particles are even higher in Cr and, more importantly, are widely separated compared with the parent σ particles, particularly in the U700 system.

3. The wide gaps of rather low-Cr diffusion zone matrix provide a vulnerable path for continuing sulfidation-front progression and, hence, coating penetration.

To the extent that this interpretation is valid, the differences between Codep/U700 and Codep/René 80 fall into place. As additional circumstantial evidence, see Figure 44; these photomicrographs are regions from specimens that elsewhere showed complete coating failure.

Codep/U700 (X54) - (100 hours age plus 88 hours in hot corrosion test, Task IV) The dark particles are Cr-rich sulfides, as confirmed by X-ray

Codep/U700, Hot Corrosion Tested 88 Hours at 900° C

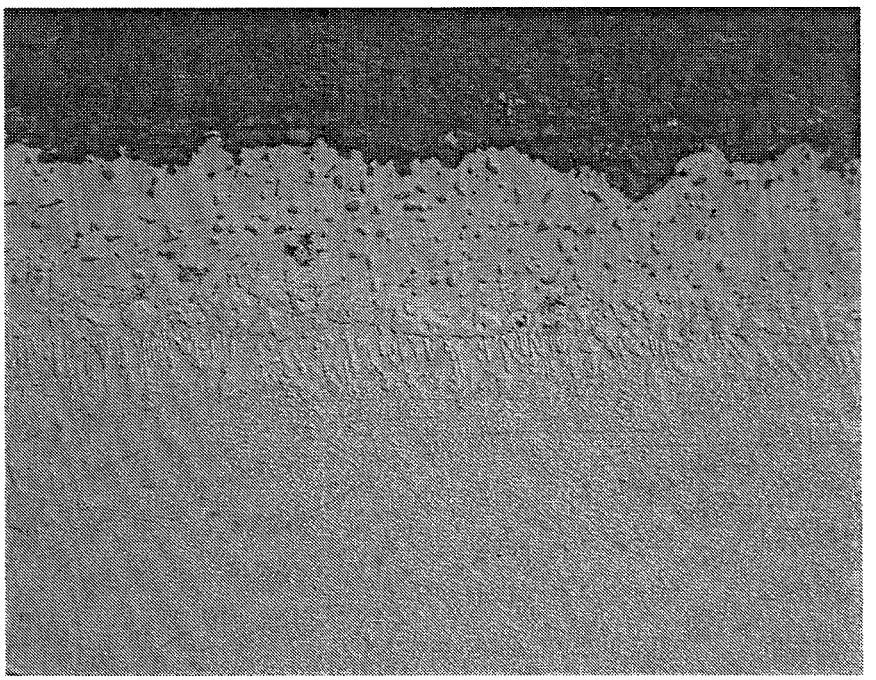

Codep/René 80, Hot Corrosion Tested 525 Hours at 900° C

Figure 44. Task IV Specimens Showing Sulfidation (500×), Isothermal Preaged for 100 Hours at 1100° C.

oscillograms, that show clear evidence of movement through the diffusion zone matrix via the large gaps between the blocky carbides.

Codep/René 80 (L21) - (100 hours age + 525 hours in hot corrosion test, Task IV) The dark particles are Cr-rich sulfides, confirmed by X-ray oscillograms, that appear to be frontally stopped or slowed down after arrival at the diffusion zone which contains a high population of closely spaced σ particles.

Additionally, it should be reiterated that compositions of the additive layer do not show any substantial differences in the two systems which would correlate with the differences in hot corrosion performance, yet the exposure times in these two examples differ by a factor of six. This suggests that the sulfidation through the additive layer of the Codep/René 80 specimen did in fact occur in a small fraction of the total exposure time, then dramatically slowed down.

As a critical test of the rapid-additive-layer/relatively slow-diffusion-zone sulfidation hypothesis, selected short burner rig tests (Task II/IV conditions) were performed to track the progression of the sulfidation front throughout coating life. Since the availability of Codep-coated specimens was limited, this effort concentrated primarily on U700/RT21, preaged for 25 hours at 1100° C. Based on previous tests of RT21 and analogous Codep results, one would expect a subsequent hot corrosion life of approximately 180 hours.

The first attempt at quantifying sulfidation progression as a function of time was to interrupt a burner rig test at approximately half-life. Figure 45 (a and b) shows cross sections of specimen X133, tested for 88 hours. The sulfidation front clearly had penetrated the additive layer, but not the diffusion zone, suggesting that sulfide advancement through the diffusion zone requires at least 50% of the life of U700/RT21 in this condition.

The small dispersed phase apparent in the additive layer is typical in the as-coated condition and has been identified by SEM energy dispersive analysis as being Cr and Mo rich. There appears to be a tendency for these particles to persist preferentially in additive layer Ni_3Al, as shown in Figure 45c.

Following the half-life results, a burner rig test of another specimen was interrupted at 23 hours, approximately 12% of total expected life. In this instance, there were no regions of additive layer penetration observed, as shown by the representative cross section in Figure 46. While there is some agglomeration of the additive layer particles (either in thin fingers of Ni_3Al or in β NiAl grain boundaries), none can be identified as sulfides.

Having established that additive layer penetration occurs between 12 and 50% of the total hot corrosion life of this preaged coating/substrate system, the next test was interrupted at around 23% (41 hours) of the total life (180 hours). Metallography found no area of severe sulfide encroachment, but there were indications, confirmed by SEM wavelength dispersive analysis, of sulfur near the interface between the diffusion zone and additive layer, as well as through the thickness of the additive layer (Figure 47).

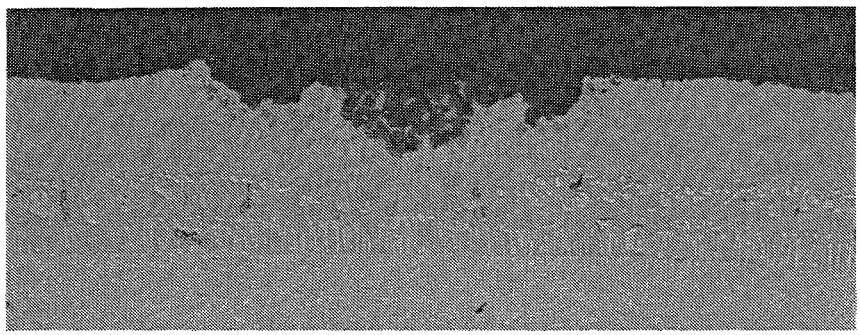

(a) Complete Sulfide Penetration of Additive Layer (250×)

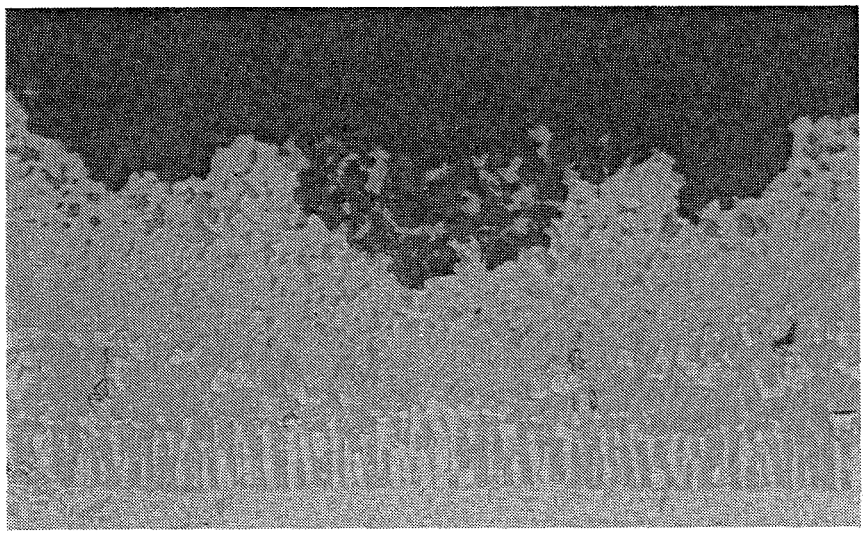

(b) Enlargement of Sulfide Pit in (a) Above (500×)

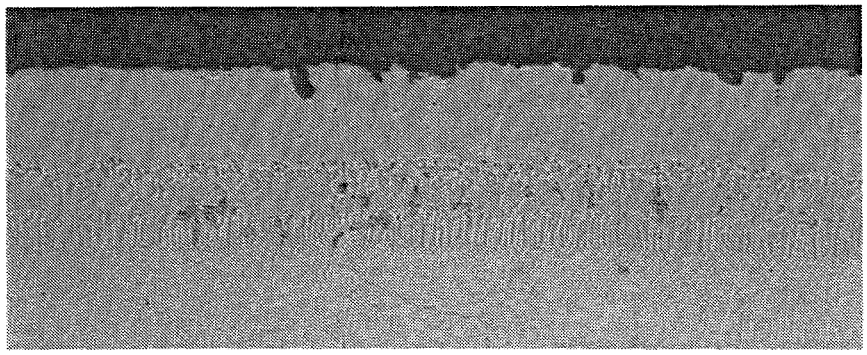

(c) Region Showing Little or No Sulfidation (250×)

Figure 45. Preaged RT21 Coated U700 (X133) after 88 Hours in Hot Corrosion Burner Rig at 900° C.

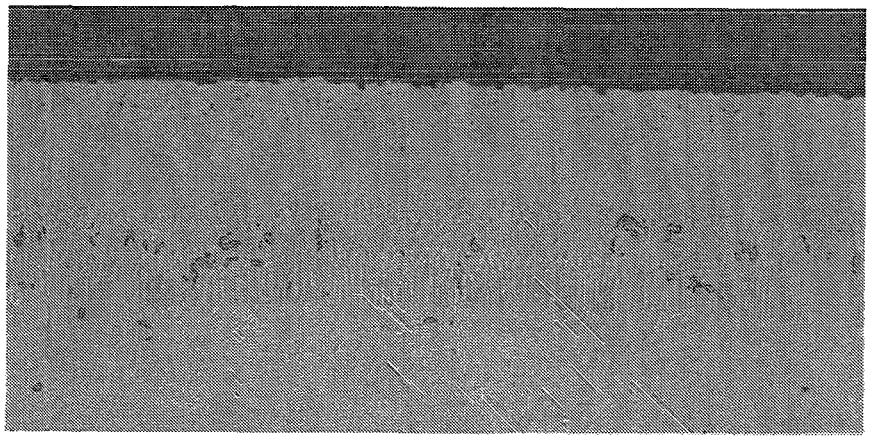

Figure 46. Preaged RT21 Coated U700 (X99) after 23 Hours in Hot Corrosion Burner Rig at 900° C (250×).

In absolute terms, the suspected 40 hours required for additive-layer penetration should not be dependent on the diffusion zone, although it may vary due to changes in chemistry during preaging. Metallographic examination of an aluminided U700 specimen, X77, in the as-coated condition, tested for 40 hours in the burner rig, showed signs of sulfidation, as shown in Figure 48, but not additive-layer penetration. A René 80/Codep burner rig test from Task II, interrupted at 103 hours (approximately 20% of the 500-hour expected life) indicates considerable additive layer sulfide penetration throughout the cross section (Figure 49). Apparently, the time required for sulfidation of the additive layer of an as-coated aluminide lies between 40 and 100 hours despite considerably longer life of the total substrate/coating system.

Sulfide penetration is a very localized phenomenon, however. In order to establish quantitatively what portion of life is spent in sulfidation of the additive layer versus the diffusion zone, one would need to evaluate several cross sections of many interrupted burner rig test specimens. The results of this preliminary (peripheral) study do provide educated starting points for the design of a test matrix to define the boundaries between the stages of this suspected dual-step phenomenon.

Having demonstrated the rapid movement of the sulfidation front through the additive layer and the severe slowdown through a diffusion zone containing closely spaced precipitates, it remains to discuss the consequences of the transformation of closely spaced σ phases in the diffusion zone to more widely separated, blocky carbides during 1100° C aging. This transformation is perceived to increase the vulnerability of the diffusion zone to sulfidation dramatically for two reasons:

- Aging causes a severe drop in Cr content in the diffusion zone matrix by a factor of two to about 7% (Table XV). Based on various published studies of Ni-base superalloys, this drop will substantially increase the sulfidation rate.

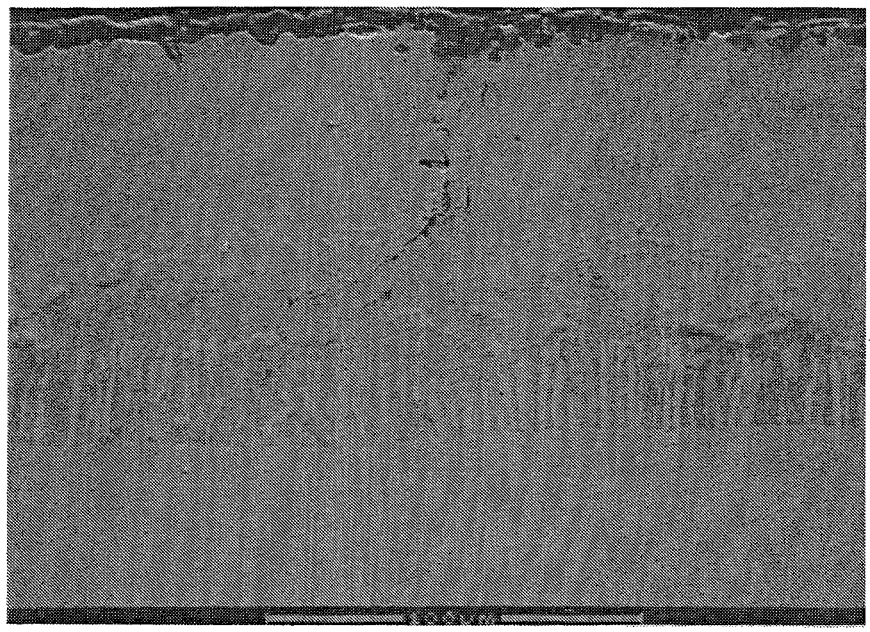

Suspected Sulfidation in Additive Layer (500×)

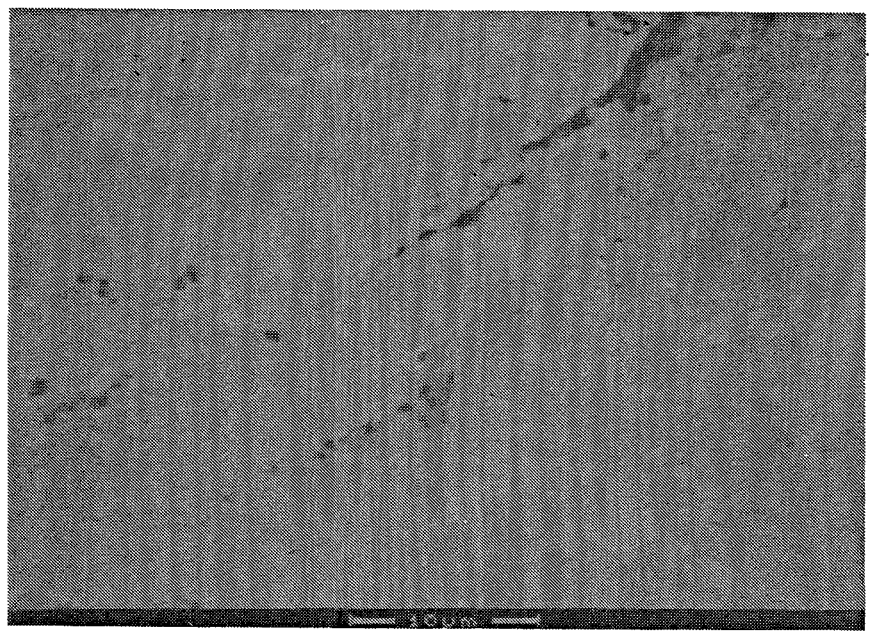

Enlargement of Above Picture (2500×)

Figure 47. SEM Pictures of Preaged RT21 Coated U700 (X107) after 41 Hours in Hot Corrosion Rig at 900° C.

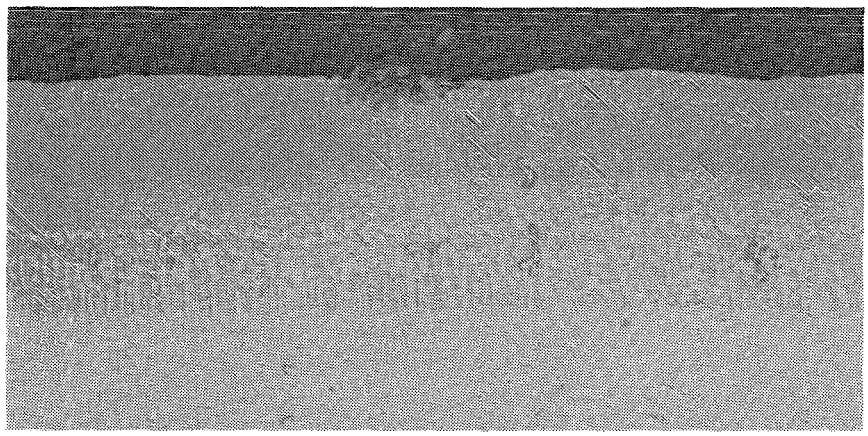

Figure 48. U700/Codep (X77), As-Coated, After 40 Hours in Hot Corrosion Burner Rig at 900° C (500×).

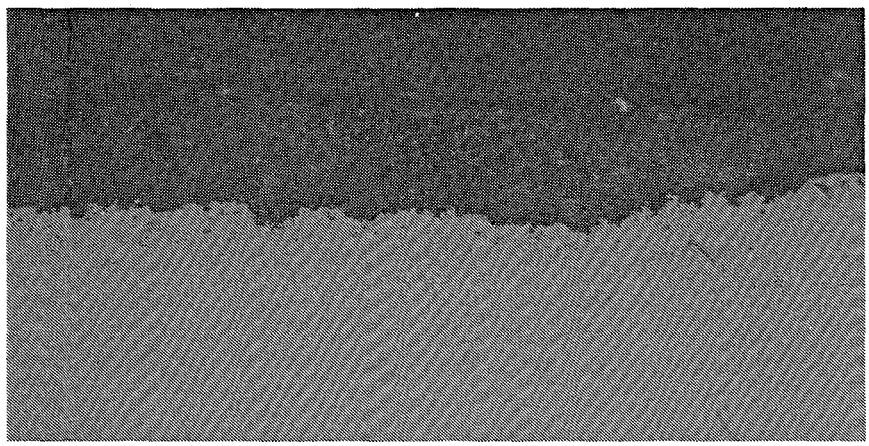

Figure 49. René 80/Codep, As-Coated, After 103 Hours in Hot Corrosion Burner Rig at 900° C (500×).

- The notion of "tortuosity factor" may be invoked (References 9 and 10). That is, if aging significantly widens the spacing between impediment phases, diffusion processes (such as sulfidation) will proceed more rapidly. This is exemplified by the Codep/U700 specimen aged for 100 hours (Figure 41). On the other hand, note the analogous Codep/René 80 specimen in Figure 42. Although considerable blocky carbides have formed, there remains an "underbrush" of σ phases that continues to provide corrosion resistance.

The concept of a more tortuous path for sulfide progression in aluminided René 80 versus U700 is supported by additional evidence obtained using phase-extraction techniques. (J. Radavich of Purdue University supplied this information in May 1986.) From a three-dimensional viewpoint, there appears to be more continuity in the diffusion zone of the René 80/Codep system compared to the discrete-particle morphology observed in U700/Codep. Figures 50 and 51 show cross sections of the substrate/coating systems after high-temperature preage, as well as the top view after electrochemical removal of the additive-layer matrix. In the case of U700, the discrete particles were identified as carbides and borides. The case of René 80 is somewhat more complex, with a multilayer diffusion zone comprising Cr-rich particles (primarily carbides) adjacent to the substrate and an interconnected boride phase adjacent to the additive layer.

Test No. 2

Results, listed in Table XIII, are displayed in Figure 52 together with previously discussed results from the ½ ppm Na test. Each plotted value is an average of two specimens. In a few cases the specimens differed considerably, yet the milder corrosion relative to the ½ ppm Na test is evident. Again, Codep-coated U700 shows life degradation increasing with aging time. These results are in qualitative agreement with laboratory data discussed previously (Reference 6) and supported by the lower Na_2SO_4 accumulation rate listed in Table XIV.

Test No. 3

Coatings lives are given in Table XIII for three groups of specimens.

Group 1 - Codep-coated U700 preaged at 1100° C: Although coatings lives for duplicate specimens were significantly different, the average values of 230 and 200 hours for 6 and 10 hours preage are reasonably consistent with previous results for other preage times, as can be seen in Figure 53.

Group 2 - Codep-coated U700 preaged at 1050° C: The intention was to preage at a lower temperature in order to cause only modest changes in the diffusion zone, anticipating little or no subsequent coating life degradation (nominal life about 500 hours with no preage). Figure 54 indicates that only minor changes occurred in the diffusion zone when compared to the as-coated

Cross-Sectional View (500×)

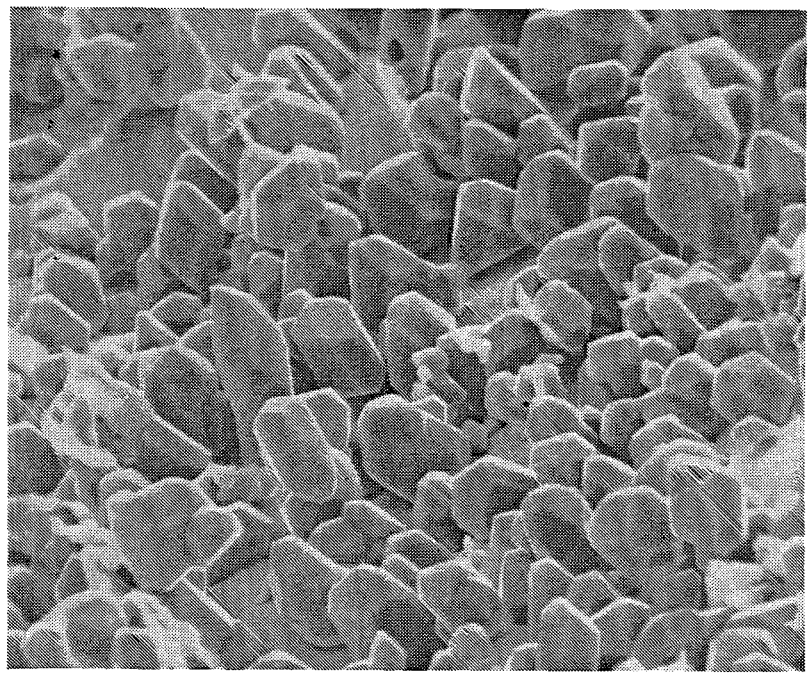

Top View of Diffusion Zone after Electrochemical Removal of Matrix (1000×)

Figure 50. SEM Pictures of Codep Coated U700 Aged at 1100° C for 100 Hours.

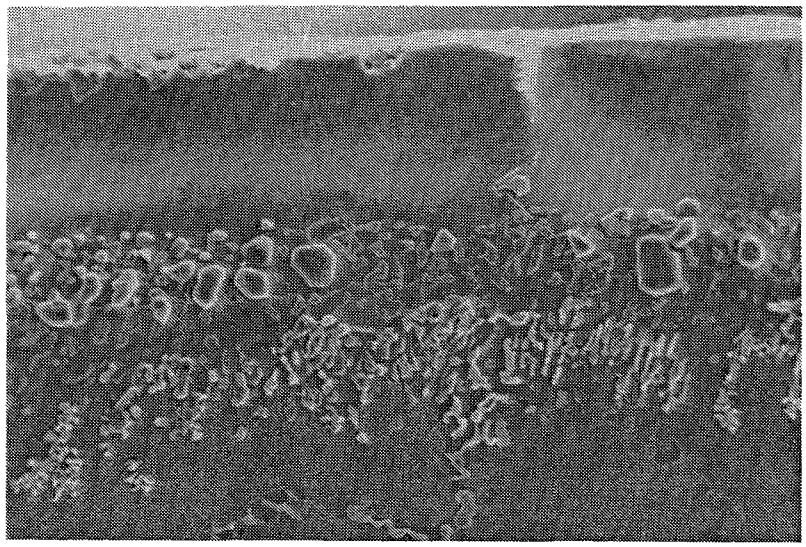

Cross-Sectional View (500×)

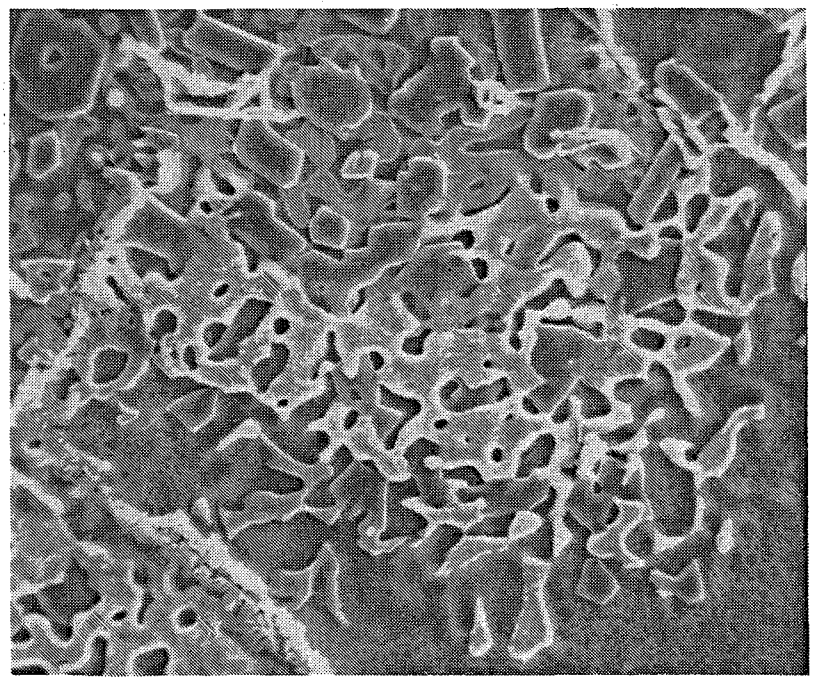

Top View of Diffusion Zone after Electrochemical Removal of Matrix (1000×)

Figure 51. SEM Pictures of Codep Coated René 80 Aged at 1100° C for 100 Hours.

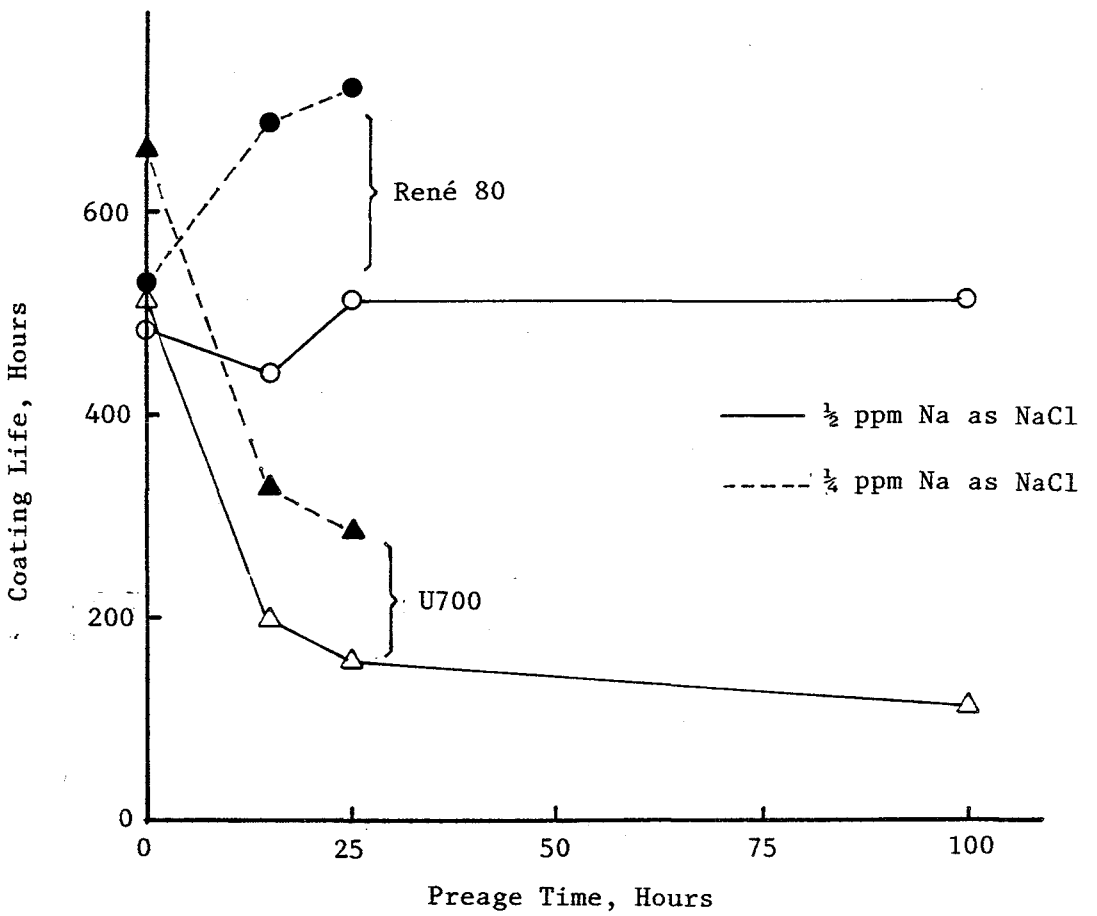

Figure 52. Codep Coating Hot Corrosion Life at 900° C as a Function of Isothermal Preage Time at 1100° C.

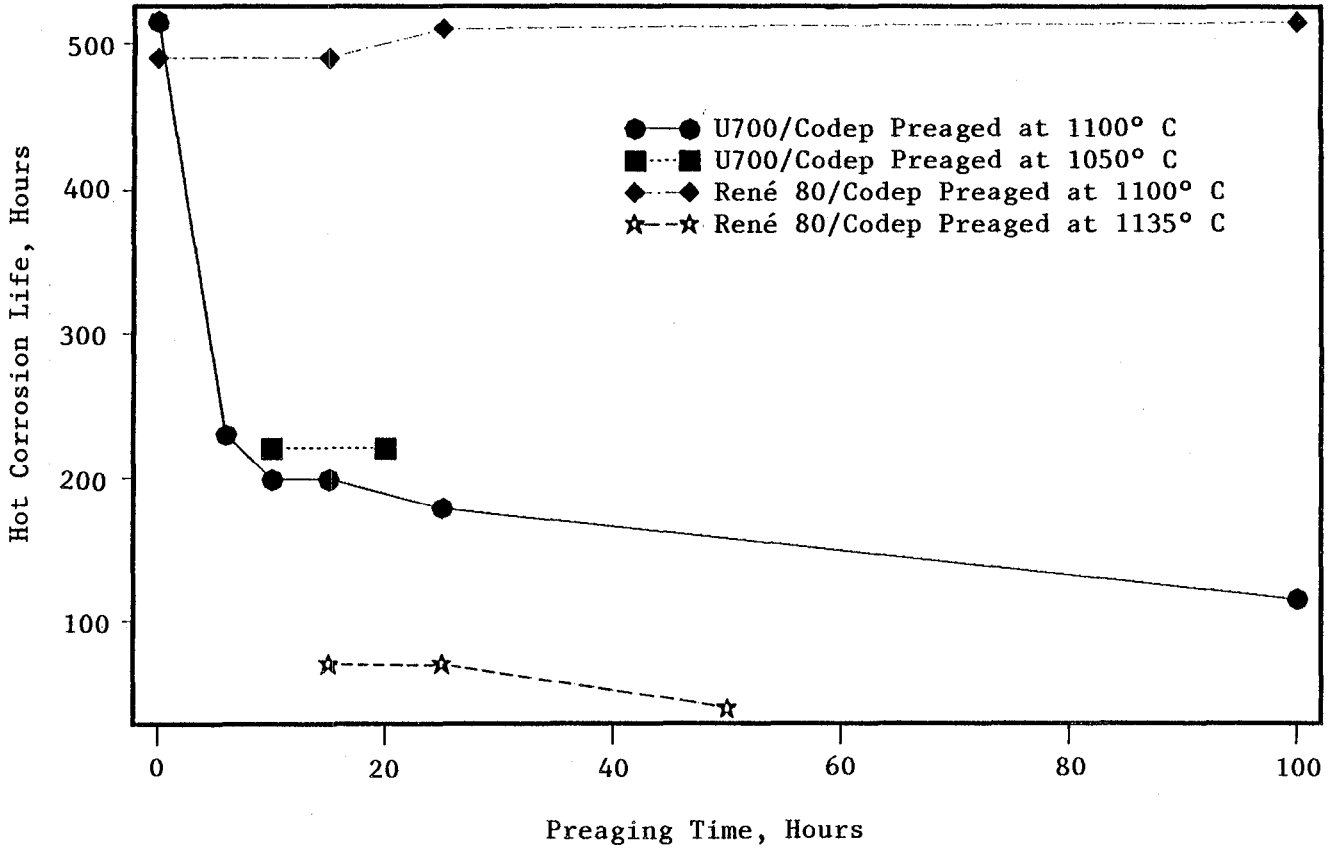

Figure 53. Hot Corrosion Codep Coating Life at 900° C for Various Isothermal Preaging Conditions.

diffusion zone microstructure depicted in Figure 41. However, the average spacing of the acicular phases has widened appreciably and is not unlike that developed in 6 hours at 1100° C. This may be the reason the hot corrosion life of the coating after 1050° C aging was more severely degraded than expected, as shown in Figure 53, although somewhat less than was caused by preaging at 1100° C. The Al content in the additive layer of the coating was found to be about 25% in both the 10-hour and 20-hour specimens (Appendix). This is the same as previously reported for 15 hours at 1100° C.

Group 3 - Codep-coated René 80 preaged at 1135° C: The intention was to preage at a higher temperature in order to cause diffusion zone changes more severe/faster than those that occur at 1100° C and hence to anticipate faster coating life degradation. Both objectives were met:

- Coating lives were severely degraded, Table XIII and Figure 53.
- Diffusion zone changes were very rapid (Figure 55). After 50 hours, the precipitates (carbides etc.) were completely gone, yet the coating/substrate interface remained well defined. For all three preage times the bulk of the additive layer contained about 15% Al; this is less than the 17-18% found in comparable specimens preaged at 1100° C (Appendix). This extensive interdiffusion caused some transformation of the β phase at the outer surface to a phase containing 5% Al, 15% Cr, and somewhat enriched in W and Mo relative to the β phase.

In summary, the three tests discussed above have satisfied most of the objectives/predictions discussed in the preceding section.

Test No. 1 - A reasonable model has been developed to explain the marked difference in hot corrosion coating lives on the two substrates, U700 and René 80, after aging at 1100° C. The model proposes that the bulk of the life of an aluminide coating resides in the corrosion resistance of the diffusion zone if that zone contains a high population of closely spaced σ phases. Aging induces transformation of σ to large, widely spaced carbides. To the extent that this occurs, and to the degree that wide paths of diffusion zone matrix are created, the overall corrosion life of the coating is significantly decreased. Application of these observations to specimen evaluation, blade coating life prediction, etc. is presently semiquantitative. Engineering judgment of the diffusion zone appearance is required.

Test No. 2 - These results provide another data point demonstrating that corrosion rate is directly related to salt-deposit film thickness.

Test No. 3 - Group 1 results provided more evidence supportive of Test 1. Group 2 results were marginal but showed that a lower age temperature for Codep/U700 specimens did in fact cause somewhat less coating hot corrosion life degradation. Group 3 results demonstrated that a higher age temperature for Codep/René 80 specimens caused rapid and major changes in the diffusion zone along with catastrophic decreases in coating hot corrosion life.

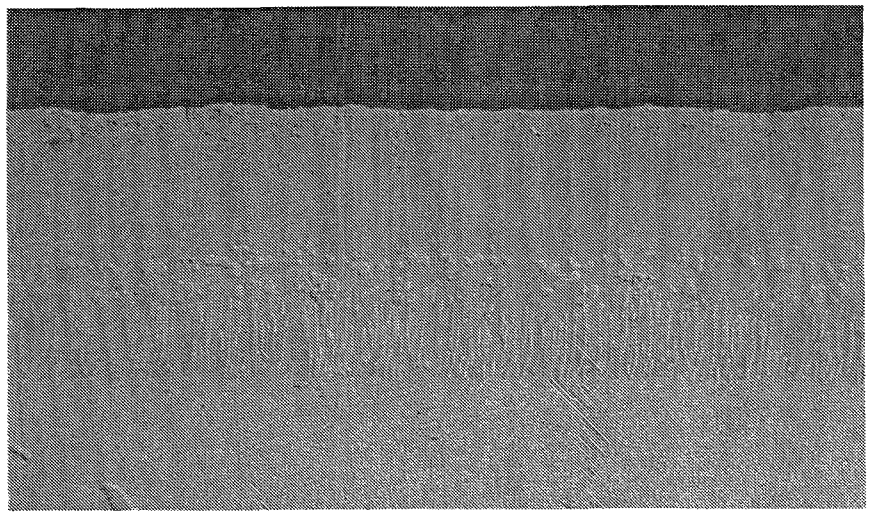

Figure 54. Codep Coated U700 (X102) after Isothermal Aging in Air at 1050° C for 10 Hours (500×).

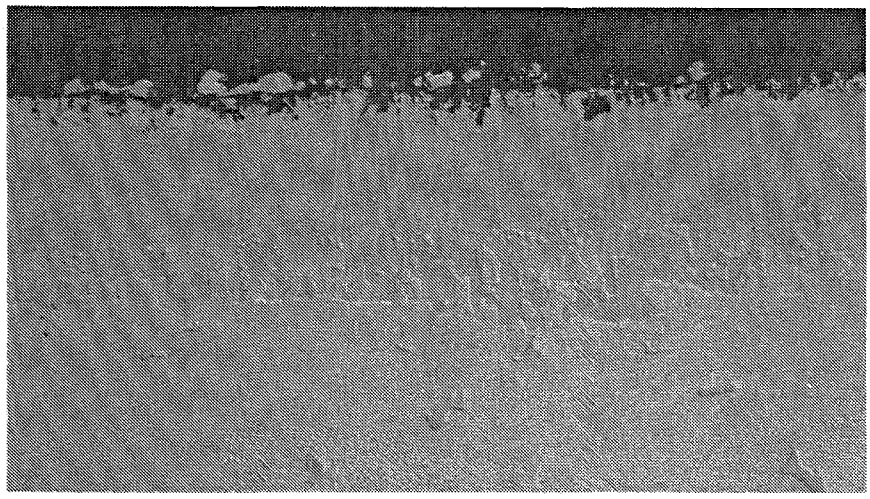

Figure 55. Codep Coated René 80 (L53) after Isothermal Aging in Air at 1135° C for 15 Hours (500×).

RECOMMENDATIONS

This program has revealed new information concerning deleterious effects of coating/substrate interdiffusion in a temperature range typical of aircraft engine takeoff conditions. However the time/temperature relationships causing a given nature and degree of change in the diffusion zone were shown to depend not only on the identity of the coating but of the substrate as well. In Task V, considerable detailed information was obtained for a typical aluminide coating (Codep) on U700 and on René 80 substrates. For coated René 80, the threshold exposure temperature, above which hot corrosion coating life is degraded, lies between 1100° and 1135° C. For coated U700, this temperature lies below 1050° C. Further experiments are needed to pinpoint the exact boundary temperature for the latter system.

Of considerable importance to broaden the scope of any life-prediction model which ensues from the present study is an extension to other materials systems. For example, the following questions should be addressed:

- What are the time/temperature relationships for aluminide coatings on other substrates? For example, several commercial turbine blade alloys contain hafnium which is known to increase significantly the hot corrosion (as-fabricated) aluminide coating life in typical burner rig tests.

- What are the time/temperature relationships for typical overlay coatings on various substrates? The present study demonstrated aging effects for NiCoCrAlY-coated specimens and suggested a significant difference between U700 and René 80 substrates, but within the constraints of the study it was not possible to pinpoint the cause, whether diffusion zone phenomena or other.

In addition to the above interdiffusion (internal) effects on coating life, the proposed model points out the importance of average salt-film thickness on the blade surface. More basic information is needed on the relationship of this parameter to hot corrosion rates, that is, controlled laboratory tests such as those reported by Fang and Shores (Reference 6). Again, various coating/substrate systems should be investigated separately to determine the extent of any substantial differences.

Information is also needed concerning the "memory effect" in which an alloy can corrode for a significant time after predeposited salts have evaporated. This can be obtained from burner rig hot corrosion tests conducted under thermal-cycling conditions above and below the salt-dewpoint temperature or under conditions of intermittent salt ingestion.

Internal and environmental aspects of the proposed model both require extensive supporting information from further, continuing study/interpretation of field experience. Among these needs are the following:

- Air surveys should be conducted to measure contaminant levels at various airports as a function of geographical location and weather conditions. Include, when possible, measurements at modest elevations (up to 3000 feet).

- Mission analyses should be conducted to aid further blade/vane evaluations and correlate with all available flight-pattern information (as in Task I). This should include a broad range of corrosion severity to determine the extent correlations suggested by Figures 7 and 8 (based on extreme cases) should be represented as bands rather than lines.

- Ultimately, mission analysis etc. (above) must be performed for various engine designs (primarily the General Electric CF6-50 in Task I) to determine the magnitude of sensitivity of the proposed life-prediction model to design differences.

In addition to the above recommendations directly related to development and verification of a life-prediction model, it is appropriate to comment on the technique of coil-inductance measurements for following the course of degradation and to suggest specific questions for which it may provide insight otherwise unattainable. In this study, such measurements were periodically made, but in most cases comparison with metallographic observations awaited extensive degradation and demonstrated only that both rate and magnitude of change of corrosion and of coil inductance agreed reasonably well.

Not explored in this study were the implications of, for example, the small negative changes for short burner rig exposures of coated specimens (see Figures 38 and 39). Such tests coupled with detailed electron microprobe analyses might be fruitful. Also, information concerning incubation period versus breakaway degradation, documented with coil-inductance measurements and metallographic evaluations, should be obtained from burner rig hot corrosion tests for various exposure times. Finally, it is suggested that the question be explored whether exposure at takeoff temperatures influences oxidation life as well as hot corrosion life of coatings.

CONCLUSIONS

This study involves the determination of surface chemistry effects of oxide scale and coating composition on the hot corrosion life of selected alloys in the coated and uncoated conditions in burner rig tests. The burner rig data are used to develop a hot corrosion life-prediction model embracing both coating/alloy composition variables and environmental variables. Evaluation of service-run turbine components that have suffered hot corrosion establishes a baseline of microstructures and extent of metal degradation as a function of operating history. This evaluation identified sulfidation with microstructures similar to those produced in burner rig tests; qualitatively the extent of corrosion appeared to be inversely proportional to average length of mission. This correlation probably reflects fraction of time under takeoff conditions (higher temperatures) and, perhaps, fraction of time near ground level (higher propensity for contamination).

Burner rig tests conditions were: 900° C, hourly thermal cycling, 0.5 ppm sodium as NaCl in the gas stream, Mach 0.3 velocity. The alloys were Udimet 700 and René 80, uncoated and with RT21, Codep, or NiCoCrAlY coatings. These tests, up to 1000 hours, included as-processed specimens and specimens aged at 1100° C in oxidizing or inert environments for up to 600 hours.

Coil inductance changes, used for periodic nondestructive inspection of specimens, were found useful in following the course of corrosion for uncoated alloys for which degradation is rather uniform and generally extensive. However, such changes are much smaller and less instructive for coated specimens for which degradation is localized and failure is defined when the relatively thin (less than 100 μm) coating is breached.

Results showed that, for all three coatings, life at 900° C is shortened significantly by preaging at 1100° C for 100 hours or more, and far more for U700 than for René 80 substrates. Also, aging in vacuum degraded life similar to aging in air, suggesting that interdiffusion effects are more important than surface-composition changes caused by oxidation.

Therefore the life-prediction model proposed is a combination of two unrelated parameters: average contaminant environment and coating/substrate interdiffusion phenomena occurring at takeoff temperatures. Both of these require detailed information concerning engine operating conditions and flight route structure.

To obtain information in support of this model, additional burner rig tests were performed using Codep/U700 and Codep/René 80 specimens. The tests identified a temperature, in the range 1100° - 1135° C, at which relatively short exposures of Codep/René 80 degrade hot corrosion life. For Codep/U700, this threshold temperature is somewhat below 1050° C. One test was performed at half the standard salt ingestion level and confirmed the expected decrease in hot corrosion rate.

APPENDIX

ELECTRON MICROPROBE ANALYSES OF CODEP COATED SPECIMENS

Tables XVI - XXI summarize detailed compositional data for as-coated and for many of the as-aged, Codep-coated specimens hot corrosion tested in this program. All aging treatments were under isothermal conditions in static air. Included are:

- Measurements of the coating additive layer and the substrate alloy immediately below the diffusion zone using an elongated raster (1 × 65 μm, described previously).

- Spot analyses of a variety of precipitate particles in the diffusion zone and the matrix surrounding them.

Reference is made to the following photomicrographs:

- Figure 41: Coated U700 before and after 1100° C aging.

- Figure 42: Coated René 80 before and after 1100° C aging.

- Figure 54: Coated U700 after 1050° C aging.

- Figure 55: Coated René 80 after 1135° C aging.

Table XVI. EMP Analysis of Codep Coated Specimens Isothermally Aged 0 Hours at 1100° C.

Material	Weight Percent							Additive Layer, μm from Surface	Note
	Ti	Cr	Co	Ni	W	Al	Mo		
Codep/René 80 (L96)	0.8	4.9	6.1	54.3	1.0	32.0	0.8	6	1
	0.8	4.3	6.0	55.9	1.3	31.1	0.6	17	1
	0.5	2.7	6.8	58.8	0.6	30.6	0.0	26	1
	4.8	9.5	7.8	53.2	2.4	21.1	1.1	35	1
	7.1	14.7	8.7	57.1	3.8	4.6	4.0		2
	5.1	25.1	10.5	31.0	9.9	8.6	9.9		2
	43.1	5.8	3.4	21.3	12.3	1.4	12.8		2
	8.8	12.4	8.5	58.1	3.1	7.6	2.4		4
	5.1	13.7	9.3	61.2	3.8	4.2	2.7		5
	5.0	14.0	9.5	Bal	4.0	3.0	4.0		6
Codep/U700 (X26)	1.2	6.6	10.0	50.1		30.8	1.3	3	1
	1.1	5.8	10.3	51.2		30.7	0.8	11	1
	1.0	5.2	10.1	52.7		30.4	0.6	19	1
	0.5	2.1	10.4	58.0		29.1	0.0	29	1
	3.3	6.1	12.0	55.5		22.6	0.6	39	1
	2.6	32.2	16.9	29.8		5.8	12.4		2
	2.3	38.3	17.3	20.9		6.2	14.5		2
	4.0	26.1	15.6	36.6		8.3	9.2		2
	2.0	59.7	4.7	12.4		7.3	13.2		2
	3.8	34.3	15.9	26.7		6.5	12.4		2
	4.3	16.5	13.4	44.9		17.1	3.7		4
	3.7	14.3	14.4	59.4		5.1	2.9		5
	3.4	14.5	15.0	Bal		4.3	4.2		6

Notes:
1. Elongated raster analysis of additive layer.
2. Spot analysis of acicular particles in diffusion zone.
3. Spot analysis of blocky particles in diffusion zone.
4. Spot analysis of diffusion zone matrix.
5. Elongated raster analysis of substrate immediately below diffusion zone.
6. Substrate nominal.

Table XVII. EMP Analysis of Codep Coated Specimens Isothermally Aged 15 Hours at 1100° C.

Material	Weight Percent							Additive Layer, μm from Surface	Note
	Ti	Cr	Co	Ni	W	Al	Mo		
Codep/René 80 (L93)	2.7	6.7	7.1	64.8	0.4	18.0	0.1	5	1
	2.8	6.9	7.2	64.7	0.4	17.8	0.1	12	1
	2.9	7.5	7.1	64.5	0.5	17.1	0.4	18	1
	3.3	7.3	7.5	64.2	0.5	17.0	0.1	25	1
	3.8	7.1	7.5	63.8	0.5	16.9	0.5	31	1
	4.0	7.5	7.3	62.6	1.2	16.7	0.8	38	1
	2.5	23.9	10.4	18.3	22.3	2.9	19.9		2
	1.1	27.5	11.6	30.8	11.3	5.6	12.0		2
	8.3	27.7	11.1	17.9	16.8	3.3	14.9		2
	1.1	52.1	3.7	15.4	12.0	6.0	9.6		3
	0.6	57.3	3.0	11.8	11.9	5.6	9.8		3
	0.8	64.1	2.4	4.6	12.7	5.2	10.3		3
	4.2	8.3	8.7	60.8	1.2	16.4	0.5		4
	5.6	14.6	9.1	58.7	3.4	5.3	3.0		5
Codep/U700 (X27)	1.0	9.8	11.0	49.4		25.7	3.0	3	1
	1.2	6.4	11.4	52.7		27.0	1.3	10	1
	1.2	8.0	11.1	51.9		25.7	2.1	17	1
	1.1	4.7	10.9	57.2		25.3	0.7	25	1
	1.2	5.1	10.8	59.0		23.8	0.0	36	1
	3.0	6.2	11.9	57.7		21.0	0.1	45	1
	3.8	17.1	15.8	45.5		11.1	6.6		2
	4.7	12.2	14.3	52.9		12.8	3.1		2
	3.7	17.0	14.9	46.7		11.0	6.5		2
	2.5	26.7	6.8	27.0		5.4	30.8		2
	2.5	65.6	4.1	5.2		5.9	15.9		3
	0.9	55.4	6.0	17.7		7.3	12.1		3
	1.5	49.8	6.9	22.8		9.3	9.4		3
	5.4	8.7	14.1	53.8		17.0	1.0		4
	4.4	15.3	14.4	55.6		6.7	3.6		5

Notes:

1. Elongated raster analysis of additive layer.
2. Spot analysis of acicular particles in diffusion zone.
3. Spot analysis of blocky particles in diffusion zone.
4. Spot analysis of diffusion zone matrix.
5. Elongated raster analysis of substrate immediately below diffusion zone.

Table XVIII. EMP Analysis of Codep Coated Specimens Isothermally Aged 25 Hours at 1100° C.

Material	Weight Percent							Additive Layer, μm from Surface	Note
	Ti	Cr	Co	Ni	W	Al	Mo		
Codep/René 80 (L23)	3.0	6.6	7.4	63.4	0.5	18.8	0.1	3	1
	3.1	6.7	7.7	64.4	0.5	17.6	0.0	9	1
	3.4	7.0	7.9	63.8	0.4	17.6	0.1	15	1
	3.5	7.0	7.7	63.8	0.4	17.6	0.0	22	1
	3.6	6.8	7.7	63.6	0.6	17.7	0.0	29	1
	3.6	6.9	7.7	63.3	0.5	17.7	0.3	36	1
	3.7	7.1	7.8	63.2	0.5	17.6	0.2	43	1
	4.0	7.4	7.6	62.5	1.5	16.1	0.9	49	1
	1.2	33.0	12.0	20.4	13.8	3.7	15.9		2
	0.7	32.4	12.1	19.3	15.6	3.3	16.6		2
	1.9	24.6	1.8	12.8	30.9	2.8	25.2		2
	0.4	65.0	2.3	4.9	11.4	5.0	11.1		3
	6.0	7.5	8.3	60.5	1.1	16.3	0.3		4
	5.2	16.3	8.8	56.0	4.3	6.1	3.3		5
Codep/U700 (X57)	1.0	5.7	11.0	60.7		21.5	0.2	5	1
	1.6	6.4	11.2	59.7		20.5	0.5	15	1
	2.6	6.0	12.1	59.2		19.9	0.2	25	1
	3.8	6.6	12.8	58.1		18.5	0.2	36	1
	3.4	6.5	12.8	58.2		18.9	0.3	46	1
	5.0	7.8	14.4	55.7		16.1	0.7		2
	3.4	15.7	14.6	49.2		12.3	4.6		2
	1.4	32.3	17.0	27.3		4.6	16.8		2
	0.5	69.5	3.6	4.4		5.5	15.7		3
	0.7	68.6	3.7	7.1		5.7	13.4		3
	0.8	68.0	3.7	6.4		6.0	14.3		3
	5.0	8.2	13.9	55.7		16.6	0.5		4
	4.6	15.2	15.3	54.7		6.8	3.4		5

Notes:

1. Elongated raster analysis of additive layer.
2. Spot analysis of acicular particles in diffusion zone.
3. Spot analysis of blocky particles in diffusion zone.
4. Spot analysis of diffusion zone matrix.
5. Elongated raster analysis of substrate immediately below diffusion zone.

Table XIX. EMP Analysis of Codep Coated Specimens Isothermally Aged 100 Hours at 1100° C.

Material	Weight Percent							Additive Layer, μm from Surface	Note
	Ti	Cr	Co	Ni	W	Al	Mo		
Codep/René 80 (L26)	3.9	5.2	8.5	65.6	0.6	16.2	0.0	8	1
	3.3	5.6	8.5	64.3	0.5	17.7	0.1	11	1
	3.1	5.9	8.9	63.3	0.5	18.2	0.1	13	1
	3.0	5.9	8.8	64.0	0.5	17.7	0.0	15	1
	3.2	5.8	8.8	64.8	0.4	17.0	0.1	17	1
	3.0	5.8	8.8	64.3	0.3	17.6	0.1	19	1
	3.1	5.8	8.7	64.4	0.4	17.6	0.0	23	1
	3.2	6.3	8.4	63.0	1.1	17.2	0.8	27	1
	3.6	7.5	8.2	60.0	2.3	16.2	2.3	30	1
	5.0	11.0	8.2	36.2	18.0	2.2	19.5		2
	4.7	14.8	8.6	18.0	25.8	1.8	26.3		2
	4.8	13.7	8.3	21.6	25.4	2.1	24.1		2
	0.6	65.5	2.2	4.7	10.2	5.7	11.1		3
	6.9	60.0	2.1	5.7	10.0	5.3	10.0		3
	1.1	63.8	2.4	5.1	10.6	5.6	11.4		3
	0.9	64.2	2.3	4.9	10.9	5.5	11.3		3
	5.7	5.1	8.4	66.4	1.2	12.7	0.4		4
	4.9	14.3	10.7	57.3	3.4	5.8	3.2		5
Codep/U700 (X77)	3.1	6.3	12.5	59.1		18.5	0.4	4	1
	3.2	6.3	12.9	59.1		17.9	0.4	9	1
	3.2	6.2	13.0	59.7		17.4	0.5	13	1
	3.3	6.2	13.0	59.8		17.3	0.4	19	1
	3.4	6.0	13.2	59.7		17.3	0.5	26	1
	3.4	6.3	13.2	59.3		17.3	0.5	35	1
	3.4	7.0	13.1	59.2		17.1	0.2	42	1
	3.3	20.7	4.1	13.5		3.1	53.8		2
	3.3	21.0	3.9	14.0		3.5	52.7		2
	2.8	18.9	4.7	25.8		2.7	44.1		2
	3.6	24.2	2.9	7.8		2.5	57.3		2
	0.3	68.6	3.5	4.5		6.6	15.9		3
	0.3	71.4	3.5	4.4		6.3	13.5		3
	0.5	67.7	3.9	6.0		6.4	14.9		3
	3.5	6.9	12.0	60.6		16.5	0.5		4
	2.8	17.1	18.9	49.3		7.0	4.8		5

Notes:
1. Elongated raster analysis of additive layer.
2. Spot analysis of acicular particles in diffusion zone.
3. Spot analysis of blocky particles in diffusion zone.
4. Spot analysis of diffusion zone matrix.
5. Elongated raster analysis of substrate immediately below diffusion zone.

Table XX. EMP Analysis of Codep Coated U700 Specimens as a Function of Isothermal Air Age Time at 1050° C and at 1100° C.

Code, Temperature (° C), Age Hours	Weight Percent						Additive Layer, μm from Surface	Note
	Ti	Cr	Co	Ni	Al	Mo		
X102,	1.1	5.3	9.3	57.2	25.7	1.3	8	1
1050°,	1.1	5.2	9.4	57.6	25.3	1.3	14	1
10	0.5	3.3	10.1	61.2	24.7	0.1	21	1
	1.5	4.5	11.3	60.3	22.2	0.2	26	1
	2.4	5.2	12.2	59.7	20.5	0.1	31	1
X120,	0.3	4.0	11.7	56.2	27.3	0.5	4	1
1050°,	0.5	4.1	11.4	57.1	26.4	0.4	16	1
20	1.2	4.3	11.2	59.1	23.8	0.5	27	1
	2.5	5.2	12.3	58.5	21.2	0.3	38	1
	3.7	6.2	13.1	57.3	19.1	0.4	45	1
	1.5	37.6	19.7	20.1	2.3	18.3		2
	0.7	74.4	4.4	5.5	0.9	13.5		3
	1.2	68.7	4.5	9.1	2.9	12.8		3
	1.1	65.8	4.6	11.9	3.2	12.8		3
	4.8	14.4	15.0	47.3	15.5	3.0		4
X4,	0.6	3.2	10.1	63.5	22.4	0.4	5	1
1100°,	0.7	3.7	10.3	62.5	22.7	0.1	14	1
6	2.3	5.2	12.0	60.3	19.8	0.4	22	1
	3.4	6.6	13.1	57.8	18.7	0.4	28	1
X70,	0.9	4.4	10.8	62.2	21.5	0.2	7	1
1100°,	1.5	4.9	11.5	61.5	20.4	0.3	15	1
10	2.2	5.8	12.1	60.8	18.7	0.5	24	1
	3.0	6.4	12.8	58.8	18.3	0.6	32	1

Notes:
1. Elongated raster analysis of additive layer.
2. Spot analysis of acicular particles in diffusion zone.
3. Spot analysis of blocky particles in diffusion zone.
4. Spot analysis of diffusion zone matrix.

Table XXI. EMP Analysis of Codep Coated René 80 Specimens as a Function of Isothermal Air Age Time at 1135° C.

Code, Aging Hours	Weight Percent							Additive Layer, μm from Surface	Note
	Ti	Cr	Co	Ni	W	Al	Mo		
L53, 15	2.8	17.7	11.7	57.0	2.5	3.5	3.0		1
	5.3	9.4	8.0	63.3	0.8	12.2	0.9	10	2
	3.5	7.8	7.6	65.6	0.5	14.5	0.5	18	2
	3.5	8.0	7.5	65.0	0.6	14.8	0.7	24	2
	3.6	8.0	7.5	65.0	0.6	14.8	0.6	32	2
	2.8	17.6	11.5	56.3	3.0	5.8	3.0		3
	5.5	13.8	6.4	22.8	26.4	1.3	23.8		3
	2.0	25.6	1.1	7.1	34.7	1.1	28.5		3
	3.6	7.2	7.3	64.0	2.4	13.9	1.6		4
L43, 25	5.8	15.2	10.6	56.5	3.0	5.6	3.4		1
	3.3	7.6	7.3	66.2	0.8	14.0	0.7	15	2
	3.4	7.2	7.3	65.9	0.7	14.8	0.6	22	2
	3.3	7.5	7.3	66.3	0.5	14.5	0.6	30	2
L135, 50	2.6	15.1	10.4	58.9	3.4	6.1	3.5		1
	6.2	6.2	6.2	65.2	0.8	14.7	0.7	8	2
	2.9	6.6	6.4	67.4	0.7	15.4	0.5	15	2
	2.0	6.4	6.4	68.7	0.8	15.2	0.5	22	2
	1.9	6.2	6.5	69.4	0.6	14.8	0.6	30	2

Notes:
1. Spot analysis of outer light phase (see Figure 55).
2. Elongated raster analysis of additive layer.
3. Spot analysis of diffusion zone precipitates (see Figure 55).
4. Spot analysis of diffusion zone matrix.

REFERENCES

1. Luthra, K.L. and Shores, D.A., "Mechanism of Na_2SO_4 Induced Corrosion at 600-900° C," J. Electrochem. Soc., Vol. 127 (10), 1980, pp 2202-2210.

2. Wortman, D.J., Fryxell, R.E., Luthra, K.L., and Bergman, P.A., "Mechanism of Low Temperature Hot Corrosion: Burner Rig Studies," Thin Solid Films, Vol. 64, 1979, pp 281-288.

3. Deadmore, D.L., "Application of Induction Coil Measurements to the Study of Superalloy Hot Corrosion and Oxidation," NASA TM83560, January 1984.

4. Grisik, J.J., Miner, R.G., and Wortman, D.J., "Performance of Second Generation Airfoil Coatings in Marine Service," Thin Solid Films, Vol. 73, 1980, pp 397-406.

5. Fryxell, R.E. and Bessen, I.I., "Coating Life Assessment in Gas Turbines Operated for Ship Propulsion," Proc. of 1974 Gas Turbine Materials in the Marine Environment Conference, Castine, MA, pp 257-276, July 24-26 1974.

6. Fang, W.C. and Shores, D.A., "The Effect of Salt Deposit Thickness on Hot Corrosion Rates," Abstract 211, The Electrochemical Society, Extended Abstracts, Vol. 79-2, Fall Meeting, Los Angeles, CA, October 14-19, 1979, pp 564-566.

7. McCarron, R.L., Lindblad, N.R., and Chatterji, D., "Environmental Resistance of Pure and Alloyed γ' Ni_3Al and β-NiAl," Corrosion, Vol. 32 (12), 1976, pp 476-481.

8. Redden, T.K., "Ni-Al Coating - Base Metal Interactions in Several Nickel-Base Alloys," Trans. Met. Soc. AIME, Vol. 242, 1968, pp 1695-1702.

9. Szekely, Julian, Evans, James, and Sohn Hong Yong, Gas Solid Reactions, Academic Press, New York, 1976, p 27.

10. Luthra, K.L. and Worrell, W.L., "Simultaneous Sulfidation-Oxidation of Nickel at 603° C in Argon - SO_2 Atmospheres," Met. Trans. A, Vol. 9A, 1978, pp 1055-1061.

End of Document